Asynchronous Parametric Excitation in Dynamical Systems

Zur Erlangung des akademischen Grades Doktor-Ingenieur (Dr.-Ing.)
Genehmigte Dissertation von Artem Karev aus Kormilovka, Russland
Tag der Einreichung: 30.09.2020, Tag der Prüfung: 26.01.2021

1. Gutachten: Prof. Dr. Dr. h.c. Peter Hagedorn
2. Gutachten: Prof. Dr. rer. nat. Michael Schäfer
3. Gutachten: a.o. Univ.-Prof. Dr. techn. Fadi Dohnal

Darmstadt

TECHNISCHE UNIVERSITÄT DARMSTADT

Fachbereich Maschinenbau

Asynchronous Parametric Excitation in Dynamical Systems

Genehmigte Dissertation von Artem Karev

1. Gutachten: Prof. Dr. Dr. h.c. Peter Hagedorn
2. Gutachten: Prof. Dr. rer. nat. Michael Schäfer
3. Gutachten: a.o. Univ.-Prof. Dr. techn. Fadi Dohnal

Tag der Einreichung: 30.09.2020
Tag der Prüfung: 26.01.2021

Darmstadt

Bitte zitieren Sie dieses Dokument als:
URN: urn:nbn:de:tuda-tuprints-175546
URL: http://tuprints.ulb.tu-darmstadt.de/17554

Dieses Dokument wird bereitgestellt von tuprints,
E-Publishing-Service der TU Darmstadt
http://tuprints.ulb.tu-darmstadt.de
tuprints@ulb.tu-darmstadt.de

Die Veröffentlichung steht unter folgender Creative Commons Lizenz:
Namensnennung – Weitergabe unter gleichen Bedingungen 4.0 International
https://creativecommons.org/licenses/by-sa/4.0/

Erklärungen laut Promotionsordnung

§8 Abs. 1 lit. c PromO

Ich versichere hiermit, dass die elektronische Version meiner Dissertation mit der schriftlichen Version übereinstimmt.

§8 Abs. 1 lit. d PromO

Ich versichere hiermit, dass zu einem vorherigen Zeitpunkt noch keine Promotion versucht wurde. In diesem Fall sind nähere Angaben über Zeitpunkt, Hochschule, Dissertationsthema und Ergebnis dieses Versuchs mitzuteilen.

§9 Abs. 1 PromO

Ich versichere hiermit, dass die vorliegende Dissertation selbstständig und nur unter Verwendung der angegebenen Quellen verfasst wurde.

§9 Abs. 2 PromO

Die Arbeit hat bisher noch nicht zu Prüfungszwecken gedient.

Darmstadt, 30.09.2020

A. Karev

Abstract

The overall objective of this thesis is to obtain a comprehensive understanding of the stability behavior of general parametrically excited systems. Even though the manifold resonance effects caused by time-periodic variation of system parameters have been intensively studied since the mid-19th century, several aspects still remain unexplored. While, historically, parametric excitation had been prominent predominantly for its destabilizing impact (resonance), in recent decades, also its stabilizing impact (anti-resonance) had attained significant attention. Owing to this historical development, the coexistence of resonance and anti-resonance at certain frequencies in the case of asynchronous excitation was not identified. Further, most of the existing studies dealing with the appearance of different resonance effects are limited to simple systems featuring neither circulatory nor gyroscopic terms, making the response of more complex systems to parametric excitation unpredictable.

In the present contribution, the stability behavior of systems featuring circulatory and gyroscopic terms subject to asynchronous parametric excitation is investigated employing the semi-analytical method of normal forms. First, novel stability patterns are identified revealing global stabilizing and destabilizing effects. More importantly, it is shown that, contrary to the previous knowledge, resonance and anti-resonance may both simultaneously appear in the vicinity of certain resonance frequencies with a particularly steep transition between them. Even for complex systems featuring circulatory terms, these effects can be easily assessed qualitatively and quantitatively using the symbolic expressions derived for the most representative stability features. The results are validated on an electronic system following the simulation-based approach. Finally, with the enhanced understanding of the parametric stability phenomena, two exemplary mechanical systems, including a minimal model of a disk brake, are analyzed. The analysis emphasizes the practical significance of the coexistence of resonance and anti-resonance and advocates more accurate consideration of possible asymmetries, i.e., parametric excitation, in the brake squeal analysis.

Kurzfassung

Das übergeordnete Ziel dieser Arbeit ist es, ein umfassendes Verständnis des Stabilitätsverhaltens von allgemeinen parametererregten Systemen zu erhalten. Obwohl die vielfältigen Resonanzeffekte, die durch die zeitperiodische Variation von Systemparametern hervorgerufen werden, seit Mitte des 19. Jahrhunderts intensiv untersucht werden, bleiben einige Aspekte noch unerforscht. Während historisch die Parametererregung vor allem in Bezug auf ihre destabilisierende Wirkung (Resonanz) untersucht wurde, hat in den letzten Jahrzehnten auch ihre stabilisierende Wirkung (Antiresonanz) große Aufmerksamkeit erlangt. Aufgrund dieser historischen Entwicklung wurde die Koexistenz von Resonanz und Antiresonanz bei bestimmten Frequenzen im Falle der asynchronen Erregung nicht erkannt. Zudem beschränken sich die meisten der vorhandenen Studien zum Auftreten verschiedener Resonanzeffekte auf einfache Systeme, die weder zirkulatorische noch gyroskopische Terme in den Bewegungsgleichungen aufweisen. Das macht die Auswirkungen der Parametererregung in komplexeren Systemen nicht voraussagbar.

In dieser Arbeit wird das Stabilitätsverhalten von Systemen mit zirkulatorischen und gyroskopischen Termen bei asynchroner Parametererregung mit Hilfe der semi-analytischen Methode der Normalformen untersucht. Dabei wird ein neuartiges Stabilitätsverhalten mit globalen stabilisierenden und destabilisierenden Effekten entdeckt. Vor allem wird gezeigt, dass, im Gegensatz zu den bisherigen Erkenntnissen, Resonanz und Antiresonanz gleichzeitig, mit einem steilen Übergang dazwischen, auftreten können. Selbst bei komplexen Systemen mit zirkulatorischen Termen lassen sich diese Effekte mit den hergeleiteten symbolischen Ausdrücken qualitativ und quantitativ leicht beurteilen. Das neuartige Stabilitätsverhalten wird auf einem elektronischen System durch einen simulationsbasierten Ansatz validiert. Mit dem verbesserten Verständnis der asynchronen Parametererregung werden schließlich zwei beispielhafte mechanische Systeme, darunter ein Minimalmodell einer Scheibenbremse, untersucht. Dabei wird die praktische Bedeutung der Koexistenz von Resonanz und Antiresonanz betont und eine sorgfältige Berücksichtigung möglicher Asymmetrien, d.h. Parametererregung, bei der Bremsenquietschanalyse angeregt.

Contents

1 Introduction

1.1 Motivation

Parametric excitation in dynamical systems is nowadays known for its manifold stability effects. The presence of periodically varying system parameters, e.g., stiffness or inertia, expressed through time-periodic coefficients in the linearized equations of motion, may contribute to destabilization or also stabilization of the system's equilibrium. However, historically, for over one century since its discovery in the mid-19th century, the studies on parametric excitation had been focused on its destabilizing effects with the prominent fundamental and combination resonances. Contrary to the resonance due to external excitation, in the case of parametric resonance the trivial solution may become unstable so that linear damping does not limit the amplitude of vibration [26]. Due to the numerous resonance areas with possible instabilities, the parametric excitation remained a rather undesired property of mechanical systems for a long time [76, 8]. On the other hand, the stabilizing effect – called anti-resonance – discovered originally by Tondl in 1978, has been thoroughly studied only in the last two decades [72, 15, 21]. In case of anti-resonance, by exciting the system with a certain frequency, beneficial energy transfer between differently strong damped vibration modes is induced [20] so that it is possible to stabilize an unstable autonomous system or also enhance the existing damping [17].

The discovery of the new effects and better understanding of the underlying principles has given rise to practical applications with deliberately introduced parametric excitation. On the one hand, the destabilizing effects are used in energy harvesting applications [77, 3] as well as in parametric amplifiers [22]; on the other hand, the anti-resonance effect is introduced in order to attenuate vibrations and to enhance dissipative properties [16]. Another quickly growing field of application is the microelectromechanical systems (MEMS). In the field of MEMS, there are several applications employing both stabilizing and destabilizing effects, e.g., highly sensitive mass sensing [54] and rapid switching in mechanical resonators [58,

64], respectively.

And yet, despite all the theoretical studies and various practical applications, there still remain gaps concerning the studies on more general systems, especially those where the parametric excitation is not synchronous, i.e., when the individual system parameters experience variation though of the same frequency, but with a phase shift. For example, it is known that in a certain special case, asynchronous excitation can lead to total instability making the trivial solution less stable for all excitation frequencies, which is in contrast to all other known parametric resonance effects being limited to rather narrow frequency ranges [10, 24]. Neither has this global effect of total instability been studied for the general case, nor has its connection to the other "local" stability effects been established so far.

Therefore there is a special interest in exploring the general stability effects of asynchronous parametric excitation which might improve the performance of existing applications or even foster new ones. This looks especially promising in the modern multi-physics applications, e.g., MEMS, with numerous flexible possibilities to introduce parametric excitation of the desired form.

Apart from the cases with deliberately introduced parametric excitation, there are mechanical problems where time-periodicity is naturally present, but its action is still not fully understood. In particular more complex systems featuring circulatory terms are affected: As the stability effects of parametric excitation have been mostly studied only for simpler systems without circulatory terms, most of the extensive knowledge accumulated on this subject cannot be directly applied here, especially for the case of asynchronous excitation. In this way, it is uncertain what kinds of stability effects – resonance or anti-resonance – can be expected once the circulatory terms appear in the equations of motion.

An example is given by disk brakes with asymmetry introduced, e.g., through ventilation channels. Since disk brakes are often affected by squealing resulting in a major comfort issue, there are several models aiming at investigating the onset of squealing [75]. As shown in one of the recent minimal disk brake models, with the disk brake being a complex system with rotating parts and frictional contact, the corresponding equations of motion feature non-conservative circulatory terms and any asymmetry might easily lead to asynchronous parametric excitation [75]. A numerical analysis of this system revealed stability behavior which cannot be explained with the current state of knowledge on parametric excitation [70]. Apparently, the interaction of circulatory terms and parametric excitation, in particular asynchronous excitation, introduces additional complexity to the system's stability behavior needing thorough investigation.

1.2 Literature overview

Dynamical systems with time-periodic coefficients, i.e., parametric excitation, have been studied since the mid-19th century when the typical resonances at the excitation frequency of twice the natural eigenfrequency were first observed by Faraday and Melde [28, 52]. As studied in detail by Lord Rayleigh in 1883 [46], the possible stability effects in such systems are limited to (mostly destabilizing) fundamental resonances involving only one eigenfrequency. With the prominent examples of Mathieu and Hill equations [50, 32], one-dimensional systems remained the only known examples of parametric excitation for a long period of time. In was not until 1940 that the new type of destabilizing combination resonance involving two eingenfrequencies was identified by Cesari [10] and studied more deeply for the first time by Mettler in 1949 [53]. Since then parametrically excited systems have attracted a lot of attention in theory and practice, mostly for their destabilizing properties. Another milestone in the studies on time-periodic systems is marked by the discovery of stabilizing properties of combination anti-resonance in 1978 by Tondl [72]. Further extensive elaboration of anti-resonance by Dohnal [15] led to first practical applications of parametric excitation for vibration mitigation in rotordynamics [16, 11].

Most of the theoretical studies and practical applications on time-periodic systems deal with synchronous parametric excitation. In this case, all time-periodic excitation terms of a multi-dimensional system are varying in phase. There is a substantial body of work on such systems covering in detail several aspects like the analytical approximations of Lyapunov characteristic exponents and stability boundary curves [4, 67, 24, 25] as well as experimental investigations [2, 16, 61, 11]. Also various types of stability effects have be extensively studied, including the destabilizing (resonance) as well as stabilizing (anti-resonance) effects [72, 14, 19, 21].

Considerably less attention has been paid to asynchronous parametric excitation. The first theoretical study on a parametrically excited system with out-of-phase excitation terms was done by Cesari in 1940 [10]. Cesari showed that in a system of two undamped Mathieu equations coupled via parametric excitation with a $\pi/2$ phase shift, the trivial solution is unstable for all excitation frequencies. The effect was later called *total instability* [9]. In 1976, for the first time, the stability effects of different phase relations (i.e., asynchronous excitation) combined with non-uniform damping were extensively studied by Schmieg [68]. In this work, the stability problem was first approached theoretically using the method of slowly varying phase and amplitude for the derivation of stability boundaries and Lyapunov characteristic exponents (LCEs). However, while the complex symbolic expression for

LCEs was derived by Schmieg in general form allowing the study of both stabilizing and destabilizing effects of parametric excitation, the analysis was limited to the destabilizing effect only, as the anti-resonance effect was not yet known at that time. The theoretical findings were also validated experimentally. Since the required phase shift in the off-diagonal excitation terms cannot be easily realized in a mechanical system, the validation was performed on an equivalent electronic system, where arbitrary phase relations are readily implemented. Schmieg's investigations remain the only experimental work done on asynchronous parametric excitation to this day.

Eicher and Dohnal also studied asynchronous parametric excitation from different perspectives. Eicher thoroughly studied the destabilizing behavior focusing, however, only on the stability boundaries [27, 24]. The symbolic expressions for the boundary curves were derived by the method of successive approximation [24]. The impact of asynchronous excitation was observed in terms of shifted stability boundaries, while the actual reason for the shift was not recognized. Dohnal extensively studied the stabilizing effect of general harmonic excitation focusing mostly on stability conditions and stability boundaries applying the averaging method [15, 17]. The LCEs, denoted by Dohnal as equivalent damping, were discussed in detail for the special cases of in-phase and anti-phase parametric excitation [14]. Further, equivalent damping for the general case of asynchronous excitation was discussed briefly in [15], focusing, however, again on the stabilizing effect. In this way, the stability effects of asynchronous parametric excitation have been studied either from the destabilizing or the stabilizing perspective only.

Considering the complexity of the studied systems, the majority of studies on parametric excitation treats dynamical systems with decoupled unperturbed autonomous equations of motion – the only coupling is via parametric excitation [27, 67]. The results of these studies cannot be applied to systems featuring gyroscopic or circulatory terms as decoupling of such systems is not possible [44]. The gyroscopic coupling was included in studies on asynchronous parametric excitation conducted by Dohnal in context of anti-resonance [15, 17]. However, no specific stability effects attributed to the gyroscopic terms alone were identified. Further, a few studies on synchronously excited systems with circulatory terms indicate that the presence of circulatory terms does not significantly change the general appearance of resonance and anti-resonance [5, 12]. Though, little is known about its precise impact on the stability boundaries and the characteristic exponents especially in the more general case with asynchronous excitation: A short study of a minimal model of a disk brake with asymmetric bearing featuring both asynchronous excitation and circulatory

terms revealed stability behavior with alternating stabilized and destabilized areas which cannot be explained with the existing knowledge [70, 40]. In this way, the most general case with gyroscopic and circulatory coupling as well as with asynchronous parametric excitation remains unexplored. While the stability analysis of such systems can still be easily carried out numerically, the precise conditions for the appearance of various resonance effects are unknown, so that only limited qualitative insight can be obtained.

Apart from the traditional field of mechanics, in recent years parametric excitation experiences an increasing interest in the area of electromechanical structures, in particular microelectromechanical structures (MEMS) [54]. In the rich field of MEMS applications there are several examples of beneficial use of destabilizing properties of parametric excitation, e.g., atomic force microscopy [63], highly sensitive mass sensing [73] and parametric amplification [59] . While the majority of the applications utilize only the basic fundamental resonances, there also attempts to make use of the anti-resonance with the aim of targeted dissipation control while maintaining high quality factors, i.e., low damping levels [58, 64]. Due to the multi-physical nature of MEMS, there is a variety of mechanisms to introduce parametric excitation, e.g., electrostatic actuation, piezoelectric elements and feedback control [65]. This flexibility makes MEMS a highly promising field for the application of potential new stability effects arising from asynchronous parametric excitation.

1.3 Research objectives

The literature review in section 1.2 reveals several major gaps in the studies on parametric excitation. The objective of this thesis is to systematically analyze the following unexplored aspects.

The first aspect deals with general asynchronous parametric excitation, while both displacement- and velocity-proportional excitation is considered. In particular, possible generalizations of total instability are to be investigated in systems with non-uniform damping. Further, it is presently known that resonance and anti-resonance appear separately at sum and difference combination resonance frequencies and swap their positions depending on whether the excitation is symmetric or skew-symmetric. The study of general asynchronous excitation is supposed to enlighten the transition process from resonance to anti-resonance at a combination resonance frequency.

The second main aspect consists in creating a solid base for the analysis of parametrically excited systems featuring also circulatory terms. The impact of circulatory terms on the

appearance and magnitude of fundamental and combination resonances is to be thoroughly investigated.

In order to obtain profound understanding of the complex stability phenomena, the semi-analytical method of normal forms will be used. By deriving an approximate time-autonomous representation of the original time-periodic system, concise analytical expressions can be obtained providing insight into the impact of individual parameters, e.g., the phase angles of asynchronous excitation or the circulatory terms.

Eventually, the new findings are to be applied for the analysis of mechanical examples featuring both circulatory terms and asynchronous excitation. The new insights are supposed to provide proper understanding of complex stability behavior previously only observed by numerical Floquet analysis.

1.4 Outline

The thesis is structured as follows. In chapter 2 the theoretical background on the stability of time-periodic systems is presented. Starting with the introduction of stability definitions and criteria, the chapter proceeds with the discussion of parametric resonance effects, paying special attention to synchronous and asynchronous types of excitation. The chapter concludes with the presentation of the semi-analytical method of normal forms applied throughout the thesis for the treatment of time-periodic systems.

In chapter 3 the global stability effects of parametric excitation are discussed studying general dynamical systems with displacement- and/or velocity-proportional excitation. After deriving approximate analytical expressions qualitatively describing the stability behavior, conditions for the appearance of global stabilizing and destabilizing effects are derived. It is shown that the previously known case of “total instability” is only a special case of a more general phenomenon. Most of the results of this chapter have been originally published in [40].

The following chapter 4 deals with the newly discovered phenomenon of coexistence of resonance and anti-resonance in the neighborhood of combination resonances. The complex stability behavior in these areas is described introducing characteristic points characterizing the most prominent stability features. Starting with a simple system in order to study the general aspects of coexistence, the phenomenon is subsequently studied for a more complex mechanical system featuring circulatory and gyroscopic terms. Section 4.1 of this chapter has been originally published in [42].

The purely theoretical results obtained in the previous chapters are validated in chapter 5 using a simulation-based approach. Simulation of an electronic circuit, which dynamics is equivalent to the mechanical systems studied before, is carried out to complete the existing experimental results by the newly discovered effects. The results of this chapter have been originally published in [39].

Various aspects of asynchronous parametric excitation, including fundamental resonances and nonlinear effects, are studied in chapters 6 and 7 for the sake of completeness. Most of the results in chapter 7 have been originally published in [43].

Chapter 8 deals with mechanical examples. The accumulated knowledge on asynchronous excitation is now applied to two examples highlighting different aspects. In the first academic example of a rotating disk, representing a simple system featuring circulatory terms, the appearance of parametric resonances in unexpected areas, i.e., in the lower frequency range, is demonstrated. In the second example, a minimal model of a disk brake developed to investigate the appearance of brake squeal is considered. The introduction of asymmetric properties, and with this also introduction of asynchronous parametric excitation, led to unusual stability behavior which could not be previously explained. Only the application of the newly acquired knowledge on the coexistence of resonance and anti-resonance made it possible to understand the complex stability behavior of this system.

Chapter 9 concludes the results of the thesis and gives outlook for further research.

2 Theoretical framework

2.1 Stability of dynamical systems

In the studies of dynamical systems, the question of stability is often of particular interest. In order to address this question, a mathematical representation of the considered system is required. For this purpose a general dynamical system, linearized at an equilibrium, can be described by equations of motion of the form

$$\mathbf{M}\,\ddot{\mathbf{q}} + [\mathbf{D} + \mathbf{G} + \mathbf{B}(t)]\,\dot{\mathbf{q}} + [\mathbf{K} + \mathbf{N} + \mathbf{C}(t)]\,\mathbf{q} = \mathbf{0} \tag{2.1}$$

with

$$\mathbf{M} = \mathbf{M}^T > 0, \tag{2.2a}$$

$$\mathbf{D} = \mathbf{D}^T \geq 0, \qquad \mathbf{G} = -\mathbf{G}^T, \tag{2.2b}$$

$$\mathbf{K} = \mathbf{K}^T > 0, \qquad \mathbf{N} = -\mathbf{N}^T, \tag{2.2c}$$

$$\mathbf{B}(t) = \mathbf{B}(t+T), \qquad \mathbf{C}(t) = \mathbf{C}(t+T) \tag{2.2d}$$

and $\mathbf{q} \in \mathbb{R}^n$ representing the column vector of generalized coordinates. In mechanical systems the different matrices collect system's properties of different physical origins. $\mathbf{M}$ and $\mathbf{K}$ follow from the geometry and from material parameters and describe inertia and stiffness properties, respectively. The damping matrix $\mathbf{D}$ is in general small and may have different physical origins. The gyroscopic matrix $\mathbf{G}$ follows from the kinematics, while the circulatory matrix $\mathbf{N}$ is always associated with a non-conservative (i.e., non-potential) force field, which may even lead to an energy source or an energy sink. The circulatory terms often appear due to the contact forces between sliding solid bodies with Coulomb friction.

As certain system properties, e.g., stiffness or damping, may experience periodic variation, there might be time-periodic coefficients in the equations of motion which are collected in matrices $\mathbf{B}(t)$ and $\mathbf{C}(t)$ representing zero-average time-periodic velocity- and displacement-

proportional terms, respectively. Systems featuring time-periodic coefficients in the equations of motion are called *parametrically excited* system. In contrast to external excitation, the equations of motion remain homogeneous. Even though the inertia terms may, in general, also experience periodic variation, in most mechanical examples a suitable reference frame can be chosen, so that either the displacement- or acceleration-proportional terms are constant. In short, a system containing all of the above characteristics will be denoted as $\mathbf{MDGKN} + \mathbf{B}(t) + \mathbf{C}(t)$ system.

The stability of a general system (2.1) can be assessed in terms of its motion as a response to a perturbation of an equilibrium position. The mathematical formalization of the stability of motion was introduced by Lyapunov in 1892 and forms the basis of today's stability definition [47]:

a) The equilibrium position $\mathbf{q}_R$ is called *Lyapunov stable* if for each $\varepsilon > 0$ there exists $\delta > 0$ so that the following applies: All solutions of (2.1) which are within the distance δ from $\mathbf{q}_R$ at time t_0 will remain within the distance ε from $\mathbf{q}_R$ for all times $t > t_0$.

b) The equilibrium position $\mathbf{q}_R$ is called *asymptotically stable*, if it is Lyapunov stable and there exists $r > 0$ such that every solution starting within the distance r from $\mathbf{q}_R$ at time t_0 will converge to $\mathbf{q}_R$ for $t \to \infty$.

b) If the equilibrium position is neither asymptotically stable nor Lyapunov stable it is considered as *unstable*.

While the Lyapunov stability definitions are rather abstract and general, the practical stability analysis requires more tangible criteria to decide whether a solution is stable or not. For autonomous systems, i.e., for systems with $\mathbf{B}(t) = \mathbf{0}$ and $\mathbf{C}(t) = \mathbf{0}$, the stability can be assessed rather straightforwardly by considering the eigenvalue problem of the corresponding first order system composed by the constant system matrices only, Eqs. (2.2a)-(2.2c). For time-periodic systems, which represent the subject throughout this thesis, obtaining a quantity characterizing the stability of the trivial solution requires several additional steps. In particular, knowing the system matrices is no longer sufficient, but, instead, the knowledge of solutions at certain time is required which represents a major challenge. In the next section time-periodic dynamical systems are discussed in detail in context of Floquet theory.

2.2 Floquet theory

The presence of time-periodic coefficients, i.e., parametric excitation, may significantly affect the stability of the trivial solution. However, as the solutions of such systems cannot be obtained analytically, stability analysis represents a major challenge. In this concern, the implications of the Floquet theory, which provides information on the form of the solutions of time-periodic systems, are of great use for an efficient stability assessment.

The starting point of the following discussion, based on [31] and [62], is the representation of equations of motion, Eq. (2.1), as a system of first order differential equations

$$\dot{\mathbf{x}} = \mathbf{A}(t)\mathbf{x}, \quad \text{with} \quad \mathbf{A}(t+T) = \mathbf{A}(t), \tag{2.3}$$

with $\mathbf{x} \in \mathbb{R}^{2n}$ obtained through the coordinate transformation $\mathbf{x} = (\mathbf{q}, \dot{\mathbf{q}})^{\mathrm{T}}$. The quadratic $2n \times 2n$-dimensional system matrix $\mathbf{A}(t)$ is periodic with period T. According to the *Floquet theorem*, every fundamental solution of system (2.3) has the form

$$\mathbf{\Phi}(t) = \mathbf{P}(t)e^{\mathbf{B}t}, \quad \text{with} \quad \mathbf{P}(t+T) = \mathbf{P}(t), \tag{2.4}$$

where $\mathbf{P}(t)$ is a periodic $n \times n$ matrix and $\mathbf{B}$ is a constant $n \times n$ matrix. Equation (2.4) is also called *Floquet normal form*. An important corollary of the theorem is that a time-periodic transformation exists to transform (2.3) into an autonomous system, i.e., system with constant coefficients.

The corresponding transformation is given by

$$\mathbf{x}(t) = \mathbf{P}(t)\mathbf{y}, \tag{2.5}$$

which inserted into (2.3) gives

$$\dot{\mathbf{y}} = \mathbf{P}^{-1}(t)\left(\mathbf{A}(t)\mathbf{P}(t) - \dot{\mathbf{P}}(t)\right)\mathbf{y}. \tag{2.6}$$

With the relations

$$\dot{\mathbf{P}} = \dot{\mathbf{\Phi}}(t)e^{-\mathbf{B}t} - \mathbf{\Phi}(t)\mathbf{B}e^{-\mathbf{B}t}, \tag{2.7a}$$

$$\dot{\mathbf{\Phi}}(t)e^{-\mathbf{B}t} = \mathbf{\Phi}^{-1}(t)\dot{\mathbf{\Phi}}(t)\mathbf{P}(t) = \mathbf{A}(t)\mathbf{P}(t), \tag{2.7b}$$

(2.6) leads a system with constant coefficients

$$\dot{\mathbf{y}} = \mathbf{B}\mathbf{y}. \tag{2.8}$$

In this way, any solution of the original time-periodic system (2.3) is given as a linear combination of functions of the form $e^{\lambda t}p(t)$ with $p(t+T) = p(t)$ a polynomial in t with periodic coefficients.

Further, with the monodromy matrix $\mathbf{M}$ defined as

$$\mathbf{\Phi}(t+T) = \mathbf{\Phi}(t)\mathbf{M}, \tag{2.9}$$

the fundamental solution at $\mathbf{\Phi}(t+T)$ is also given by

$$\mathbf{P}(t+T)e^{\mathbf{B}(t+T)} = \mathbf{P}(t)e^{\mathbf{B}t}\mathbf{M}, \tag{2.10}$$

so that the matrix exponential $e^{\mathbf{B}T}$ is simply given as

$$e^{\mathbf{B}T} = \mathbf{M}. \tag{2.11}$$

Therefore, the eigenvalues of the monodromy matrix $\mathbf{M}$ can be used to assess the stability using the following definitions:

- the eigenvalues of the monodromy matrix ρ_i, $i = 1, 2, ..., 2N$, are called *characteristic* or *Floquet multipliers*
- any η_i, $i = 1, 2, ..., 2N$, such that $\rho_i = e^{\eta_i T}$ is called *characteristic* or *Floquet exponent*

In terms of Floquet multipliers, the necessary and the sufficient conditions for the stability of system (2.3) are given as follows:

- the trivial solution of system (2.3) is *Lyapunov stable* if the Floquet multipliers satisfy the condition $|\rho_i| \leq 1$ and those with $|\rho_i| = 1$ are semi-simple
- the trivial solution of system (2.3) is *asymptotically stable* if the Floquet multipliers satisfy the condition $|\rho_i| < 1$

In the simplest case, the monodromy matrix can be obtained as

$$\mathbf{M} = \mathbf{\Phi}^{-1}(0)\mathbf{\Phi}(T) \quad \text{with} \quad \mathbf{\Phi}(0) = \mathbf{I}, \tag{2.12}$$

so that only the fundamental solution at $t = T$ with unity initial conditions is required. On the one hand, this represents an efficient way of assessing the stability of a time-periodic system. On the other hand, however, as the fundamental solution cannot be obtained analytically, numerical integration has to be performed with the consequence that all of the studied system's parameters have to be assigned numerical values. Therefore, as opposed to its numerical efficiency, the approach provides limited insight in qualitative studies.

In the following, the procedure of numerically obtaining the monodromy matrix and evaluating its eigenvalues with the purpose of assessing the stability is called *Floquet analysis*.

2.3 Lyapunov characteristic exponents

Parametric excitation, i.e., the presence of time-periodic terms in the equations of motion, affects the stability of the trivial solution in several ways, described in detail in section 2.4. Depending on the structure of the excitation matrix and on the excitation frequency, there might be stabilizing, destabilizing or even no stability effect at all. There are many parameters with complex interdependencies deciding upon which effect is at hand in a particular case. The prevalent aim of the current study it to understand the contribution of individual parameters, in particular, of the phase angles in case of asynchronous excitation. However, as already mentioned, the stability problem in presence of time-periodic coefficients cannot be solved analytically. Although a quick overview can be obtained numerically applying the Floquet stability analysis, it does not provide a proper insight, but only a snapshot for certain parameter values.

In order to obtain more insight, an analytical approximation method has to be applied. In the present contribution, the method of normal forms, presented in detail in section 2.5, will be applied in order to obtain an approximate linear autonomous representation of the original time-periodic system. The stability of this linear autonomous system is then easily studied analytically by investigating its eigenvalues. Further, the approximate analytical results are to be verified by comparison with the numerical results obtained via Floquet analysis of the original system. These, however, are usually given in terms of the eigenvalues of the monodromy matrix, i.e., the Floquet multipliers. Obviously, in order to compare these results, a uniform stability criterion is required.

An appropriate uniform stability criterion is given by the *Lyapunov characteristic exponents* (LCEs) which are defined for both types of systems. The LCEs are widely used in the stability analysis of dynamical systems and are equal to the *characteristic numbers* introduced by

LYAPUNOV taken with the inverse sign [47, 7]. For a linear dynamical system

$$\dot{\mathbf{x}} = \mathbf{A}(t)\mathbf{x}, \quad \mathbf{A}(t) \in \mathbb{R}^{N\times N} \tag{2.13}$$

and its linear independent solutions $\mathbf{x}_i(t)$, $i = 1, ..., N$, the LCE corresponding to each solution is given by

$$\lambda_i = \limsup_{t\to\infty} \frac{1}{t} \ln |\mathbf{x}_i(t)|. \tag{2.14}$$

For linear autonomous systems ($\mathbf{A}(t) = \mathbf{A}(0) = \mathbf{A}, t \geq 0$) as well as for linear time-periodic systems ($\mathbf{A}(t + T) = \mathbf{A}(t)$) the solutions are both of the type

$$\mathbf{x}_i(t) = \mathrm{e}^{\nu_i t}\mathbf{p}_i(t). \tag{2.15}$$

In the autonomous case, ν_i and $\mathbf{p}_i(t)$ represent the eigenvalues of the system matrix $\mathbf{A}$ and polynomials in t with *constant* coefficients, respectively. In a periodic system, ν_i and $\mathbf{p}_i(t)$ denote the *Floquet exponents* and polynomials in t with *time-periodic* coefficients, respectively. Considering the definition of the LCEs in Eq. (2.14) and the structure of the solution in Eq. (2.15), the LCEs can be expressed as the real parts of the system's eigenvalues and as the real parts of the Floquet exponents for the constant and time-periodic system, respectively [48]. With the Floquet exponents η_i defined through Floquet multipliers ρ_i as

$$\rho_i = \mathrm{e}^{\eta_i T}, \tag{2.16}$$

the LCEs can also be obtained directly from the Floquet multipliers, i.e., the eigenvalues of the monodromy matrix, by

$$\lambda_i = \frac{1}{T} \ln |\rho_i|. \tag{2.17}$$

For the trivial solution to be asymptotically stable, all LCEs have to be negative. The largest LCE deciding upon stability will be denoted as Λ with $\Lambda = (\lambda_i)_{max}$. This uniform stability criterion enables comparison between autonomous and time-periodic systems. Moreover, the LCEs, in contrast to the Floquet multipliers, are not distorted by different periods T, which enables comparison of stability characteristics for different excitation frequencies Ω as well.

Another essential advantage of studying the stability effects in terms of the LCEs is that

both stabilizing and destabilizing effects are automatically accounted for, in contrast to considering stability boundaries only as it is often done in studies on parametric excitation. Having the LCEs, the stability boundaries can be easily obtained by setting $\Lambda = 0$.

2.4 Parametric resonance effects

In the following, the various stability effects of parametric excitation are discussed in terms of LCEs, differentiating between the more common and well-studied case of synchronous excitation and the case of asynchronous excitation needing deeper investigations.

2.4.1 Synchronous excitation

The different effects of synchronous parametric excitation are demonstrated by means of the following two-degrees-of-freedom $\mathbf{MDK} + \mathbf{C}(t)$ system

$$\begin{pmatrix} 1 & 0 \\ 0 & 1 \end{pmatrix} \begin{pmatrix} \ddot{q}_1 \\ \ddot{q}_2 \end{pmatrix} + \begin{pmatrix} \delta_{11} & 0 \\ 0 & \delta_{22} \end{pmatrix} \begin{pmatrix} \dot{q}_1 \\ \dot{q}_2 \end{pmatrix} + \left[\begin{pmatrix} \omega_1^2 & 0 \\ 0 & \omega_2^2 \end{pmatrix} + \varepsilon_\kappa \begin{pmatrix} \cos(\Omega t) & \cos(\Omega t) \\ \pm\cos(\Omega t) & \cos(\Omega t) \end{pmatrix} \right] \begin{pmatrix} q_1 \\ q_2 \end{pmatrix} = \mathbf{0} \tag{2.18}$$

with non-uniform damping, $\delta_{11} \neq \delta_{22}$, and synchronous displacement-proportional parametric excitation of amplitude ε_κ (including the cases with symmetric and anti-symmetric off-diagonal excitation terms). Even though, the excitation with anti-symmetric off-diagonal terms (lower sign in Eq. (2.18)) is as a special case of asynchronous excitation with the phase shift of π, it is considered together with the symmetric, i.e., synchronous, case for having very similar stability impact [17].

The stability effects of synchronous parametric excitation are limited to narrow frequency areas originating at specific resonance frequencies given by

$$\Omega = \frac{|\omega_k \mp \omega_l|}{p}, \quad k, l = 1, 2, ... \tag{2.19}$$

with ω_k and ω_l denoting the k-th and the l-th circular eigenfrequencies (i.e., natural frequencies) of the underlying autonomous system [4]. The denominator $p \in \mathbb{N}$ represents the order of the resonance; the higher orders, $p > 1$, are usually much less significant. The resonances of the first kind, also called fundamental or principal resonances, involve only one eigenfrequency, that is $k{=}l$. The excitation terms on the main diagonal are primarily responsible for the fundamental resonances. The resonances of the second kind – combina-

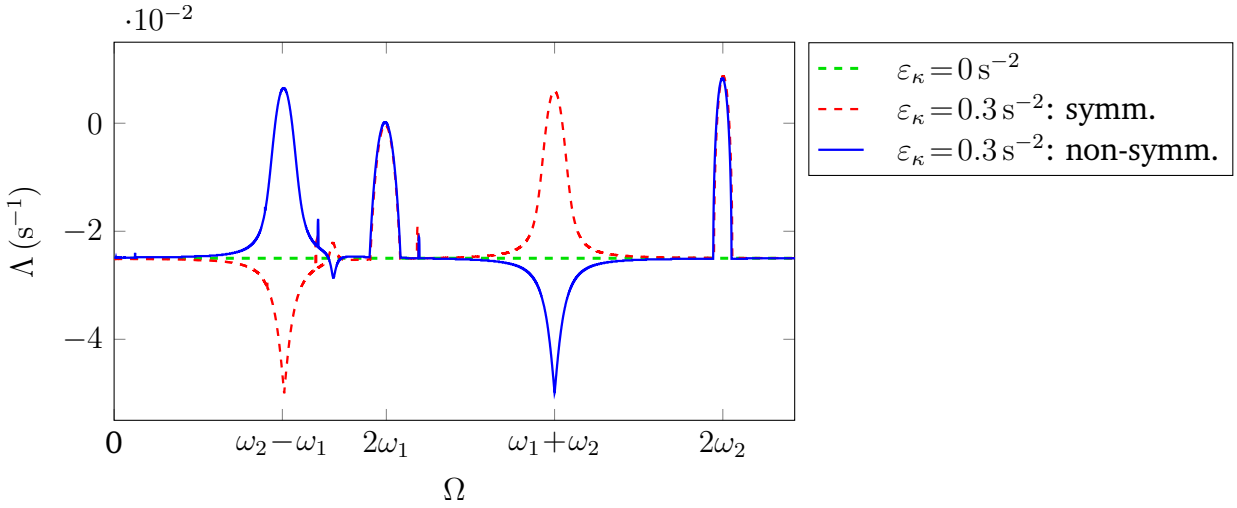

Figure 2.1: Stability effects of displacement-proportional synchronous parametric excitation in system (2.18): the largest LCE Λ for varying excitation frequency Ω with $\omega_1 = 1\,\mathrm{s}^{-1}$, $\omega_2 = \sqrt{5}\,\mathrm{s}^{-1}$, $\delta_{11} = 0.15\,\mathrm{s}^{-1}$, $\delta_{22} = 0.05\,\mathrm{s}^{-1}$

tion resonances – involve two different eigenfrequencies with $k \neq l$, so that they only appear in systems with at least two degrees of freedom. The excitation terms on the antidiagonal are primarily responsible for the combination resonances.

In systems with positive definite stiffness matrix, $\mathbf{K} > \mathbf{0}$, as assumed throughout this thesis, the fundamental resonances always have a destabilizing effect on the trivial solution, while parametric excitation with a frequency close to a combination resonance may have either a destabilizing or, in special cases, also a stabilizing effect called anti-resonance. The destabilizing effects have been known for a long time (since mid-19th century for fundamental and since 1940 for combination resonances), whereas the phenomenon of anti-resonance remained concealed for many years and was discovered relatively recently in 1978 by Tondl [72]. As shown later by Dohnal [15], the phenomenon of anti-resonance is based on the energy flow from a less strongly damped mode of vibration to a more strongly damped mode initiated by the parametric coupling. Therefore, the presence of non-uniform damping is necessary for the appearance of anti-resonance.

The stability impact of parametric excitation in system (2.18) is now studied in terms of the largest LCE Λ obtained through numerical Floquet analysis. Figure 2.1 shows the results of the numerical stability analysis comparing the stability of the trivial solution for the unperturbed case ($\varepsilon_\kappa = 0$) and for the case with parametric excitation ($\varepsilon_\kappa = 0.3$). All of the standard effects are clearly demonstrated: the dominant resonance areas of the first order including the fundamental resonances at $\Omega = 2\omega_i$, $i = 1, 2$, as well as the combination

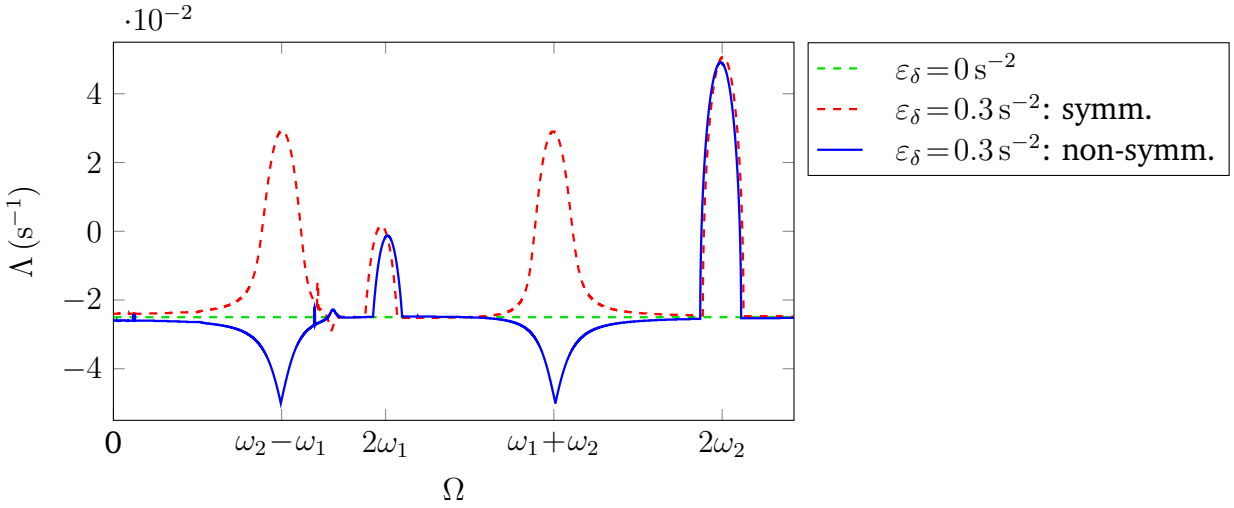

Figure 2.2: Stability effects of velocity-proportional synchronous parametric excitation in system (2.20): the largest LCE Λ for varying excitation frequency Ω with $\omega_1 = 1\,\mathrm{s}^{-1}$, $\omega_2 = \sqrt{5}\,\mathrm{s}^{-1}$, $\delta_{11} = 0.15\,\mathrm{s}^{-1}$, $\delta_{22} = 0.05\,\mathrm{s}^{-1}$

resonance and anti-resonance at combination resonance frequencies $\Omega = |\omega_1 \pm \omega_2|$. In the given case with synchronous excitation the areas of combination resonance and anti-resonance are separated – there is either one of them at each combination resonance frequency. The decision upon which one is at the sum and which one is at the difference frequency depends on the structure of the excitation matrix: There is resonance (anti-resonance) at the sum frequency and anti-resonance (resonance) at the difference frequency for symmetric (anti-symmetric) off-diagonal excitation terms, see e.g. [17].

For the case of velocity-proportional excitation, the main difference to the displacement-proportional case consists in the combination resonances behaving in the same way at the sum and at the difference combination resonance areas: There is either resonance or anti-resonance at both resonance areas [18]. The stability behavior is demonstrated for the following $\mathbf{MDK} + \mathbf{B}(t)$ system

$$\begin{pmatrix} 1 & 0 \\ 0 & 1 \end{pmatrix} \begin{pmatrix} \ddot{q}_1 \\ \ddot{q}_2 \end{pmatrix} + \left[\begin{pmatrix} \delta_{11} & 0 \\ 0 & \delta_{22} \end{pmatrix} + \varepsilon_\delta \begin{pmatrix} \cos(\Omega t) & \cos(\Omega t) \\ \pm\cos(\Omega t) & \cos(\Omega t) \end{pmatrix} \right] \begin{pmatrix} \dot{q}_1 \\ \dot{q}_2 \end{pmatrix} + \begin{pmatrix} \omega_1^2 & 0 \\ 0 & \omega_2^2 \end{pmatrix} \begin{pmatrix} q_1 \\ q_2 \end{pmatrix} = \mathbf{0} \tag{2.20}$$

with non-uniform damping, $\delta_{11} \neq \delta_{22}$, and synchronous velocity-proportional parametric excitation of amplitude ε_δ (including the cases of symmetric and anti-symmetric off-diagonal excitation terms). Figure 2.2 shows the stability impact in terms of the largest LCE compared to the unperturbed case.

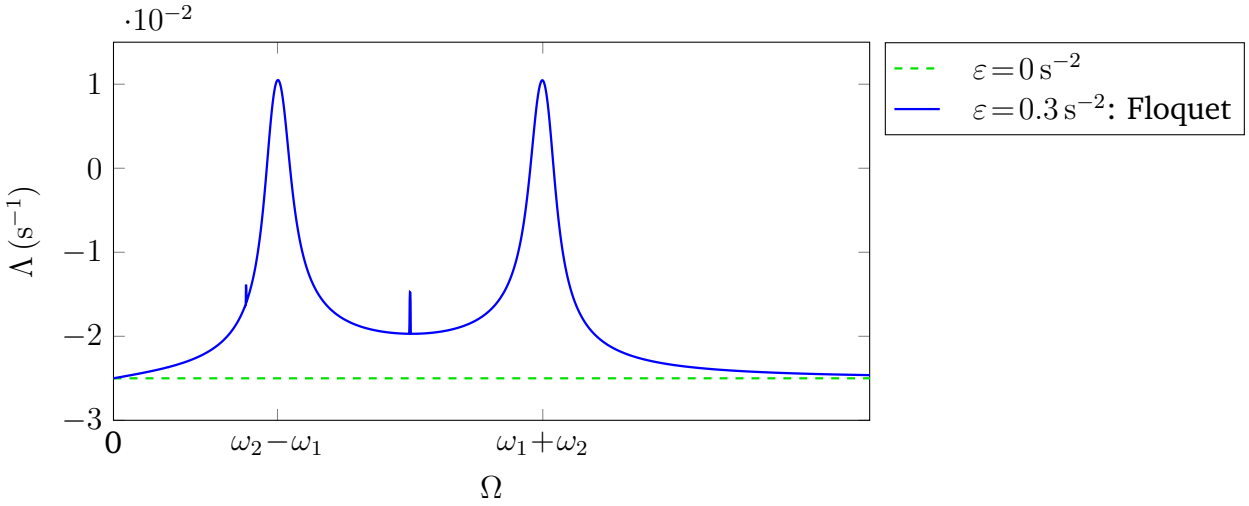

Figure 2.3: "Total instability" due to parametric excitation in system (2.21): the largest LCE Λ for varying excitation frequency Ω with $\omega_1 = 1\,\mathrm{s}^{-1}$, $\omega_2 = \sqrt{5}\,\mathrm{s}^{-1}$, $\delta = 0.05\,\mathrm{s}^{-1}, \zeta = \pi/2$

2.4.2 Asynchronous excitation

In contrast to synchronous excitation, the stability impact of asynchronous excitation is not limited to a certain frequency range, instead, it affects the trivial solution for all excitation frequencies. This global stability impact, also called *total instability* [9], can be demonstrated with the following simple uniformly damped system with out-of-phase parametric excitation

$$\begin{pmatrix} 1 & 0 \\ 0 & 1 \end{pmatrix} \begin{pmatrix} \ddot{q}_1 \\ \ddot{q}_2 \end{pmatrix} + \begin{pmatrix} \delta & 0 \\ 0 & \delta \end{pmatrix} \begin{pmatrix} \dot{q}_1 \\ \dot{q}_2 \end{pmatrix} + \left[\begin{pmatrix} \omega_1^2 & 0 \\ 0 & \omega_2^2 \end{pmatrix} + \varepsilon \begin{pmatrix} 0 & \cos(\Omega t) \\ \cos(\Omega t + \zeta) & 0 \end{pmatrix} \right] \begin{pmatrix} q_1 \\ q_2 \end{pmatrix} = \mathbf{0}. \tag{2.21}$$

The numerical stability analysis of this system, Fig. 2.3, shows that, indeed, the trivial solution is made less stable through the presence of parametric excitation over the whole range of Ω. Moreover, the sum and difference combination resonances appear simultaneously.

Two features are essential for the appearance of total instability: uniform damping and a phase shift in the off-diagonal terms. The global behavior of a more general case with non-uniform damping has not yet been studied systematically, but covering only specific aspects. In 1976 Schmieg studied a similar non-uniformly damped system in terms of characteristic exponents focusing on "local" destabilizing behavior around combination resonance areas only [68]. In 1980s Eicher studied also a general $\mathbf{MDK} + \mathbf{C}(t)$ system with asynchronous excitation and non-uniform damping focusing, however, again only on the

destabilizing aspects by deriving the stability boundaries [27]. On the other hand, in recent decades Dohnal extensively studied anti-resonance showing that the stabilizing effect is as well possible for the case of asynchronous excitation [17, 15].

In this way, there is a large gap in the studies on asynchronous excitation. In particular, the gap consists in the missing knowledge on the transition between the two synchronous cases, with symmetric and the anti-symmetric off-diagonal excitation terms, presented in the section 2.4.1: It has not been shown yet how the combination resonance and the anti-resonance swap their locations and what is the connection to the global effect.

2.5 The method of normal forms

The stability problem of a time-periodic system cannot be approached fully analytically. For a specific problem with given parameter values, a numerical solution can be easily obtained applying the Floquet theory. However, in order to obtain a better insight into the appearance of different resonance areas and to understand the influence of individual parameters, an analytical approximation method has to be applied. Several analytical approximation methods have been successfully applied for the analysis of time-periodic systems: the averaging methods [29, 68, 15], the method of multiple scales [22] and the method of normal forms [34]. The method of multiple scales and the method of normal forms provide equivalent results and differ only in the transformation procedure [56]. Also the averaging methods provide results equivalent to the method of normal forms, at least in the first order approximation [68, 42]. The method of normal forms will be applied throughout this thesis.

The application of the method of normal forms involves a rather lengthy transformation process with the following basic steps. In the first preparing step the time-periodicity in the considered linear non-autonomous systems is eliminated through a “state-space expansion” which introduces nonlinear (quadratic) terms. Now, the normal form transformation is applied to the nonlinear system aiming at eliminating as many of the nonlinear terms as possible. The few remaining nonlinear terms are called *resonant*. Apart from these, the process of elimination introduces higher order nonlinear terms. Neglecting these higher order terms makes out the approximation. In the next step, the time-dependency is reintroduced in place of the few remaining nonlinear terms obtaining a linear non-autonomous system again. The new transformed time-dependency, however, is now of a much simpler form and can be eliminated by a polar coordinate transformation. In this way, a linear autonomous

system is obtained as an approximation to the original time-periodic system. The general background on the method of normal forms can be found in [55, 56]. Details of the following analysis are based on [34, 33, 13]. The procedure was implemented in the software package MATHEMATICA [49].

The basic steps of the method are presented exemplary for system (2.21) featuring asynchronous excitation leading to total instability. In the first step the system is written as a time-autonomous first order system of the form

$$\dot{u}_1 = u_2, \tag{2.22a}$$

$$\dot{u}_2 = -\omega_1^2 u_1 - \delta_{11} u_7 u_2 - \frac{1}{2}\varepsilon(u_5 + u_6)u_3, \tag{2.22b}$$

$$\dot{u}_3 = u_4, \tag{2.22c}$$

$$\dot{u}_4 = -\omega_2^2 u_3 - \delta_{22} u_7 u_4 - \frac{1}{2}\varepsilon(u_5 e^{j\zeta} + u_6 e^{-j\zeta})u_1, \tag{2.22d}$$

$$\dot{u}_5 = j\Omega u_5, \tag{2.22e}$$

$$\dot{u}_6 = -j\Omega u_6, \tag{2.22f}$$

$$\dot{u}_7 = 0 \tag{2.22g}$$

with $u_1 = q_1$, $u_2 = \dot{q}_1$, $u_3 = q_2$, $u_4 = \dot{q}_2$ and $u_5 = e^{j\Omega t}$, $u_6 = e^{-j\Omega t}$, $u_7 = 1$. The dummy variable u_7 has been introduced in order to move all linear velocity-proportional terms to the set of nonlinear terms. In this way, the subsequent analysis steps, in particular the modal transformation, are considerably simplified, though the assumption of small velocity-proportional terms holds. In matrix notation (2.22) reads

$$\dot{\mathbf{u}} = \mathbf{A}\mathbf{u} + \bar{\mathbf{f}}(\mathbf{u}), \tag{2.23}$$

where $\bar{\mathbf{f}}$ contains nonlinear (quadratic) terms, including those originating from the linear damping. The linear part of (2.22) can be decoupled by a modal transformation $\mathbf{u} = \mathbf{R}\mathbf{x}$ resulting in

$$\dot{\mathbf{x}} = \mathbf{\Lambda}\mathbf{x} + \mathbf{R}^{-1}\bar{\mathbf{f}}(\mathbf{R}\mathbf{x}) \tag{2.24a}$$

$$= \mathbf{\Lambda}\mathbf{x} + \mathbf{f}_2(\mathbf{x}) + \mathbf{f}_3(\mathbf{x}) + \dots \tag{2.24b}$$

$$= \mathbf{f}(\mathbf{x}) \tag{2.24c}$$

with the diagonal matrix

$$\mathbf{\Lambda} = \mathrm{diag}(\lambda_1, \ldots, \lambda_n) = \mathrm{diag}(j\omega_1, -j\omega_1, j\omega_2, -j\omega_2, j\Omega, -j\Omega, 0), \tag{2.25}$$

with ω_1 and ω_2 denoting the circular eigenfrequencies of the undamped autonomous part of system (2.21) and $\mathbf{f}_i(\mathbf{x})$ containing nonlinear terms of i^{th} order.

The basic idea of the normal form transformation is to eliminate as many nonlinear terms of (2.24) as possible by the near-identity transformation

$$\mathbf{x} = \mathbf{g}(\mathbf{y}) = \mathbf{y} + \mathbf{g}_2(\mathbf{y}) + \mathbf{g}_3(\mathbf{y}) + \ldots \tag{2.26}$$

yielding the system in normal form

$$\dot{\mathbf{y}} = \mathbf{h}(\mathbf{y}) = \mathbf{\Lambda}\mathbf{y} + \mathbf{h}_2(\mathbf{y}) + \mathbf{h}_3(\mathbf{y}) + \ldots \ , \tag{2.27}$$

where $\mathbf{g}_i(\mathbf{y})$ and $\mathbf{h}_i(\mathbf{y})$ contain nonlinear terms of i^{th} order. Inserting (2.26) and (2.27) in (2.24c) yields

$$\frac{\partial \mathbf{g}(\mathbf{y})}{\partial \mathbf{y}} \mathbf{h}(\mathbf{y}) = \mathbf{f}(\mathbf{g}(\mathbf{y})). \tag{2.28}$$

This partial differential equation can be solved for the coefficients of $\mathbf{g}_i(\mathbf{y})$ and $\mathbf{h}_i(\mathbf{y})$ under the condition that as many nonlinear terms of $\mathbf{h}(\mathbf{y})$ as possible are eliminated. In doing so, all monomials $y_1^{m_1} y_2^{m_2} \cdots y_n^{m_n}$ (in the present case $n = 7$) can be eliminated except the ones for which the resonance condition

$$\lambda_j = m_1\lambda_1 + m_2\lambda_2 + \ldots + m_n\lambda_n, \ j = 1, \ldots, n \tag{2.29}$$

is fulfilled (resonant terms), where m_j are natural numbers. In the present case, the resonance condition reads

$$\{\pm\omega_1, \pm\omega_2, \pm\Omega, 0\} = m_1\omega_1 - m_2\omega_1 + m_3\omega_2 - m_4\omega_2 + m_5\Omega - m_6\Omega + m_7 0. \tag{2.30}$$

It has to be mentioned that while eliminating second order terms, new third order terms are created. This process of creating new higher order terms continues every next order, so that in practice the transformation will be interrupted at some certain order and the higher order terms will be truncated.

Obviously, the resonant terms depend on the excitation frequency Ω and normal forms have to be derived separately for specific frequency ranges, e.g., for each fundamental and combination resonance area. There is also a possibility to derive a normal form for Ω not equal to any of the fundamental or combination resonances, as presented in [43]. That is, the normal form is then valid for all Ω except for narrow frequency ranges associated with the standard fundamental and combination resonances and can be used to explore the global effects of parametric excitation. The resonant terms are still identified by the resonance condition (2.30), which in this case has to be fulfilled for arbitrary Ω. This kind of normal form will be further referred to as *normal form for non-resonant parametric excitation*.

The normal form for system (2.22) reads

$$\dot{y}_1 = \quad j\omega_1 y_1 - \frac{\delta}{2} y_1 y_7 - j\frac{\delta^2}{8\omega_1} y_1 y_7^2 + j\varepsilon^2 \frac{(\omega_1^2 - \omega_2^2 + \Omega^2)\cos(\zeta) - 2j\omega_2 \sin(\zeta)}{4\omega_1 \left[\Omega^2 - (\omega_1 - \omega_2)^2\right]\left[\Omega^2 - (\omega_1 + \omega_2)^2\right]} y_1 y_5 y_6 + h_{14}(\mathbf{y}), \tag{2.31a}$$

$$\dot{y}_2 = -j\omega_1 y_2 - \frac{\delta}{2} y_2 y_7 + j\frac{\delta^2}{8\omega_1} y_2 y_7^2 - j\varepsilon^2 \frac{(\omega_1^2 - \omega_2^2 + \Omega^2)\cos(\zeta) + 2j\omega_2 \sin(\zeta)}{4\omega_1 \left[\Omega^2 - (\omega_1 - \omega_2)^2\right]\left[\Omega^2 - (\omega_1 + \omega_2)^2\right]} y_2 y_5 y_6 + h_{24}(\mathbf{y}), \tag{2.31b}$$

$$\dot{y}_3 = \quad j\omega_2 y_3 - \frac{\delta}{2} y_3 y_7 - j\frac{\delta^2}{8\omega_1} y_3 y_7^2 - j\varepsilon^2 \frac{(\omega_1^2 - \omega_2^2 - \Omega^2)\cos(\zeta) - 2j\omega_2 \sin(\zeta)}{4\omega_2 \left[\Omega^2 - (\omega_1 - \omega_2)^2\right]\left[\Omega^2 - (\omega_1 + \omega_2)^2\right]} y_3 y_5 y_6 + h_{34}(\mathbf{y}), \tag{2.31c}$$

$$\dot{y}_4 = -j\omega_2 y_4 - \frac{\delta}{2} y_4 y_7 + j\frac{\delta^2}{8\omega_1} y_4 y_7^2 + j\varepsilon^2 \frac{(\omega_1^2 - \omega_2^2 - \Omega^2)\cos(\zeta) + 2j\omega_2 \sin(\zeta)}{4\omega_2 \left[\Omega^2 - (\omega_1 - \omega_2)^2\right]\left[\Omega^2 - (\omega_1 + \omega_2)^2\right]} y_4 y_5 y_6 + h_{44}(\mathbf{y}), \tag{2.31d}$$

$$\dot{y}_5 = \quad j\Omega y_5, \tag{2.31e}$$

$$\dot{y}_6 = -j\Omega y_6, \tag{2.31f}$$

$$\dot{y}_7 = 0. \tag{2.31g}$$

The solutions of the differential equations (2.31e) and (2.31f) can be easily calculated and substituted in (2.31a) to (2.31d). The equations (2.31a)-(2.31f) are pairwise complex conjugate. For the given example, the transformation is carried out up to the third order terms.

In the next step the linear damping and the time-dependency are reintroduced. Applying an additional polar coordinate transformation

$$y_1 = \frac{1}{2} r_1 e^{j\varphi_1},\ y_2 = \frac{1}{2} r_1 e^{-j\varphi_1},\ y_3 = \frac{1}{2} r_2 e^{j\varphi_2},\ y_4 = \frac{1}{2} r_2 e^{-j\varphi_2}, \tag{2.32}$$

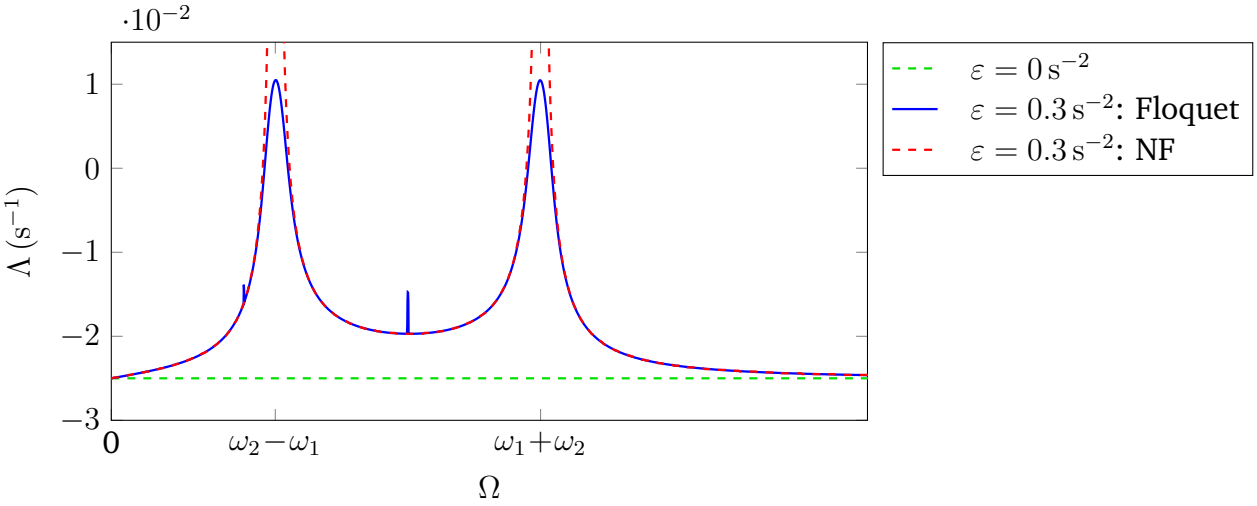

Figure 2.4: Numerical (Floquet) and analytical (NF) results for system (2.21): the largest LCE Λ for varying excitation frequency Ω with $\omega_1 = 1\,\mathrm{s}^{-1}$, $\omega_2 = \sqrt{5}\,\mathrm{s}^{-1}$, $\delta = 0.05\,\mathrm{s}^{-1}, \zeta = \pi/2$

real autonomous representation can be obtained as follows

$$\dot{r}_1 = \left[-\frac{1}{2}\delta + \frac{\varepsilon^2\,\Omega\sin(\zeta)}{2\left[\Omega^2-(\omega_1-\omega_2)^2\right]\left[\Omega^2-(\omega_1+\omega_2)^2\right]}\right] r_1, \tag{2.33}$$

$$\dot{r}_2 = \left[-\frac{1}{2}\delta - \frac{\varepsilon^2\,\Omega\sin(\zeta)}{2\left[\Omega^2-(\omega_1-\omega_2)^2\right]\left[\Omega^2-(\omega_1+\omega_2)^2\right]}\right] r_2, \tag{2.34}$$

$$\dot{\varphi}_1 = \omega_1 - \frac{\delta^2}{8\,\omega_1} + \frac{\varepsilon^2(\Omega^2+\omega_1^2-\omega_2^2)\cos(\zeta_c)}{4\omega_1[\Omega^2-(\omega_1+\omega_2)^2][\Omega^2-(\omega_1-\omega_2)^2]}, \tag{2.35}$$

$$\dot{\varphi}_2 = \omega_2 - \frac{\delta^2}{8\,\omega_2} + \frac{\varepsilon^2(\Omega^2-\omega_1^2+\omega_2^2)\cos(\zeta_c)}{4\omega_2[\Omega^2-(\omega_1+\omega_2)^2][\Omega^2-(\omega_1-\omega_2)^2]}. \tag{2.36}$$

The amplitude and the phase equations are linear and decoupled. The stability of this system, which represents an approximation of the original time-periodic system, can now be easily studied applying the complex eigenvalue analysis to the amplitude equations. The LCEs are then given by the real parts of the eigenvalues.

Figure 2.4 shows a comparison between the numerical Floquet analysis and the results of the normal form analysis (NF) for the case of non-resonant parametric excitation. The advantages and disadvantages of the method are clearly demonstrated. On the one hand, the complex stability behavior for the case of asynchronous excitation is approximated by concise analytical expressions allowing insight into the impact of individual parameters, Eqs. (2.33)-(2.34). On the other hand, the derived normal form is valid only for one specific resonance case: in this example the normal form is valid for all excitation frequencies, except

for the areas around the fundamental and combination resonances. In the same manner, the normal form has to be derived individually for each fundamental or combination resonance case.

3 Global stability effects of asynchronous parametric excitation

Stability investigations of general non-conservative parametrically excited systems with asynchronous excitation are presented. Focusing on the global stability effects outside of the traditional resonance areas, systems with two degrees of freedom are considered featuring displacement- and/or velocity-proportional parametric excitation with variable phase relations. In particular, facing the lack of studies on this subject, special attention is paid to time-periodic systems containing gyroscopic and circulatory terms. Through the application of the semi-analytical method of normal forms, general conditions for the appearance of possible global effects are derived. Apart from the "total instability" – until recently the only known global effect – new stabilizing and destabilizing effects affecting the stability over the whole range of excitation frequencies are discovered. The derived conditions show that such global effects are expected to be rather common in complex mechanical system, especially those, featuring circulatory terms. The qualitative analytical results are also confirmed by numerical stability analysis based on Floquet theory.

3.1 Investigated systems

The primary interest here is the investigation of possible global stability effects of parametric excitation, i.e., stability effects outside of the known fundamental and combination resonance areas. In the studies of the corresponding frequency region conducted by Dohnal with the averaging method accounting for the linear detuning parameter [15, 17], no global stability impact of parametric excitation was identified. However, this contradicts to the previous results on total instability [10, 25] and to numerical observations, Fig. 2.3. Therefore, in order to account for possible global stability effects, a higher order normal form transformation will be used, as outlined in section 2.5.

In the following sections, a thorough analysis of three linear two-degrees-of-freedom systems featuring gyroscopic and circulatory terms as well as different types of parametric excitation is conducted. **System I** is a general $\mathbf{MDGKN}+\mathbf{C}(t)$ system featuring parametric excitation in the displacement-proportional terms with variable phase angles

$$\begin{pmatrix}1 & 0\\ 0 & 1\end{pmatrix}\begin{pmatrix}\ddot{q}_1\\ \ddot{q}_2\end{pmatrix}+\begin{pmatrix}\delta_{11} & \delta_c+\gamma\\ \delta_c-\gamma & \delta_{22}\end{pmatrix}\begin{pmatrix}\dot{q}_1\\ \dot{q}_2\end{pmatrix} + \left[\begin{pmatrix}k_{11} & n\\ -n & k_{22}\end{pmatrix}+\varepsilon_\kappa\begin{pmatrix}\cos(\Omega t) & \cos(\Omega t+\zeta_{12})\\ \cos(\Omega t+\zeta_{21}) & \cos(\Omega t+\zeta_{22})\end{pmatrix}\right]\begin{pmatrix}q_1\\ q_2\end{pmatrix}=\mathbf{0}. \tag{3.1}$$

System II is an $\mathbf{MDGKN}+\mathbf{B}(t)$ system featuring parametric excitation in the velocity-proportional terms with variable phase angles

$$\begin{pmatrix}1 & 0\\ 0 & 1\end{pmatrix}\begin{pmatrix}\ddot{q}_1\\ \ddot{q}_2\end{pmatrix}+\left[\begin{pmatrix}\delta_{11} & \delta_c+\gamma\\ \delta_c-\gamma & \delta_{22}\end{pmatrix}+\varepsilon_\delta\begin{pmatrix}\cos(\Omega t) & \cos(\Omega t+\psi_{12})\\ \cos(\Omega t+\psi_{21}) & \cos(\Omega t+\psi_{22})\end{pmatrix}\right]\begin{pmatrix}\dot{q}_1\\ \dot{q}_2\end{pmatrix} + \begin{pmatrix}k_{11} & n\\ -n & k_{22}\end{pmatrix}\begin{pmatrix}q_1\\ q_2\end{pmatrix}=\mathbf{0}. \tag{3.2}$$

At last, the most general $\mathbf{MDGKN}+\mathbf{B}(t)+\mathbf{C}(t)$ system is introduced. This **system III** combines systems I and II and features both velocity- and displacement-proportional parametric excitation

$$\begin{pmatrix}1 & 0\\ 0 & 1\end{pmatrix}\begin{pmatrix}\ddot{q}_1\\ \ddot{q}_2\end{pmatrix}+\left[\begin{pmatrix}\delta_{11} & \delta_c+\gamma\\ \delta_c-\gamma & \delta_{22}\end{pmatrix}+\varepsilon_\delta\begin{pmatrix}\cos(\Omega t) & \cos(\Omega t+\psi_{12})\\ \cos(\Omega t+\psi_{21}) & \cos(\Omega t+\psi_{22})\end{pmatrix}\right]\begin{pmatrix}\dot{q}_1\\ \dot{q}_2\end{pmatrix} + \left[\begin{pmatrix}k_{11} & n\\ -n & k_{22}\end{pmatrix}+\varepsilon_\kappa\begin{pmatrix}\cos(\Omega t+\zeta_{11}) & \cos(\Omega t+\zeta_{12})\\ \cos(\Omega t+\zeta_{21}) & \cos(\Omega t+\zeta_{22})\end{pmatrix}\right]\begin{pmatrix}q_1\\ q_2\end{pmatrix}=\mathbf{0}. \tag{3.3}$$

All systems I to III described by Eqs. (3.1)-(3.3) will be studied by applying the method of normal forms. An extension of system I with non-uniform amplitude of variation has been treated separately in [41]. The results revealed no qualitative changes in the stability effects, so that in the following only the cases of uniform excitation amplitude are treated for the sake of clarity.

3.2 Displacement-proportional excitation

In the following section the results of the normal form analysis are presented. Based on these results, conditions for the existence of global effects are formulated. Further, the influence of global effects on the stability of the trivial solution is analyzed in detail.

3.2.1 Normal form for non-resonant parametric excitation: system I

The approximate autonomous representation is derived by means of the normal form developed up to the third order, while the higher order terms are neglected. For system I, featuring only displacement-proportional excitation, the results are given by

$$\dot{r}_1 = \left(A_1 - \varepsilon_\kappa^2\, B_\zeta(\Omega)\right) r_1, \tag{3.4a}$$

$$\dot{r}_2 = \left(A_2 + \varepsilon_\kappa^2\, B_\zeta(\Omega)\right) r_2, \tag{3.4b}$$

$$\dot{\varphi}_1 = \omega_1 - C_1\delta_{11}^2 + C_2\delta_{11}\delta_{22} - C_3\delta_{22}^2 - C_4\gamma^2 - C_5\delta_{11}\gamma + C_6\delta_{22}\gamma + C_7\delta_c^2, \tag{3.4c}$$

$$\dot{\varphi}_2 = \omega_2 + D_1\delta_{11}^2 - D_2\delta_{11}\delta_{22} - D_3\delta_{22}^2 + D_4\gamma^2 + D_5\delta_{11}\gamma - C_6\delta_{22}\gamma - C_7\delta_c^2, \tag{3.4d}$$

where polar coordinates

$$y_1 = \frac{1}{2}\omega_1 r_1 e^{j\varphi_1},\ y_2 = \frac{1}{2}\omega_1 r_1 e^{-j\varphi_1},\ y_3 = \frac{1}{2}\omega_2 r_2 e^{j\varphi_2},\ y_4 = \frac{1}{2}\omega_2 r_2 e^{-j\varphi_2} \tag{3.5}$$

have been introduced. The resulting equations are linear in $r_{1,2}$ and $\varphi_{1,2}$. The most important coefficients strongly affecting the stability of the trivial solution read

$$A_1 = -\frac{1}{4}(\delta_{11}+\delta_{22}) - \frac{4\gamma n - (k_{11}-k_{22})(\delta_{11}-\delta_{22})}{4\sqrt{(k_{11}-k_{22})^2 - 4n^2}}, \tag{3.6a}$$

$$A_2 = -\frac{1}{4}(\delta_{11}+\delta_{22}) + \frac{4\gamma n - (k_{11}-k_{22})(\delta_{11}-\delta_{22})}{4\sqrt{(k_{11}-k_{22})^2 - 4n^2}}, \tag{3.6b}$$

$$B_\zeta(\Omega) = \frac{\Omega\left[(k_{22}-k_{11})\sin(\zeta_{12}-\zeta_{21}) - n(\sin\zeta_{12} + \sin\zeta_{21} - \sin(\zeta_{12}-\zeta_{22}) - \sin(\zeta_{21}-\zeta_{22}))\right]}{2\sqrt{(k_{11}-k_{22})^2 - 4n^2}\left[\Omega^2 - (\omega_1-\omega_2)^2\right]\left[\Omega^2 - (\omega_1+\omega_2)^2\right]}, \tag{3.6c}$$

where ζ_{kl}, $k,l = 1,2$, represent the phase angles of parametric excitation, Eq. (3.1). While A_1 and A_2 represent the approximate real parts of the (unperturbed) original system's eigenvalues, the coefficient $B_\zeta(\Omega)$ describes the contribution of parametric excitation and decides upon the presence of global effects and their nature. The linearized approximate analytical expressions of equations (3.4) and (3.6) provide great insight and will be dis-

cussed in detail. The coefficients C_i and D_i, $i = 1 \dots 7$, appearing in the decoupled phase equations (3.4c)-(3.4d) depend on the system parameters k_{11}, k_{22}, n and do not have any effect on the stability.

There are two characteristic features of system (3.4). First, the amplitude equations (3.4a) and (3.4b) are decoupled and do not depend on the phase angle equations (3.4c)-(3.4d). Second, the amplitude equations are also linear and autonomous, so that the stability analysis of the equilibrium is performed by simply considering the coefficients of r_1 and r_2, which directly represent the real eigenvalues of the linear system (3.4a)-(3.4b). Therefore the LCEs are given directly by

$$\lambda_{1,2} = A_{1,2} \pm \varepsilon_\kappa^2 B_\zeta(\Omega). \tag{3.7}$$

It should be noted that in this third order approximation the off-diagonal damping terms δ_c do not contribute to the LCEs. Therefore δ_c is set to zero in the following analysis.

3.2.2 Conditions for the existence of global effects: system I

The global effects of parametric excitation for system I are fully described by Eqs. (3.4a)-(3.4b). For both degrees of freedom, r_1 and r_2, the contribution of parametric excitation is of the same magnitude, however, due to the different signs the consequences are opposite. While the real part of one eigenvalue is decreased by $\varepsilon_\kappa^2 B_\zeta(\Omega)$, the other one is increased by the same amount. The decision about which one is decreased and which one increased depends strongly on parameters k_{11}, k_{22}, n, on the excitation frequency Ω, and, in particular, on the phase relations ζ_{kl} with $k, l = 1, 2$. The relations of ζ_{kl} decide also whether any global effects appear at all. In the next step, general conditions for the appearance of global effects of parametric excitation are derived.

For the appearance of global effects the coefficients of r_1 and r_2 related to parametric excitation should not be equal zero

$$\varepsilon_\kappa^2 B_\zeta(\Omega) \neq 0. \tag{3.8}$$

Considering Eq. (3.6c), the corresponding necessary and sufficient condition is then given

by

$$\frac{\varepsilon_\kappa^2\Omega\left[(k_{22}-k_{11})\sin(\zeta_{12}-\zeta_{21})-n(\sin\zeta_{12}+\sin\zeta_{21}-\sin(\zeta_{12}-\zeta_{22})-\sin(\zeta_{21}-\zeta_{22}))\right]}{2\sqrt{(k_{11}-k_{22})^2-4n^2}\left[\Omega^2-(\omega_1-\omega_2)^2\right]\left[\Omega^2-(\omega_1+\omega_2)^2\right]}\neq 0. \tag{3.9}$$

Apart from the trivial requirements with $\varepsilon_\kappa \neq 0$ and $\Omega \neq 0$, there is a number of further requirements depending on ζ_{kl}. It is also apparent that the velocity-proportional terms do not play any role for the appearance of global effects, at least up to the square terms of ε_κ. As the denominator of (3.9) is not supposed to be equal to zero, this leads to

$$(k_{22}-k_{11})\sin(\zeta_{12}-\zeta_{21})-n(\sin\zeta_{12}+\sin\zeta_{21}-\sin(\zeta_{12}-\zeta_{22})-\sin(\zeta_{21}-\zeta_{22}))\neq 0. \tag{3.10}$$

For a system without circulatory forces, i.e., for $n = 0$, Eq. (3.10) provides the expected condition of $\zeta_{12} - \zeta_{21} \neq \pi z$, $z \in \mathbb{Z}$. For a system containing circulatory forces, apart from $\zeta_{12} - \zeta_{21} \neq \pi z$, there are additional conditions leading to global effects:

$$\zeta_{12} = \zeta_{21} = \pi z \wedge \zeta_{22} \neq \pi z, \tag{3.11a}$$

$$\zeta_{12} = \zeta_{21} \neq \pi z \wedge \zeta_{22} \neq 2\zeta_{12}+\pi(2z+1) \wedge \zeta_{22} \neq 2\pi z, \quad \text{with} \quad z \in \mathbb{Z}. \tag{3.11b}$$

Eqs. (3.11a)-(3.11b) show that in a circulatory system a phase shift on the main diagonal of the excitation matrix is sufficient for the existence of global effects. Since a phase shift on the main diagonal is much more common and easier to obtain than a phase shift in the coupling terms, global effects in such systems are expected to be much more relevant than it has been believed so far.

3.2.3 Stabilizing and destabilizing global effects: system I

In contrast to the previously known exclusively destabilizing global effect of total instability, which was observed for simple $\mathbf{MDK} + \mathbf{C}(t)$ systems with uniform damping matrix, the derived autonomous representation (3.4) reveals the existence of global stabilizing effects as well. Thereby, total instability becomes just a special case of a more general phenomenon.

For a more vivid demonstration of the global effects, a simple system featuring all of the relevant characteristics is analyzed. Such a system is given by the following $\mathbf{MDK} + \mathbf{C}(t)$

system

$$\ddot{\mathbf{q}}(t) + \begin{pmatrix} \delta_{11} & \delta_c \\ \delta_c & \delta_{22} \end{pmatrix} \dot{\mathbf{q}}(t) + \left[\begin{pmatrix} \omega_1^2 & 0 \\ 0 & \omega_2^2 \end{pmatrix} + \varepsilon_\kappa \begin{pmatrix} \cos(\Omega t) & \cos(\Omega t + \zeta_{12}) \\ \cos(\Omega t + \zeta_{21}) & \cos(\Omega t + \zeta_{22}) \end{pmatrix} \right] \mathbf{q}(t) = \mathbf{0}. \tag{3.12}$$

The corresponding autonomous representation is obtained by setting $\gamma = 0\,\mathrm{s}^{-1}$ and $n = 0\,\mathrm{s}^{-2}$ in Eqs. (3.6a)-(3.6c). Further, as for $n = 0\,\mathrm{s}^{-2}$ only the anti-diagonal excitation terms are involved in the global effects, the phase angles ζ_{12} and ζ_{21} are replaced by $\zeta_c = \zeta_{21} - \zeta_{12}$ resulting in

$$\dot{r}_1 = \left[-\frac{1}{2}\delta_{11} + \frac{\varepsilon_\kappa^2\, \Omega \sin\zeta_c}{2\left[\Omega^2 - (\omega_1 - \omega_2)^2\right]\left[\Omega^2 - (\omega_1 + \omega_2)^2\right]} \right] r_1, \tag{3.13a}$$

$$\dot{r}_2 = \left[-\frac{1}{2}\delta_{22} - \frac{\varepsilon_\kappa^2\, \Omega \sin\zeta_c}{2\left[\Omega^2 - (\omega_1 - \omega_2)^2\right]\left[\Omega^2 - (\omega_1 + \omega_2)^2\right]} \right] r_2. \tag{3.13b}$$

Eqs. (3.13a)-(3.13b) clearly show that the contribution of parametric excitation depends particularly on ζ_c and Ω. Both parameters affect not only the magnitude, but also the sign of the contribution. While the behavior of $\sin\zeta_c$ is trivial, the dependence on Ω is given as follows:

$$\begin{cases} \left[\Omega^2 - (\omega_1 - \omega_2)^2\right]\left[\Omega^2 - (\omega_1 + \omega_2)^2\right] > 0 & \text{for} \quad \Omega < |\omega_1 - \omega_2| \wedge \Omega > \omega_1 + \omega_2, \\ \left[\Omega^2 - (\omega_1 - \omega_2)^2\right]\left[\Omega^2 - (\omega_1 + \omega_2)^2\right] < 0 & \text{for} \quad |\omega_1 - \omega_2| < \Omega < \omega_1 + \omega_2. \end{cases} \tag{3.14}$$

The above inequality shows that the global effects are qualitatively different for different ranges of the excitation frequency Ω: The contribution of parametric excitation in Eqs. (3.13a)-(3.13b) changes its sign near the combination resonance frequencies leading to alternating stabilizing and destabilizing impact. Next, two different scenarios are considered. The first scenario is rather a special case with uniform damping ($\delta_{11} = \delta_{22}$) leading to a purely destabilizing global effect known as the total instability. Second, a general case with non-uniform damping, i.e., with $\delta_{11} \neq \delta_{22}$, resulting in wide stabilizing and destabilizing areas depending on Ω is treated.

Uniform damping – total instability: system I

The effect of total instability is demonstrated by the use of the autonomous approximation obtained via the normal form transformation. Assuming a uniform damping with $\delta_{11} =$

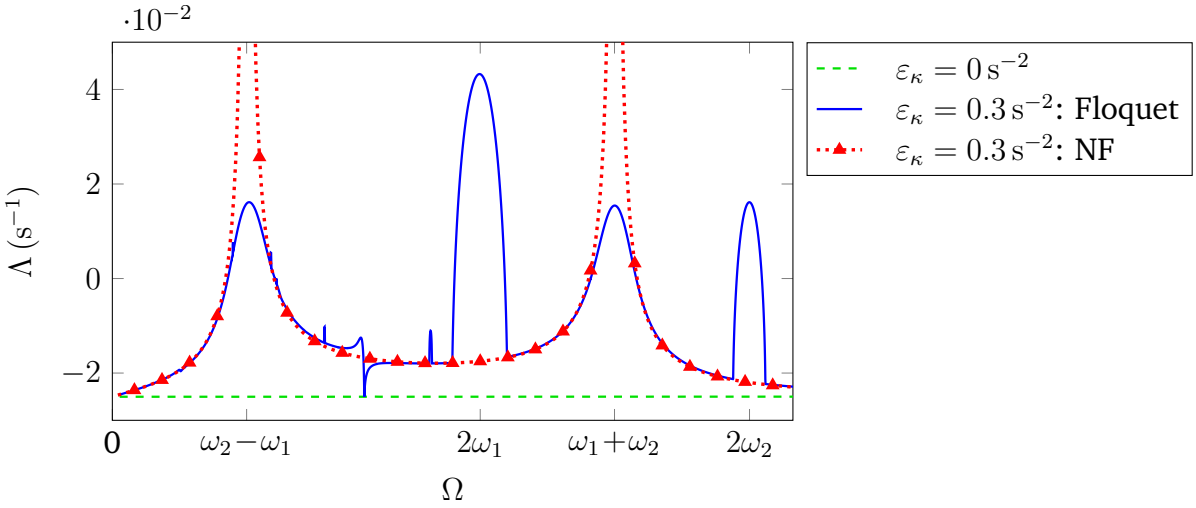

Figure 3.1: Purely destabilizing global effect (total instability) of displacement-proportional parametric excitation in system (3.12) with $\omega_1 = 1\,\mathrm{s}^{-1}$, $\omega_2 = \sqrt{3}\,\mathrm{s}^{-1}$, $\delta_{11} = \delta_{22} = \delta_u = 0.05\,\mathrm{s}^{-1}$, $\delta_c = 0\,\mathrm{s}^{-1}$, $\zeta_{12} = 0$, $\zeta_{21} = \zeta_c = \pi/2$, $\zeta_{22} = 0$

$\delta_{22} = \delta_u$ and a constant phase angle $\zeta_c = \frac{\pi}{2}$, system (3.13) is simplified to

$$\dot{r}_{1,2} = \left[-\frac{1}{2}\delta_u \pm \frac{\varepsilon_\kappa^2\,\Omega}{2\left[\Omega^2 - (\omega_1-\omega_2)^2\right]\left[\Omega^2 - (\omega_1+\omega_2)^2\right]} \right] r_{1,2}. \tag{3.15}$$

The stability of the trivial solution is defined by the largest LCE, represented here simply by the coefficients of $r_{1,2}$ in Eq. (3.15). As the constant damping term δ_u is the same for both r_1 and r_2 and the contribution of parametric excitation changes its sign depending on the region of Ω, the largest LCE is switching between the first and the second one, so that the parametric excitation will lead to an increase of the largest LCE, and thus to a destabilization, for all values of the excitation frequency Ω. In particular, for $\delta_u = 0\,\mathrm{s}^{-1}$ the trivial solution becomes unstable for all Ω.

The stability behavior in terms of the largest LCE is depicted in Fig. 3.1 clearly showing that compared to the unperturbed case with $\varepsilon_\kappa = 0\,\mathrm{s}^{-2}$, the parametric excitation with $\varepsilon_\kappa = 0.3\,\mathrm{s}^{-2}$ leads to a less stable trivial solution for all Ω. The results of the normal form transformation (NF) are further compared to numerical results (Floquet) revealing a high level of agreement over wide areas of Ω, except for the areas around fundamental and combination resonances, which is also the expected behavior for the normal form derived for non-resonant parametric excitation.

Figure 3.2 shows the critical values of ε_κ, above which the trivial solution becomes unstable, i.e., $\Lambda = 0\,\mathrm{s}^{-1}$. This is the classical stability map representation used in the analysis

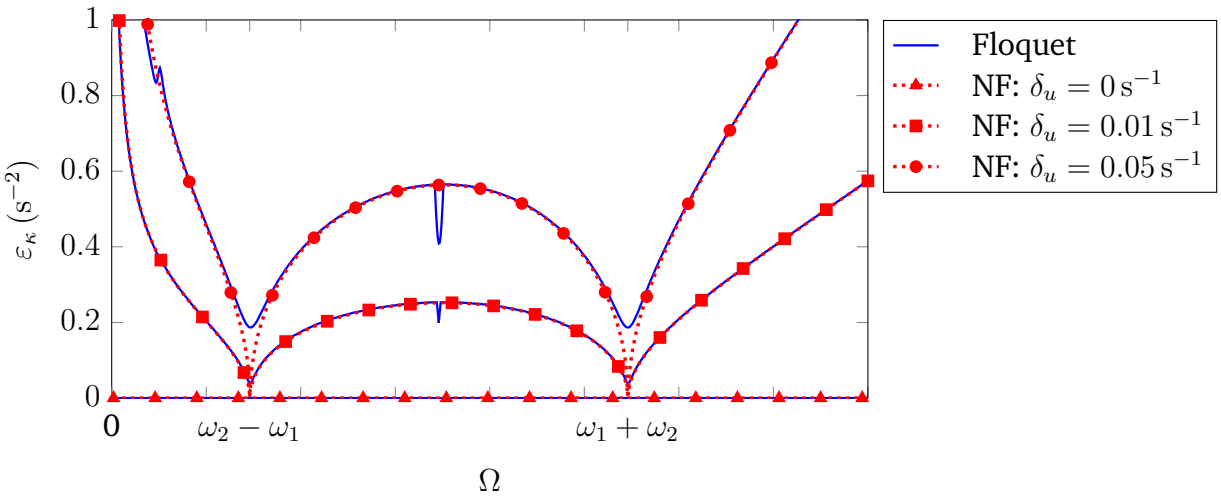

Figure 3.2: Critical ε-values for the instability of the trivial solution; solid: numerical integration (Floquet) of system (3.12), dotted: normal form (NF) in the non-resonant case, Eq. (3.13). Parameter values: $\omega_1 = 1\,s^{-1}$, $\omega_2 = \sqrt{3}\,s^{-1}$, $\zeta_{12} = 0$, $\zeta_{21} = \zeta_c = \pi/2$, $\zeta_{22} = 0$

of parametrically excited system. Obviously, this representation providing only binary data on the stability, i.e., either “stable” or “unstable”, is not optimal for understanding the global effects. It only reveals the impact of the variation amplitude ε_κ on the stability boundaries, while the actual impact of parametric excitation on the stability of the trivial solution compared to the unperturbed case is missing. Nevertheless, it highlights the impact of increasing the amplitude of variation ε and demonstrates that linear damping δ_u can quickly mask total instability making the trivial solution stable. Again, these normal form results are valid for non-resonant Ω only; in particular, Eq. (3.15) is not valid in the vicinity of the combination resonances. Nevertheless, Fig. 3.2 shows that the results of the non-resonant normal form match very well with the numerical results over wide regions of the exictation frequency Ω.

Non-uniform damping – the general case: system I

In case of a non-uniform damping, the global effects of parametric excitation vary depending on the range of Ω: the effect will be qualitatively different for Ω between the combination resonances ($|\omega_1 - \omega_2| < \Omega < \omega_1 + \omega_2$) and below the difference or above the sum combination resonances ($\Omega < |\omega_1 - \omega_2|$ and $\Omega > \omega_1 + \omega_2$). The stability behavior is described by Eqs. (3.13a)-(3.13b).

Due to the second power of the small parameter ε_κ in (3.13), the stability determining

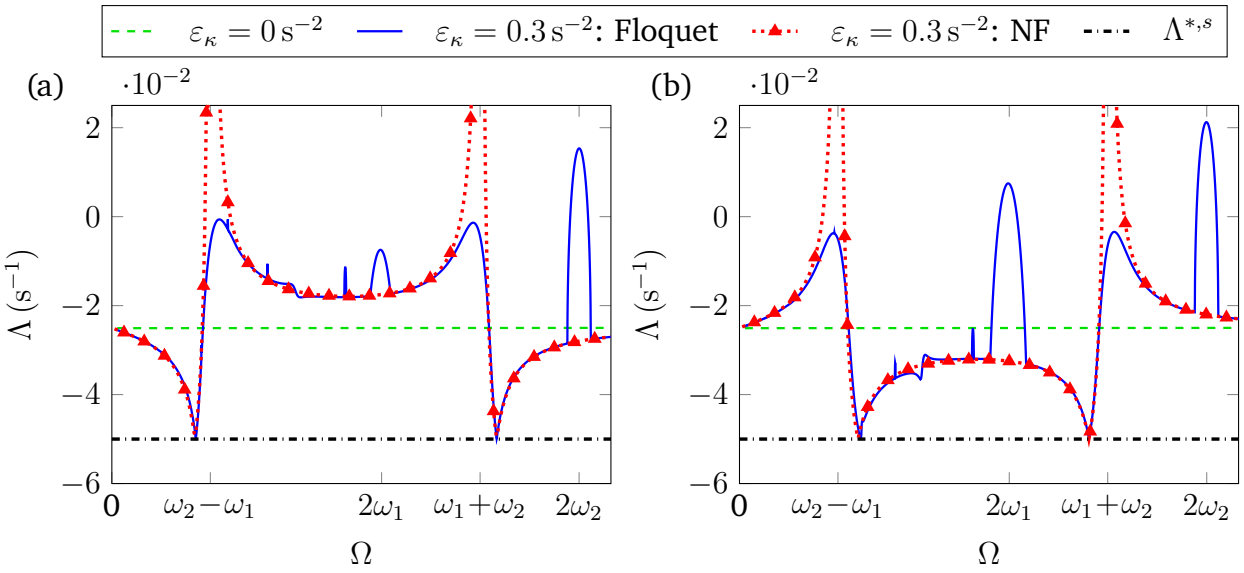

Figure 3.3: Global stability effects of displacement-proportional parametric excitation in system (3.12) with $\omega_1 = 1\,\mathrm{s}^{-1}$, $\omega_2 = \sqrt{3}\,\mathrm{s}^{-1}$, $\delta_{11} = 0.15\,\mathrm{s}^{-1}$, $\delta_{22} = 0.05\,\mathrm{s}^{-1}$, $\delta_c = 0\,\mathrm{s}^{-1}$, $\zeta_{12} = 0$, $\zeta_{22} = 0$; $\Lambda^{*,s} = -0.05\,\mathrm{s}^{-1}$ acc. to Eq. (3.16). Part (a): $\zeta_{21} = \zeta_c = \pi/2$. Part (b): $\zeta_{21} = \zeta_c = -\pi/2$

eigenvalue will remain the one corresponding to the degree of freedom with lower damping, except for the narrow areas in the vicinity of both combination resonances due to the poles at $\Omega = |\omega_1 - \omega_2|$ and $\Omega = \omega_1 + \omega_2$. However, at the same time the sign of the parametric excitation contribution is still changing according to inequality (3.14). In this way, while having a destabilizing global effect between the combination resonances, outside of this range the trivial solution is stabilized (case I), and vice versa (case II). Which one of the two cases occurs depends, on the one hand, on the damping parameters δ_{11} and δ_{22}, on the other hand, on the phase relations in the parametric excitation, here specifically on ζ_c. The corresponding stability behavior in terms of the largest LCE for $\delta_{11} > \delta_{22}$ is presented in Fig. 3.3, while the cases are switched by varying the phase angle $\zeta_c = \pm\pi/2$. The results obtained from the approximate autonomous representation derived through the normal form transformation (NF) are again compared to the numerical results (Floquet) showing high agreement over wide regions of Ω, except for the excitation frequencies around the fundamental and combination resonances.

As can bee seen from Eqs. (3.13a)-(3.13b), the magnitude of the stabilizing and destabilizing global effects depends exclusively on the parameters of parametric excitation: its amplitude ε_κ, excitation frequency Ω as well as the phase relation ζ_c. Due to the poles, the strongest stabilization and destabilization areas are both located directly at the combination

resonance frequencies. Further, the position $\Omega^{*,s}$ and the magnitude $\Lambda^{*,s}$ of the highest stabilization can be determined analytically by equating the LCEs λ_1 and λ_2, i.e., coefficients of r_1 and r_2, since, as shown by Fig. 3.3, the lowest maximum of the two LCEs is located at their intersection. While the analytical expression for $\Omega^{*,s}$ is rather complex, the magnitude of the highest stabilization $\Lambda^{*,s}$ depends only on the linear damping parameters

$$\Lambda^{*,s} = -\frac{1}{4}(\delta_{11} + \delta_{22}). \tag{3.16}$$

Surprisingly, this corresponds exactly to the maximum damping in case of anti-resonance as derived by Dohnal [14], which indicates a certain correlation between the two effects. However, the considered frequency region is too close to combination resonance frequencies, so that more detailed analysis will be performed in section 4.1 with appropriate normal forms instead of the normal form derived for the non-resonant parametric excitation. Nevertheless, as can be seen from Fig. 3.3, the predicted magnitude of $\Lambda^{*,s} = 0.05\,\mathrm{s}^{-1}$ for the chosen parameter values is met precisely by the numerical Floquet analysis.

3.3 Velocity-proportional excitation

The following section presents the results of the normal form analysis for system II described by Eq. (3.2). As in the previous section, the conditions for the existence of global effects are formulated, followed by the investigation of the influence of global effects on the trivial solution.

3.3.1 Normal form for non-resonant parametric excitation: system II

For the system with velocity-proportional excitation, the autonomous approximation is very similar to the previously considered system of displacement-proportional excitation: The signs of the parametric contributions for r_1 and r_2 in Eqs. (3.4a)-(3.4b) are changed and an additional coefficient is introduced:

$$\dot{r}_1 = \left(A_1 + \varepsilon_\delta^2 \frac{1}{2}(k_{11} + k_{22} - \Omega^2)\, B_\psi(\Omega) \right) r_1, \tag{3.17a}$$

$$\dot{r}_2 = \left(A_2 - \varepsilon_\delta^2 \frac{1}{2}(k_{11} + k_{22} - \Omega^2)\, B_\psi(\Omega) \right) r_2, \tag{3.17b}$$

while $B_\psi(\Omega)$ corresponds to $B_\zeta(\Omega)$ from Eq. (3.6c) with the phase angles ζ_{kl} replaced by ψ_{kl}. The basic features and the influence of phase relations in the excitation terms remain the same. As in the case of displacement-proportional excitation, the off-diagonal damping terms δ_c do not contribute to the LCEs in this third order approximation.

3.3.2 Conditions for the existence of global effects: system II

The conditions for the existence of global effects in a system with velocity-proportional excitation are given by

$$\varepsilon_\delta^2 \left(k_{11} + k_{22} - \Omega^2\right) B_\psi(\Omega) \neq 0. \tag{3.18}$$

In this way they contain all conditions derived for systems with displacement-proportional excitation (Eqs. (3.9)-(3.11b)) supplemented by another simple necessary condition

$$\Omega \neq \sqrt{k_{11} + k_{22}}. \tag{3.19}$$

Independently of any phase relations in the excitation terms, the global effect in a system with velocity-proportional parametric excitation vanishes for the Ω value given by the inequality (3.19). Moreover, the sign of the complete contribution changes depending on the sign of the expression $[k_{11} + k_{22} - \Omega^2]$, with the change occurring at

$$\Omega = \sqrt{k_{11} + k_{22}}. \tag{3.20}$$

3.3.3 Stabilizing and destabilizing global effects: system II

For the demonstration of the global effects a simplified $\mathbf{MDK} + \mathbf{B}(t)$ system is chosen

$$\ddot{\mathbf{q}}(t) + \left[\begin{pmatrix} \delta_{11} & \delta_c \\ \delta_c & \delta_{22} \end{pmatrix} + \varepsilon_\delta \begin{pmatrix} \cos(\Omega t) & \cos(\Omega t + \psi_{12}) \\ \cos(\Omega t + \psi_{21}) & \cos(\Omega t + \psi_{22}) \end{pmatrix} \right] \dot{\mathbf{q}}(t) + \begin{pmatrix} \omega_1^2 & 0 \\ 0 & \omega_2^2 \end{pmatrix} \mathbf{q}(t) = \mathbf{0}. \tag{3.21}$$

The corresponding autonomous representation is obtained by setting $\gamma = 0\,\mathrm{s}^{-1}$ and $n = 0\,\mathrm{s}^{-2}$ in (3.6a)-(3.6c). Further, as for $n = 0\,\mathrm{s}^{-2}$ only the anti-diagonal excitation terms are involved in the global effects, the phase angles ψ_{12} and ψ_{21} are replaced by $\psi_c = \psi_{21} - \psi_{12}$ resulting

in

$$\dot{r}_1 = \left[-\frac{1}{2}\delta_{11} - \frac{\varepsilon_\delta^2(\omega_1^2 + \omega_2^2 - \Omega^2)\,\Omega \sin\psi_c}{4\left[\Omega^2 - (\omega_1 - \omega_2)^2\right]\left[\Omega^2 - (\omega_1 + \omega_2)^2\right]} \right] r_1, \tag{3.22a}$$

$$\dot{r}_2 = \left[-\frac{1}{2}\delta_{22} + \frac{\varepsilon_\delta^2(\omega_1^2 + \omega_2^2 - \Omega^2)\,\Omega \sin\psi_c}{4\left[\Omega^2 - (\omega_1 - \omega_2)^2\right]\left[\Omega^2 - (\omega_1 + \omega_2)^2\right]} \right] r_2. \tag{3.22b}$$

As in the case of displacement-proportional excitation, the contribution of parametric excitation depends particularly on ψ_c and Ω. Again, both parameters affect the magnitude and the sign of the contribution. Additionally to the change of signs at $\Omega = |\omega_1 - \omega_2|$ and $\Omega = \omega_1 + \omega_2$, as described by Eq. (3.14), there is a change at $\Omega = \sqrt{\omega_1^2 + \omega_2^2}$ according to Eq. (3.20).

Uniform damping – total instability: system II

The effect of total instability is also present in case of velocity-proportional parametric excitation with uniform damping. Assuming $\delta_{11} = \delta_{22} = \delta_u$ and a constant phase angle $\psi_c = -\frac{\pi}{2}$, system (3.22) is simplified to

$$\dot{r}_{1,2} = \left[-\frac{1}{2}\delta_u \pm \frac{\varepsilon_\delta^2(\omega_1^2 + \omega_2^2 - \Omega^2)\,\Omega}{4\left[\Omega^2 - (\omega_1 - \omega_2)^2\right]\left[\Omega^2 - (\omega_1 + \omega_2)^2\right]} \right] r_{1,2}. \tag{3.23}$$

The total instability shows a similar pattern to what is known from systems with displacement-proportional excitation, except for one zero root between the sum and difference combination resonances, Fig. 3.4. The stability of the trivial solution is decreased for $\Omega \neq \sqrt{\omega_1^2 + \omega_2^2}$, while in case of $\delta_u = 0\,\mathrm{s}^{-1}$ the trivial solution becomes unstable.

Non-uniform damping – the general case: system II

In case of a non-uniform damping in a system with velocity-proportional parametric excitation, the global effects are again both stabilizing and destabilizing ones depending on the range of the excitation frequency Ω: the change of the behavior occurs at the two poles $\Omega = |\omega_1 \pm \omega_2|$ and at the additional zero root $\Omega = \sqrt{\omega_1^2 + \omega_2^2}$. The sequence of the destabilizing and stabilizing effects depends on the relation of the damping parameters δ_{11}, δ_{22} as well as on the phase angle ψ_c, Eq. (3.22).

Figure 3.5, depicting the stability of the trivial solution in terms of the largest LCE, shows another qualitative difference to the global effects induced by displacement-proportional excitation: The global effects persist longer for higher values of Ω. While the limit still

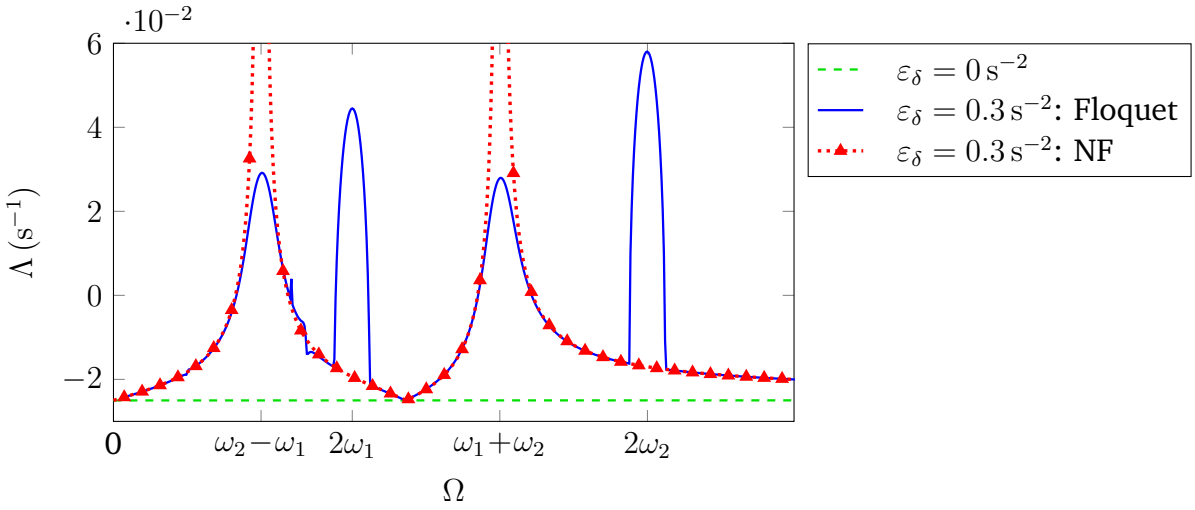

Figure 3.4: Purely destabilizing global effect (total instability) of velocity-proportional parametric excitation in system (3.21) with $\omega_1 = 1\,\mathrm{s}^{-1}$, $\omega_2 = \sqrt{5}\,\mathrm{s}^{-1}$, $\delta_{11} = \delta_{22} = \delta_u = 0.05\,\mathrm{s}^{-1}$, $\delta_c = 0\,\mathrm{s}^{-1}$, $\psi_{12} = 0$, $\psi_{21} = \psi_c = -\pi/2$, $\psi_{22} = 0$

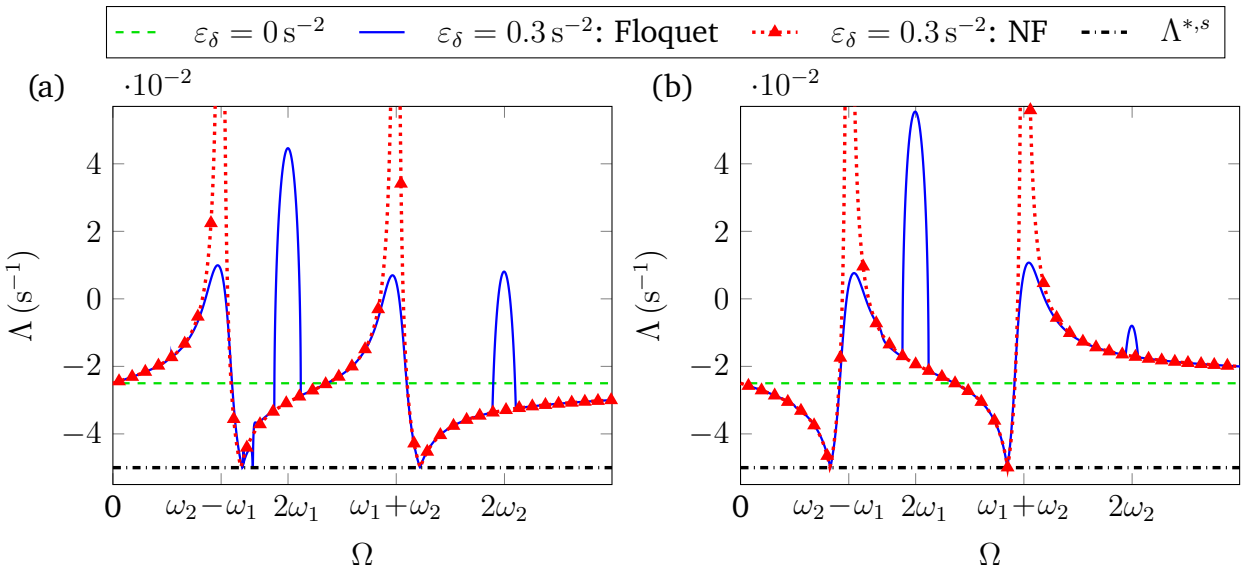

Figure 3.5: Global stability effects of velocity-proportional parametric excitation in system (3.21) with $\omega_1 = 1\,\mathrm{s}^{-1}$, $\omega_2 = \sqrt{5}\,\mathrm{s}^{-1}$, $\delta_{11} = 0.05\,\mathrm{s}^{-1}$, $\delta_{22} = 0.15\,\mathrm{s}^{-1}$, $\delta_c = 0\,\mathrm{s}^{-1}$, $\psi_{12} = 0$, $\psi_{22} = 0$; $\Lambda^{*,s} = -0.05\,\mathrm{s}^{-1}$ acc. to Eq. (3.16). Part (a): $\psi_{21} = \psi_c = -\pi/2$. Part (b): $\psi_{21} = \psi_c = \pi/2$

approaches zero for increasing Ω, the rate is much lower due to the third power of Ω in the numerator of Eq. (3.22). As in the case of system I, the magnitude of the highest stabilization is defined by the linear damping parameters and is given by (3.16). Comparing the semi-analytical and numerical results for $\varepsilon_\delta = 0.3\,\mathrm{s}^{-2}$, high agreement can be detected: The global behavior, including the highest rates of stabilization, are correctly predicted by the results obtained through the normal form transformation, Fig. 3.5. However, it has to be noted that here the variation of damping is several times greater than the constant damping terms. While these specific values were chosen for the clearer demonstration of the effects, the amplitude of variation is usually less than the average parameter value. It also has to be kept in mind that the amplitude of velocity-proportional parametric excitation is usually much smaller than that of displacement-proportional excitation, in the same manner as damping terms are usually not of the same order of magnitude as the stiffness terms. These relations lead to rather weak effects of velocity-proportional parametric excitation in general and, in particular, to weak global effects caused by this kind of excitation. For example, with $\delta_{11} = 0.05\,\mathrm{s}^{-1}$ and $\delta_{22} = 0.15\,\mathrm{s}^{-1}$, the amplitude $\varepsilon_\delta = 0.03\,\mathrm{s}^{-2}$ would be more appropriate, reducing the parametric contribution by factor 100 compared to the example in Fig. 3.5.

3.4 Combined displacement- and velocity-proportional excitation

The following section presents the results of the normal form analysis for system III described by Eq. (3.3). Following the analysis procedure of the preceding sections, the global effects are analyzed with respect to the conditions for their appearance as well as to their impact on the stability of the trivial solution.

3.4.1 Normal form for non-resonant parametric excitation: system III

The structure of the linear autonomous approximation of system III with simultaneous displacement- and velocity-proportional excitation has in general the same structure as that of the previous systems. However, the contributions of each excitation type are not simply

summed up – there is also an additional coupling term proportional to $\varepsilon_\delta \varepsilon_\kappa$:

$$\dot{r}_1 = \left(A_1 - \varepsilon_\kappa^2 B_\zeta(\Omega) + \varepsilon_\delta^2 \frac{1}{2}(k_{11} + k_{22} - \Omega^2) B_\psi(\Omega) - \varepsilon_\delta \varepsilon_\kappa B_{\zeta\psi}(\Omega) \right) r_1, \tag{3.24a}$$

$$\dot{r}_2 = \left(A_2 + \varepsilon_\kappa^2 B_\zeta(\Omega) - \varepsilon_\delta^2 \frac{1}{2}(k_{11} + k_{22} - \Omega^2) B_\psi(\Omega) + \varepsilon_\delta \varepsilon_\kappa B_{\zeta\psi}(\Omega) \right) r_2. \tag{3.24b}$$

The contribution of the constant part of the system, A_1 and A_2, as well as the individual contributions of displacement- and velocity-proportional contributions $B_\zeta(\Omega)$, $B_\psi(\Omega)$ remain the same and are given by Eqs. (3.6a)-(3.6c). The additional coupling term $B_{\zeta\psi}(\Omega)$ is given by

$$B_{\zeta\psi}(\Omega) = \frac{\beta}{4\sqrt{(k_{11} - k_{22})^2 - 4n^2}\,[\Omega^2 - (\omega_1 - \omega_2)^2]\,[\Omega^2 - (\omega_1 + \omega_2)^2]}, \quad \text{with} \tag{3.25a}$$

$$\begin{aligned}
\beta =& [(k_{11} - k_{22})\Omega^2 - (k_{11} - k_{22})^2] \cos(\zeta_{21} - \psi_{12}) \\
& - [(k_{11} - k_{22})\Omega^2 + (k_{11} - k_{22})^2] \cos(\zeta_{12} - \psi_{21}) \\
& + n(k_{11} - k_{22} - \Omega^2) \left[\cos\zeta_{21} - \cos(\zeta_{11} - \psi_{12}) + \cos(\zeta_{22} - \psi_{12}) - \cos(\zeta_{21} - \psi_{22})\right] \\
& - n(k_{11} - k_{22} + \Omega^2) \left[\cos\zeta_{12} - \cos(\zeta_{11} - \psi_{21}) + \cos(\zeta_{22} - \psi_{21}) - \cos(\zeta_{12} + \psi_{22})\right] \\
& + 2n^2 [\cos\zeta_{11} - \cos\zeta_{22} - \cos(\zeta_{11} - \psi_{22}) + \cos(\zeta_{22} - \psi_{22}) \\
& + \cos(\zeta_{12} - \psi_{12}) + \cos(\zeta_{12} - \psi_{21}) + \cos(\zeta_{21} - \psi_{21}) + \cos(\zeta_{21} - \psi_{12})].
\end{aligned} \tag{3.25b}$$

Obviously, the high complexity of $B_{\zeta\psi}(\Omega)$ is due to various possible phase relations between the excitation terms, whereas a great share of this complexity is attributed to the circulatory term n. For the case of $n = 0\,\mathrm{s}^{-2}$, the expression is substantially reduced to just two terms with simple phase relations.

3.4.2 Conditions for the existence of global effects: system III

The conditions derived in sections 3.2.2 and 3.3.2 apply to a system with simultaneous velocity- and displacement-proportional excitation as well. Apart from these, additional conditions arise from the coupling term given by Eqs. (3.25a)-(3.25b). Due to the highly entangled phase relations, no distinct rules for a general system can be derived here. Most probably, the global effects in a circulatory system with this kind of excitation will be present for *any* phase relation, while their amplitude depends on the specific phase relations, apart

from the amplitudes of excitation ε_δ and ε_κ themselves. Some more specific statements can be made for simplified systems, two of which will be presented in the following.

The first simplification consists in setting all phase angles to zero, i.e., $\psi_{kl} = 0$, $\zeta_{kl} = 0$ with $k, l = 1, 2$. In this case, there will be no global effects caused individually by the velocity- or displacement-proportional excitation and the coupled contribution described by Eq. (3.25b) simplifies to

$$\beta = -2(k_{11} - k_{22})^2 + 8n^2. \tag{3.26}$$

This means that with simultaneous synchronous velocity- and displacement-proportional parametric excitation there will *always* be global effects, except for the special case with $n = \frac{|k_{11}-k_{22}|}{2}$.

The second simplification is representative for a large number of systems which have no circulatory forces: $n = 0\,\mathrm{s}^{-2}$. In this case, Eq. (3.25b) simplifies to

$$\beta = (k_{11} - k_{22}) \left[(-k_{11} + k_{22} + \Omega^2) \cos(\zeta_{21} - \psi_{12}) - (k_{11} - k_{22} + \Omega^2) \cos(\zeta_{12} - \psi_{21}) \right]. \tag{3.27}$$

Assuming $\psi_{12} = \psi_{21}$ and $\zeta_{12} = \zeta_{21}$, since otherwise there would already be global effects from individual velocity- and displacement-proportional contributions, the only possibility that there are *no* global effects is when there is a phase shift of $\pi/2$ between the anti-diagonal terms of the velocity- and displacement-proportional excitation, precisely, it applies if $\psi_{kl} - \zeta_{lk} = \frac{\pi}{2}(2z + 1)$ with $k, l = 1, 2$, $k \neq l$ and $z \in \mathbb{Z}$. For $\psi_{kl} - \zeta_{lk} = \pi z$ the global effects are maximal. These results are in agreement with the conditions derived by Eicher [27].

These examples show that, in general, there will be global effects present in case of simultaneous displacement- and velocity-proportional excitation. However, as already outlined in section 3.3.3, the contribution of velocity-proportional parametric excitation is usually much smaller than that of displacement-proportional excitation, so that also the mixed effect described by Eq. 3.24 is expected to be less pronounced. Nevertheless, the analysis considers the most general case for the sake of completeness.

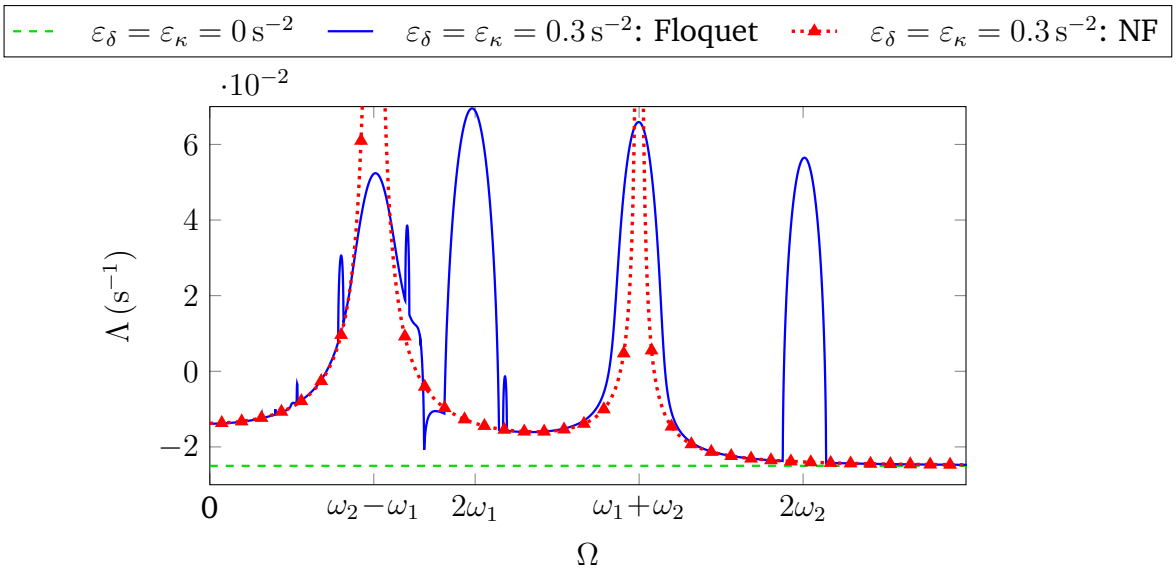

Figure 3.6: Purely destabilizing global effect (total instability) of simultaneous synchronous displacement- and velocity-proportional parametric excitation in system (3.28) with $\omega_1 = 1\,\mathrm{s}^{-1}$, $\omega_2 = \sqrt{5}\,\mathrm{s}^{-1}$, $\delta_{11} = \delta_{22} = \delta_u = 0.05\,\mathrm{s}^{-1}$, $\delta_c = 0\,\mathrm{s}^{-1}$

3.4.3 Stabilizing and destabilizing global effects: system III

For the demonstration of the global effects a simplified synchronous $\mathbf{MDK} + \mathbf{B}(t) + \mathbf{C}(t)$ system is chosen

$$\ddot{\mathbf{q}}(t) + \left[\begin{pmatrix} \delta_{11} & \delta_c \\ \delta_c & \delta_{22} \end{pmatrix} + \varepsilon_\delta \cos(\Omega t) \begin{pmatrix} 1 & 1 \\ 1 & 1 \end{pmatrix}\right] \dot{\mathbf{q}}(t) + \left[\begin{pmatrix} \omega_1^2 & 0 \\ 0 & \omega_2^2 \end{pmatrix} + \varepsilon_\kappa \cos(\Omega t) \begin{pmatrix} 1 & 1 \\ 1 & 1 \end{pmatrix}\right] \mathbf{q}(t) = \mathbf{0}. \tag{3.28}$$

The corresponding autonomous representation is obtained by setting $\gamma = 0\,\mathrm{s}^{-1}$, $n = 0\,\mathrm{s}^{-2}$ and $\psi_{kl} = \zeta_{lk} = 0$ with $k, l = 1, 2$ in Eqs. (3.24)-(3.25) and (3.6a)-(3.6c) resulting in

$$\dot{r}_1 = \left[-\frac{1}{2}\delta_{11} - \frac{\varepsilon_\delta \varepsilon_\kappa (\omega_1^2 - \omega_2^2)}{2\left[\Omega^2 - (\omega_1 - \omega_2)^2\right]\left[\Omega^2 - (\omega_1 + \omega_2)^2\right]}\right] r_1, \tag{3.29a}$$

$$\dot{r}_2 = \left[-\frac{1}{2}\delta_{22} + \frac{\varepsilon_\delta \varepsilon_\kappa (\omega_1^2 - \omega_2^2)}{2\left[\Omega^2 - (\omega_1 - \omega_2)^2\right]\left[\Omega^2 - (\omega_1 + \omega_2)^2\right]}\right] r_2. \tag{3.29b}$$

According to this, the contribution changes its sign at the combination resonance frequencies only. The magnitude of the global effects depends, as in the other cases, on Ω and ε_δ, ε_κ, but here, in addition, also on the gap between the system's eigenfrequencies. Another specific feature of this example is the non-vanishing global effect for Ω approaching zero.

Uniform damping – total instability: system III

The effect of total instability is also present in case of simultaneous synchronous parametric excitation with uniform damping. Assuming $\delta_{11} = \delta_{22} = \delta_u$, system (3.29) is simplified to

$$\dot{r}_{1,2} = \left[-\frac{1}{2}\delta_u \mp \frac{\varepsilon_\delta \varepsilon_\kappa (\omega_1^2 - \omega_2^2)}{2\left[\Omega^2 - (\omega_1 - \omega_2)^2\right]\left[\Omega^2 - (\omega_1 + \omega_2)^2\right]} \right] r_1. \tag{3.30}$$

As shown in Fig. 3.6, the effect of total instability in case of simultaneous velocity- and displacement-proportional excitation is similar to total instability due to displacement-proportional excitation, except that the contribution of parametric excitation does not approach zero for Ω approaching zero

$$\lim_{\Omega \to 0} \frac{\varepsilon_\delta \varepsilon_\kappa (\omega_1^2 - \omega_2^2)}{2\left[\Omega^2 - (\omega_1 - \omega_2)^2\right]\left[\Omega^2 - (\omega_1 + \omega_2)^2\right]} = \frac{\varepsilon_\delta \varepsilon_\kappa}{2(\omega_1^2 - \omega_2^2)}. \tag{3.31}$$

In this way, the global effect is increasing with a smaller gap between the eigenfrequencies for low values of Ω. Further, due to the absence of Ω in the numerator of Eq. (3.30), the global effect quickly approaches zero for $\Omega > \omega_1 + \omega_2$.

Non-uniform damping – the general case: system III

With a non-uniform damping there are alternating stabilizing and destabilizing areas depending on Ω. As in the case of uniform damping, there is a non-vanishing contribution of parametric excitation for Ω approaching zero. The switching of the stabilized and destabilized areas occurs at the combination resonance frequencies and is further controlled by the relation of the damping terms δ_{11} and δ_{22}. Figure 3.7 shows the global behavior of the stability of the trivial solution being in general well represented by the autonomous approximation over wide regions of Ω. While the non-vanishing contribution for low values of Ω is confirmed by the numerical analysis, the quality of the semi-analytical approximation near the sum combination resonance frequency is lower compared to the previous cases. Also the regions of the highest possible stabilization, located closely to the combination resonance frequencies, are captured less accurately. The obtained results, though being of interest from the theoretical point of view, are to be treated with care, since the involved parameters ε_κ and in particular ε_δ are usually small so that the induced effects will probably have no practical significance in standard applications.

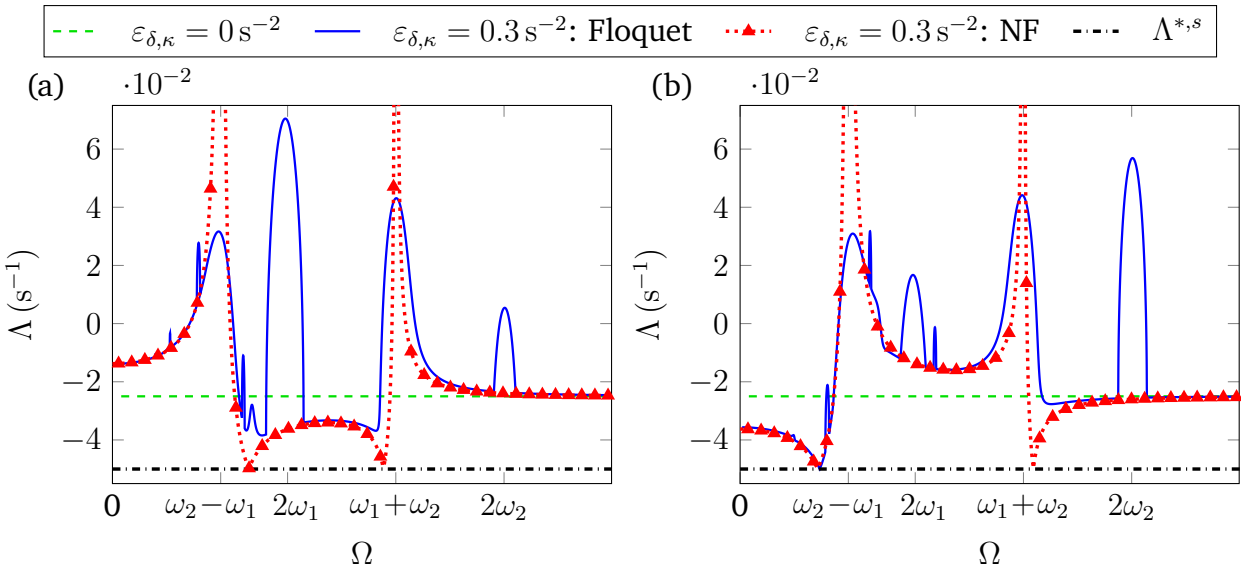

Figure 3.7: Global stability effects of simultaneous synchronous displacement- and velocity-proportional parametric excitation in system (3.28) with $\omega_1 = 1\,\mathrm{s}^{-1}$, $\omega_2 = \sqrt{5}\,\mathrm{s}^{-1}$, $\delta_c = 0\,\mathrm{s}^{-1}$; $\Lambda^{*,s} = -0.05\,\mathrm{s}^{-1}$ acc. to Eq. (3.16). Part (a): $\delta_{11} = 0.05\,\mathrm{s}^{-1}$, $\delta_{22} = 0.15\,\mathrm{s}^{-1}$. Part (b): $\delta_{11} = 0.15\,\mathrm{s}^{-1}$, $\delta_{22} = 0.05\,\mathrm{s}^{-1}$

3.5 Conclusions

In view of the lack of studies on non-conservative dynamical systems under asynchronous parametric excitation, the present contribution thoroughly investigates the stability behavior of general two-degrees-of-freedom systems containing circulatory and gyroscopic terms as well as excitation terms with variable phase relations. The semi-analytical analysis based on the normal form transformation proved to be highly suitable for qualitative analysis of parametric excitation effects. The analysis revealed that the previously known effect of total instability is only a special case of a more general phenomenon of global stability effects, which may destabilize and stabilize the trivial solution over a wide range of excitation frequencies. The chosen approach enabled the derivation of general rules for the appearance of global effects, so that potential global effects can be identified on the basis of phase relations in the excitation matrix only. According to the derived rules, the global effects of parametric excitation are expected to be quite common in complex systems containing circulatory terms.

Further, the “non-resonant” normal forms, although not valid at the combination resonance frequencies, indicate a new kind of stability behavior with pronounced stabilizing (resonance) and destabilizing (anti-resonance) effects occurring at each combination resonance area. This behavior will be studied in detail by deriving the corresponding normal forms in the

following chapter.

4 Coexistence of resonance and anti-resonance

Until recently, resonance and anti-resonance had been mostly studied individually, however, as the previous chapter has shown, there are systems where both effects appear simultaneously at each combination resonance frequency. With a steep transition between them and a high sensitivity of their relative positions, there is a need for a concurrent study of resonance and anti-resonance. In the following, the semi-analytical method of normal forms is used to derive approximate analytical expressions for characteristic points describing the magnitude and the location of the most prominent stability features, e.g., the point of strongest stabilization or destabilization.

The analysis is first performed for a simple $\mathbf{MDK} + \mathbf{C}(t)$ *system with displacement- and/or velocity-proportional parametric excitation. The analyzed system is then further extended to include constant circulatory and gyroscopic terms. The results reveal that the separate appearance of resonance and anti-resonance is, though a common one, but only a special case with synchronous parametric excitation. Furthermore, with clear conditions for the appearance of resonance and anti-resonance as well as concise symbolic expressions for the characteristic points derived by means of the normal form analysis, the stability behavior can now be described qualitatively and quantitatively on the basis of equations of motion alone, even for systems featuring circulatory terms.*

4.1 Displacement-proportional excitation: $\mathrm{MDK} + \mathbf{C}(t)$ system

As seen from the results of the previous section, the highest stabilization as well as the highest destabilization effects of parametric excitation take place near the combination resonances. The normal form for the non-resonant parametric excitation provides a great

overview of the global stability behavior and also indicates the behavior in the vicinity of the combination resonance frequencies, but at the same time it is not valid for $\Omega \approx |\omega_1 \mp \omega_2|$. For this reason, the transition from resonance to anti-resonance and in particular their simultaneous appearance is not captured. At the same time, these effects appear to be even more significant than the global effects themselves. Therefore, in order to obtain more insight into the stability behavior near the combination resonances, a separate normal form valid in the vicinity of combination resonances $\Omega \approx |\omega_1 \mp \omega_2|$ is derived.

The corresponding frequency range has attained considerable attention in the previous studies, though being analyzed either from the destabilization or from the stabilization perspective only. On the one hand, Schmieg [68] studied an asynchronously excited system only from the destabilization perspective deriving explicit symbolic expressions for the LCEs as well as for the magnitude and location of the strongest destabilization. On the other hand, Dohnal [15, 17] extensively studied synchronous and asynchronous excitation from the stabilizing perspective focusing mostly on the stability boundary curves. Additionally, in a study of equivalent damping [15], i.e., LCEs, Dohnal discussed in detail the case of synchronous excitation, while in a short note on asynchronous excitation the possibility of coexisting resonance and anti-resonance was implicitly given but not recognized. Therefore, in the following an asynchronously excited system is discussed in detail in terms of the LCEs focusing on the coexistence.

Even though, the approximate symbolic expressions for the LCEs derived by Schmieg do contain the relevant stability behavior, their complexity does not allow for sufficient insight, so that in the following *characteristic points* are introduced, described by concise and expressive symbolic expressions. The most relevant stability features are be covered by the three characteristic points P^s, P^d, P^0 describing the location and the magnitude of the strongest stabilization $P^s(\Omega^s, \Lambda^s)$, destabilization $P^d(\Omega^d, \Lambda^d)$ and the transition between the two effects $P^0(\Omega^0, \Lambda^0)$, respectively. The largest LCE Λ^0 at the transition point is simply given by the largest LCE of the unperturbed autonomous system, i.e., $\Lambda^0 = \max\{-\frac{1}{2}\delta_{11}, -\frac{1}{2}\delta_{22}\}$ for the simple case of $\mathbf{MDK} + \mathbf{C}(t)$ system. Further less decisive but still important features are given by the maximum value of the stabilization $\Lambda^{*,s}$ (once the amplitude of variation is above the threshold $\varepsilon^{2,*}$) and the threshold value of parametric variation ε^2_{th} leading to instability, i.e., with $\Lambda = 0\,\mathrm{s}^{-1}$.

For this purpose an $\mathbf{MDK} + \mathbf{C}(t)$ system with variable phase relations in the parametric

excitation is considered

$$\begin{pmatrix}\ddot{q}_1\\ \ddot{q}_2\end{pmatrix}+\begin{pmatrix}\delta_{11} & \delta_c\\ \delta_c & \delta_{22}\end{pmatrix}\begin{pmatrix}\dot{q}_1\\ \dot{q}_2\end{pmatrix}+\left[\begin{pmatrix}\omega_1^2 & 0\\ 0 & \omega_2^2\end{pmatrix}+\begin{pmatrix}\varepsilon_{11}\cos(\Omega t) & \varepsilon_{12}\cos(\Omega t+\zeta_{12})\\ \varepsilon_{21}\cos(\Omega t+\zeta_{21}) & \varepsilon_{22}\cos(\Omega t+\zeta_{22})\end{pmatrix}\right]\begin{pmatrix}q_1\\ q_2\end{pmatrix}=\mathbf{0}. \tag{4.1}$$

The corresponding normal form for $\Omega \approx |\omega_1 \mp \omega_2|$ is derived according to the procedure described and in section 2 and is given by

$$\dot{r}_1 = -\frac{\delta_{11}}{2}\, r_1 - \frac{\varepsilon_{12}}{4\,\omega_2}\sin(\varphi)\, r_2, \tag{4.2a}$$

$$\dot{r}_2 = -\frac{\delta_{22}}{2}\, r_2 \,{}_{(\pm)}\, \frac{\varepsilon_{21}}{4\,\omega_1}\sin(\varphi-\zeta_c)\, r_1, \tag{4.2b}$$

$$\dot{\varphi} = \omega_2 \,{}_{(\mp)}\, \omega_1 - \Omega - \frac{\varepsilon_{12}\cos(\varphi)\omega_1\, r_2^2 \,{}_{(\mp)}\, \varepsilon_{21}\cos(\varphi-\zeta_c)\omega_2\, r_1^2}{4\,\omega_1\omega_2\, r_1 r_2}, \tag{4.2c}$$

while the upper (lower) signs apply for difference (sum) combination resonance. This second order normal form (linear in ε_{ij}) shows that only the off-diagonal excitation terms contribute to the combination resonances. A higher order normal form, not presented here due to high complexity, shows that, indeed, the main diagonal terms do as well affect the stability in the combination resonance areas. However, as also confirmed by numerical Floquet analysis, their effect is extremely weak. Further, as only the off-diagonal excitation terms are involved, the phase angles ζ_{12} and ζ_{21} are replaced by $\zeta_{21} = \zeta_c$, $\zeta_{12} = 0$. This normal form provides an autonomous approximation, however, all three equations are nonlinear and coupled. Schmieg [68] derived nearly identical equations using the method of slowly varying phase and amplitude for a similar problem and also developed a transformation procedure in order to obtain the eigenvalues for the amplitude equations, i.e., the LCEs. While the eventual expressions for the LCEs are rather lengthy and complicated, the most important features can be discussed considering the eigenvalue problem for the amplitude equations Eqs. (4.2a)-(4.2b) with $\dot{\varphi} = 0$ and $\varphi = \varphi_0$ without explicitly solving for the LCEs. In this way, the corresponding eigenvalues for difference and sum combination resonance are given by

$$\nu_{1,2} = -\frac{\delta_{11}+\delta_{22}}{4} \mp \frac{1}{4}\sqrt{(\delta_{11}-\delta_{22})^2 \,{}_{(\mp)}\, \frac{\varepsilon_{12}\varepsilon_{21}\sin(\varphi_0)\sin(\varphi_0-\zeta_c)}{\omega_1\omega_2}}. \tag{4.3}$$

The product of the variation coefficients $\varepsilon_{12}\varepsilon_{21}$ will be further denoted as ε^2, keeping in mind that both off-diagonal excitation terms are involved. For $\varepsilon^2 = 0$ the approximated

real parts of the eigenvalues of the original autonomous system with $\nu_i = -\frac{1}{2}\delta_{ii}$, $i = 1, 2$, are obtained. For $\varepsilon^2 > 0$ and $\delta_{11} \neq \delta_{22}$, $\delta_{ii} \neq 0$, stabilizing (anti-resonance) as well as destabilizing (resonance) action of parametric excitation can be observed. Whether the area around $\Omega \approx |\omega_1 \mp \omega_2|$ is stabilized or destabilized, or even both at the same time, depends primarily on the phase angle ζ_c, but also on the relation of the damping terms, i.e., $\delta_{11} \gtrless \delta_{22}$. Eq. (4.3) also shows that the stability effects at sum and difference combination resonance areas are identical except for the phase shift of π with respect to ζ_c. Therefore, in the following two sections only the case of $\Omega \approx |\omega_1 - \omega_2|$ is discussed in detail. Three representative cases will be treated: $\zeta_c = 0$, $\zeta_c = \pi$ and variable ζ_c. Further, as the largest LCE is the one decisive for stability, only the real part of the eigenvalue with the plus sign before the root in Eq. (4.3) will be considered.

4.1.1 Parametric anti-resonance

In the first case with $\zeta_c = 0$ the largest LCE for $\Omega \approx |\omega_1 - \omega_2|$ reads

$$\Lambda = \mathrm{Re}\left(-\frac{\delta_{11} + \delta_{22}}{4} + \frac{1}{4}\sqrt{(\delta_{11} - \delta_{22})^2 - \frac{\varepsilon^2}{\omega_1 \omega_2} \sin^2(\varphi_0)} \right). \tag{4.4}$$

Assuming $\delta_{11} \neq \delta_{22}$ and with $\sin^2(\varphi_0) \geq 0$ for all φ_0, the radicand is reduced for all $\varepsilon^2 > 0$ compared to the unperturbed case with $\varepsilon^2 = 0$. This leads to a lower Λ and thus to an increased stability of the trivial solution compared to the unperturbed autonomous case. Obviously, this effect of anti-resonance disappears in case of uniform damping with $\delta_{11} = \delta_{22} = \delta_u$, as the radicand instantly becomes negative and the root expression becomes imaginary so that parametric excitation does not contribute to a change of the largest LCE. The highest stabilization through anti-resonance is achieved for vanishing or negative radicand in Eq. (4.4) and is equal to the maximum stabilization $\Lambda^{*,s}$ given by

$$\Lambda^{*,s} = -\frac{1}{4}(\delta_{11} + \delta_{22}). \tag{4.5}$$

In order to achieve $\Lambda^{*,s}$ at the point of the strongest stabilization with $\sin^2(\varphi_0) = 1$, the minimum amplitude of variation

$$\varepsilon^{2,*} = (\delta_{11} - \delta_{22})^2 \omega_1 \omega_2 \tag{4.6}$$

is required. These results agree with maximum equivalent damping by parametric excitation derived by Dohnal [15].

The required amplitude $\varepsilon^{2,*}$ grows with the increasing maximum equivalent damping $\Lambda^{*,s}$, which means that higher damping levels require stronger variation of the time-periodic parameter. Given the case that the variation is limited to some magnitude ε^2_{max}, there exists an optimal relation of the damping coefficients δ_{11} and δ_{22}, since on the one hand a more non-uniform damping increases the maximum equivalent damping, on the other hand it increases the radicand in Eq. (4.4). Therefore, the optimal case is given for vanishing radicand:

$$(\delta_{11} - \delta_{22})^2 - \frac{\varepsilon^2_{max} \sin^2(\varphi_0)}{\omega_1 \omega_2} = 0. \tag{4.7}$$

Assuming the damping coefficient relation as $\delta_{22} = \eta \delta_{11}$ with $\eta > 1$, the optimal relation of the damping coefficients for the strongest stabilization with limited amplitude of variation is given by

$$\eta = 1 + \frac{1}{\delta_{11}} \sqrt{\frac{\varepsilon^2_{max} \sin^2(\varphi_0)}{\omega_1 \omega_2}}. \tag{4.8}$$

4.1.2 Parametric resonance

In the second case with $\zeta_c = \pi$ the largest LCE reads

$$\Lambda = \mathrm{Re}\left(-\frac{\delta_{11} + \delta_{22}}{4} + \frac{1}{4} \sqrt{(\delta_{11} - \delta_{22})^2 + \frac{\varepsilon^2}{\omega_1 \omega_2} \sin^2(\varphi_0)} \right). \tag{4.9}$$

Due to the summation of two positive terms, the radicand will remain positive for all ε^2 and φ_0, so that for $\zeta_c = \pi$ the area around the difference combination resonance is always destabilized. Unlike for the anti-resonance, there is no upper limit for the destabilization – an increasing amplitude of excitation ε^2 will always lead to a stronger destabilization. For the same reason, the destabilizing effect persists also for the case of uniform damping, while the stabilizing effect disappears. These two first cases represent the current perception with resonance and anti-resonance appearing separately either at the sum or at the difference combination resonance frequencies.

4.1.3 Simultaneous parametric resonance and anti-resonance

In the general case as described by Eq. (4.3), the sign of the parametric contribution term depends on φ_0, which, as shown in Eq. (4.2c), depends on Ω. In this way, there will be both stabilizing and destabilizing effects in the vicinity of the combination resonance depending on the excitation frequency. Though the analytical expression for φ_0 and therefore for Λ can be obtained in a lengthy transformation process from Eq. (4.2c), as presented by Schmieg [68], the result is a very complex expression which does not provide any insight. However, important information considering the location and the amplitude of the strongest stabilization and destabilization can be extracted considering only the extrema of $_{(\pm)} \sin(\varphi_0) \sin(\varphi_0 - \zeta_c)$ with respect to φ_0, while the lower sign in brackets stands for the sum combination resonance case.

First, the amplitudes of the highest stabilization and destabilization in terms of the corresponding LCEs are considered. With the maxima and minima of the term $_{(\pm)} \sin(\varphi_0) \sin(\varphi_0 - \zeta_c)$ given as follows

for the difference:	for the sum:	
$\varphi_{0,max} = \dfrac{\zeta_c}{2},$	$\varphi_{0,max} = \dfrac{\zeta_c + \pi}{2},$	(4.10a)
$\varphi_{0,min} = \dfrac{\zeta_c + \pi}{2},$	$\varphi_{0,min} = \dfrac{\zeta_c}{2}$	(4.10b)

the LCEs describing the highest stabilization Λ^s and destabilization Λ^d points in the vicinity of the combination resonances read

for the difference:

$$\Lambda^{s,d} = \mathrm{Re}\left(-\frac{\delta_{11} + \delta_{22}}{4} + \frac{1}{4}\sqrt{(\delta_{11} - \delta_{22})^2 - \frac{\varepsilon^2 \left(\cos(\zeta_c) \pm 1\right)}{2\,\omega_1 \omega_2}} \right), \tag{4.11a}$$

for the sum:

$$\Lambda^{s,d} = \mathrm{Re}\left(-\frac{\delta_{11} + \delta_{22}}{4} + \frac{1}{4}\sqrt{(\delta_{11} - \delta_{22})^2 + \frac{\varepsilon^2 \left(\cos(\zeta_c) \mp 1\right)}{2\,\omega_1 \omega_2}} \right), \tag{4.11b}$$

where the upper sign in the radicand corresponds to the stabilization effect. The above equation vividly demonstrates the influence of the phase shift ζ_c, describing the emergence and decay of resonance and anti-resonance. From Eqs. (4.11a)-(4.11b) it is also obvious that the separate appearance of resonance and anti-resonance is only a special case for $\zeta_c = \pi z$,

while, in general, for $\zeta_c \neq \pi z$, $z \in \mathbb{Z}$, and $\delta_{11} \neq \delta_{22}$ both effects are present. Apparently, the conditions for the global stability effects as well as for simultaneous resonance and anti-resonance are the same. Further, Eqs. (4.11a)-(4.11b) show that even though the maximum magnitude of the parametric contribution term is the same for both effects, the strongest stabilization at $\zeta_c = 0$, if not limited to $\Lambda^{*,s}$, is higher than the strongest destabilization at $\zeta_c = \pi$. This relation is due to the property of the root function having higher rates of change for lower values of the radicand.

Further, Eqs. (4.11a)-(4.11b) can be easily solved for the threshold value of the excitation amplitude leading to instability. Setting $\Lambda^d = 0$, the threshold value is given by

$$\varepsilon^2_{th} = \frac{8\delta_{11}\delta_{22}\,\omega_1\omega_2}{1 \mp \cos\left(\zeta_c\right)}, \tag{4.12}$$

where the upper sign holds for the difference combination resonance.

Figure 4.1 depicts $\Lambda^{s,d}$ for different values of ζ_c with $\varepsilon^2 > \varepsilon^{2,*}$ for the case of difference combination resonance. Compared to the unperturbed case, $\varepsilon^2 = 0$, parametric excitation introduces resonance and anti-resonance depending on ζ_c. It can be seen that the highest stabilization is limited to $\Lambda^s = \Lambda^{*,s}$ due to the negative radicand in Eq. (4.11). The results of the semi-analytical approximation, Eq. (4.11), are also compared to numerical Floquet analysis of the original system showing excellent agreement. However, while the semi-analytical results are given by a compact and meaningful expression, the numerical results are obtained from a sweep over Ω for each specified ζ_c and a constant ε^2 requiring considerable computational effort.

Of great importance is also the location of the stabilizing and destabilizing effects, Ω^s and Ω^d respectively, which depends on the phase angle ζ_c as well as on the relation of the damping coefficients δ_{11} and δ_{22}. The approximate analytical expression can be obtained by substituting Eq. (4.10) into Eq. (4.2c) and solving for Ω. The location of the strongest stabilization and destabilization is then given by

$$\text{for the difference:} \quad \Omega \approx |\omega_1 - \omega_2|$$

$$\Omega^s = \omega_2 - \omega_1 - \frac{1}{2}\left(\delta_{11} - \delta_{22}\right)\tan\left(\frac{\zeta_c}{2}\right) \quad \text{for } \varepsilon^2 < \varepsilon^{2,*}, \tag{4.13a}$$

$$\Omega^{*,s} = \omega_2 - \omega_1 - \frac{\varepsilon^2 \sin(\zeta_c)}{4\,\omega_1\omega_2(\delta_{11} - \delta_{22})} \qquad \text{for } \varepsilon^2 > \varepsilon^{2,*}, \tag{4.13b}$$

$$\Omega^d = \omega_2 - \omega_1 + \frac{1}{2}\left(\delta_{11} - \delta_{22}\right)\cot\left(\frac{\zeta_c}{2}\right), \tag{4.13c}$$

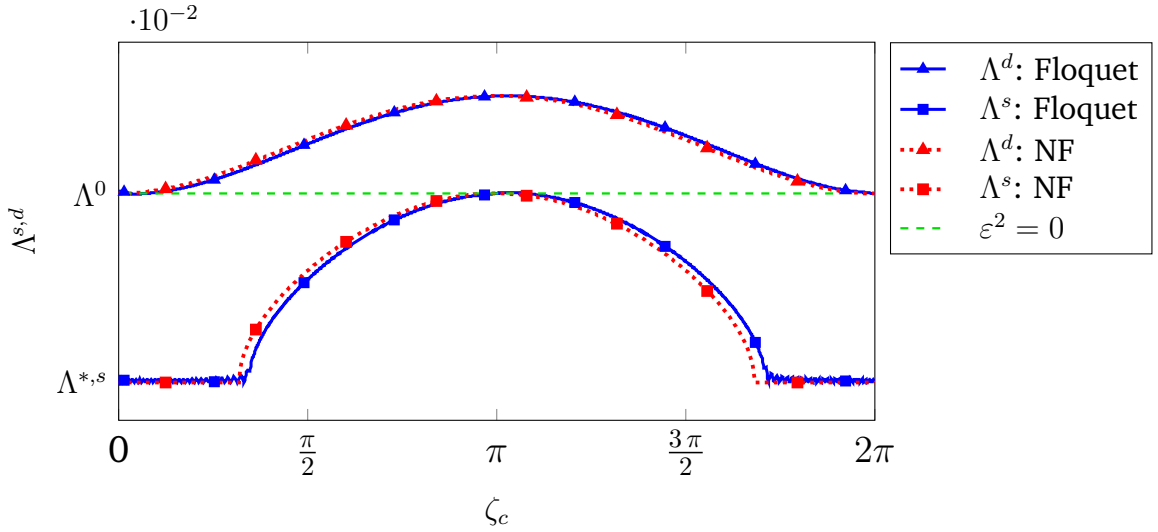

Figure 4.1: Amplitude of highest stabilization Λ^s and highest destabilization Λ^d in system (4.1) with $\Omega \approx |\omega_1 - \omega_2|$, $\varepsilon^2 = (0.15\,\mathrm{s}^{-2})^2$, $\omega_1 = 1\,\mathrm{s}^{-1}$, $\omega_2 = \sqrt{3}\,\mathrm{s}^{-1}$, $\delta_{11} = 0.05\,\mathrm{s}^{-1}$, $\delta_{22} = 0.15\,\mathrm{s}^{-1}$, $\delta_c = 0\,\mathrm{s}^{-1}$, $\zeta_{12} = 0$, $\zeta_{21} = \zeta_c$, $\zeta_{22} = 0$

for the sum: $\Omega \approx \omega_1 + \omega_2$

$$\Omega^s = \omega_2 + \omega_1 + \frac{1}{2}\,(\delta_{11} - \delta_{22})\cot\left(\frac{\zeta_c}{2}\right) \quad \text{for } \varepsilon^2 < \varepsilon^{2,*}, \tag{4.14a}$$

$$\Omega^{*,s} = \omega_2 + \omega_1 + \frac{\varepsilon^2 \sin(\zeta_c)}{4\,\omega_1\omega_2(\delta_{11} - \delta_{22})} \quad \text{for } \varepsilon^2 > \varepsilon^{2,*}, \tag{4.14b}$$

$$\Omega^d = \omega_2 + \omega_1 - \frac{1}{2}\,(\delta_{11} - \delta_{22})\tan\left(\frac{\zeta_c}{2}\right), \tag{4.14c}$$

while the upper (lower) sign applies for difference (sum) combination resonance. Surprisingly, the expressions are very compact and clear. Interestingly, the locations $\Omega^{s,d}$ do not depend on the amplitude of variation ε^2. The amplitude plays a role only for the case when the stabilizing effect has reached its maximum $\Lambda^{*,s}$, i.e., for $\varepsilon^2 > \varepsilon^{2,*}$. Figure 4.2 clearly demonstrates the changing positions of stabilized and destabilized areas for the difference combination resonance area: e.g., for the stabilized area starting directly at the difference combination resonance for $\zeta_c = 0$, moving to higher Ω values for increasing ζ_c, disappearing with ζ_c approaching π and eventually emerging on the other side for $\zeta_c > \pi$. In this way, for $\delta_{11} < \delta_{22}$ and $\omega_1 < \omega_2$, the stabilization takes place above the difference combination resonance for $\zeta_c \in [0, \pi]$ and below it for $\zeta_c \in [\pi, 2\pi]$. The destabilization is always opposite to the stabilization with respect to the combination resonance frequency. As outlined before, the same, but opposite relations also apply to the sum combination

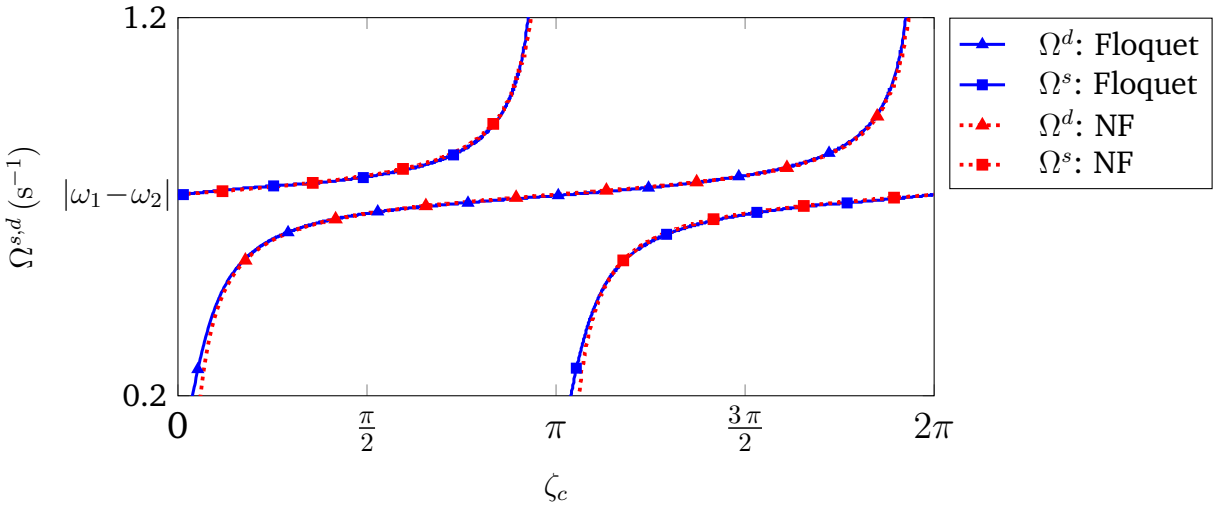

Figure 4.2: Location of the highest stabilization Ω^s and the highest destabilization Ω^d in system (4.1) with $\Omega \approx |\omega_1 - \omega_2|$, $\varepsilon^2 = (0.15\,\mathrm{s}^{-2})^2$, $\omega_1 = 1\,\mathrm{s}^{-1}$, $\omega_2 = \sqrt{3}\,\mathrm{s}^{-1}$, $\delta_{11} = 0.05\,\mathrm{s}^{-1}$, $\delta_{22} = 0.15\,\mathrm{s}^{-1}$, $\delta_c = 0\,\mathrm{s}^{-1}$, $\zeta_{12} = 0$, $\zeta_{21} = \zeta_c$, $\zeta_{22} = 0$

resonance area. These findings also agree with the behavior indicated by the normal form for non-resonant parametric excitation in Fig. 3.3.

Of interest is also the transition point Ω^0 between the stabilizing and the destabilizing behavior. It can be obtained from the zero solution of the parametric contribution term in Eq. (4.3) and the subsequent solving of the linearized Eq. (4.2c) for Ω:

$$\Omega^0 = \omega_2 \mp \omega_1 + \frac{1}{2}\left(\delta_{11} - \delta_{22}\right)\cot(\zeta_c) \mp \frac{\varepsilon^2 \sin(\zeta_c)}{8\,\omega_1\omega_2(\delta_{11} - \delta_{22})}, \tag{4.15a}$$

while the upper (lower) sign holds for the difference (sum) combination resonance. The above equation shows that, except for the ε^2-proportional terms, the transition point is exactly in the middle between the maximum stabilization and maximum destabilization, Eq. (4.13).

Table 4.1 provides an overview of the characteristic points $P^s(\Omega^s, \Lambda^{(*),s})$, $P^d(\Omega^d, \Lambda^d)$ and $P^0(\Omega^0, \Lambda^0)$ describing the location and the magnitude of the strongest stabilization and destabilization as well as of the transition point, respectively. The expressions for the destabilizing effect (Λ^d, Ω^d, ε^2_{th}) agree with the results obtained by Schmieg [68]. The expressions for the stabilizing effect (Λ^s, $\varepsilon^{2,*}$) under synchronous parametric excitation with $\zeta_c = \pi z, z \in \mathbb{Z}$ agree with the results obtained by Dohnal [15].

It has to be noted that according to Eq. (4.11), the contribution of parametric excitation is inversely proportional to the product of the eigenfrequencies. Therefore, in systems with

Difference combination resonance $\Omega \approx \lvert\omega_1 - \omega_2\rvert$		Sum combination resonance $\Omega \approx \omega_1 + \omega_2$
Λ^s	$\mathrm{Re}\left(-\frac{\delta_{11}+\delta_{22}}{4} + \frac{1}{4}\sqrt{(\delta_{11}-\delta_{22})^2 - \frac{\varepsilon^2(\cos(\zeta_c)+1)}{2\,\omega_1\omega_2}}\right)$	$\mathrm{Re}\left(-\frac{\delta_{11}+\delta_{22}}{4} + \frac{1}{4}\sqrt{(\delta_{11}-\delta_{22})^2 + \frac{\varepsilon^2(\cos(\zeta_c)-1)}{2\,\omega_1\omega_2}}\right)$
Λ^d	$\mathrm{Re}\left(-\frac{\delta_{11}+\delta_{22}}{4} + \frac{1}{4}\sqrt{(\delta_{11}-\delta_{22})^2 - \frac{\varepsilon^2(\cos(\zeta_c)-1)}{2\,\omega_1\omega_2}}\right)$	$\mathrm{Re}\left(-\frac{\delta_{11}+\delta_{22}}{4} + \frac{1}{4}\sqrt{(\delta_{11}-\delta_{22})^2 + \frac{\varepsilon^2(\cos(\zeta_c)+1)}{2\,\omega_1\omega_2}}\right)$
Ω^s $\varepsilon^2 < \varepsilon^{2,*}$	$\omega_2 - \omega_1 - \frac{1}{2}(\delta_{11}-\delta_{22})\tan\left(\frac{\zeta_c}{2}\right)$	$\omega_2 + \omega_1 + \frac{1}{2}(\delta_{11}-\delta_{22})\cot\left(\frac{\zeta_c}{2}\right)$
Ω^s $\varepsilon^2 > \varepsilon^{2,*}$	$\omega_2 - \omega_1 - \frac{\varepsilon^2\sin(\zeta_c)}{4\omega_1\omega_2(\delta_{11}-\delta_{22})}$	$\omega_2 + \omega_1 + \frac{\varepsilon^2\sin(\zeta_c)}{4\omega_1\omega_2(\delta_{11}-\delta_{22})}$
Ω^d	$\omega_2 - \omega_1 + \frac{1}{2}(\delta_{11}-\delta_{22})\cot\left(\frac{\zeta_c}{2}\right)$	$\omega_2 + \omega_1 - \frac{1}{2}(\delta_{11}-\delta_{22})\tan\left(\frac{\zeta_c}{2}\right)$
Ω^0	$\omega_2 - \omega_1 + \frac{1}{2}(\delta_{11}-\delta_{22})\cot(\zeta_c) - \frac{\varepsilon^2\sin(\zeta_c)}{8\,\omega_1\omega_2(\delta_{11}-\delta_{22})}$	$\omega_2 + \omega_1 + \frac{1}{2}(\delta_{11}-\delta_{22})\cot(\zeta_c) + \frac{\varepsilon^2\sin(\zeta_c)}{8\,\omega_1\omega_2(\delta_{11}-\delta_{22})}$
$\varepsilon^{2,*}$	$\frac{2(\delta_{11}-\delta_{22})^2\omega_1\omega_2}{1+\cos(\zeta_c)}$	$\frac{2(\delta_{11}-\delta_{22})^2\omega_1\omega_2}{1-\cos(\zeta_c)}$
ε^2_{th}	$\frac{8\delta_{11}\delta_{22}\,\omega_1\omega_2}{1+\cos(\zeta_c)}$	$\frac{8\delta_{11}\delta_{22}\,\omega_1\omega_2}{1-\cos(\zeta_c)}$

Table 4.1: Coordinates of the characteristic points $P^s(\Omega^s, \Lambda^s)$, $P^d(\Omega^d, \Lambda^d)$, $P^0(\Omega^0, \Lambda^0)$ for asynchronous parametric excitation in $\mathbf{MDK} + \mathbf{C}(t)$ system (4.1) with $\varepsilon^2 = \varepsilon_{ij}\varepsilon_{ji}$ while $i \neq j$ and $i, j = 1, 2$.

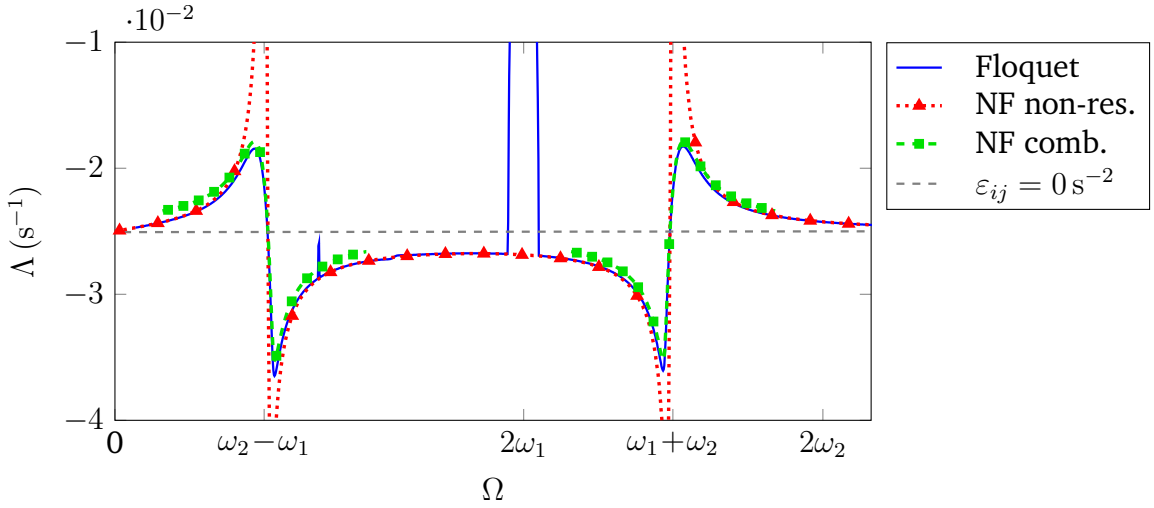

Figure 4.3: General stability behavior of system (4.1) with $\varepsilon_{11}=\varepsilon_{22}=0.15\,\mathrm{s}^{-2}$, $\varepsilon_{12}=\varepsilon_{21}=0\,\mathrm{s}^{-2}$, $\omega_1=1\,\mathrm{s}^{-1}$, $\omega_2=\sqrt{3}\,\mathrm{s}^{-1}$, $\delta_{11}=0.05\,\mathrm{s}^{-1}$, $\delta_{22}=0.15\,\mathrm{s}^{-1}$, $\delta_c=0\,\mathrm{s}^{-1}$, $\zeta_{12}=0$, $\zeta_{22}=0$, $\zeta_{21}=\zeta_c=\pi/2$

high eigenfrequencies also high variation of stiffness is required to maintain the strength of the parametric resonance effects.

The above analysis provides a deep insight into the stability behavior of an $\mathbf{MDK}+\mathbf{C}(t)$ system at the combination resonance frequencies, completing the findings obtained from the non-resonant parametric excitation and also the results of previous studies on combination resonances. The derived compact expressions can also be used as a tool for designing a system with desired properties concerning the location and the magnitude of resonance and anti-resonance. In particular, the influence of the off-diagonal phase shift parameter ζ_c, dramatically affecting the stability behavior, is described clearly and precisely. The results of the normal form transformation can be also used for the derivation of the transition curves separating stable and unstable regions in the $\varepsilon-\Omega$ space, however, this has already been extensively studied by Eicher [24] and Dohnal [15].

Both normal forms together, the one for the non-resonant parametric excitation, Eq. (3.13), and the one for the combination resonance areas, Eq. (4.2), capture all essential parametric resonance effects over the whole range of excitation frequencies, except for the fundamental resonances for which the normal forms have to be derived separately. Figure 4.3 shows the stability behavior of system (4.1), while the results of the numerical Floquet analysis are compared to the normal form analysis revealing reasonable qualitative and quantitative agreement. However, the transition between the different normal forms should be analyzed in detail in order to possibly obtain a more general function valid for all values of Ω.

4.2 Displacement-proportional excitation: $\mathbf{MDGKN} + \mathbf{C}(t)$ system

The analysis of an $\mathbf{MDGKN} + \mathbf{C}(t)$ system with respect to its global stability behavior has shown that the approximate analytical expressions become exceedingly complex due to the highly entangled interdependencies of parameters, in particular, of the phase angles in parametric excitation terms, so that extracting useful information is barely possible [40]. While the conditions for the appearance of global effects could still be successfully derived using a non-resonant normal form, an explicit analysis of the combination resonance areas does not provide as much general insight as in the previous cases with $\mathbf{MDK} + \mathbf{C}(t)$ and $\mathbf{MDK} + \mathbf{B}(t)$ systems. Still, an attempt is made to extract as much information as possible.

The following $\mathbf{MDGKN} + \mathbf{C}(t)$ system is studied:

$$\begin{pmatrix} 1 & 0 \\ 0 & 1 \end{pmatrix} \begin{pmatrix} \ddot{q}_1 \\ \ddot{q}_2 \end{pmatrix} + \begin{pmatrix} \delta_{11} & \delta_c + \gamma \\ \delta_c - \gamma & \delta_{22} \end{pmatrix} \begin{pmatrix} \dot{q}_1 \\ \dot{q}_2 \end{pmatrix} + \left[\begin{pmatrix} k_{11} & n \\ -n & k_{22} \end{pmatrix} + \begin{pmatrix} \varepsilon_{11} \cos(\Omega t) & \varepsilon_{12} \cos(\Omega t + \zeta_{12}) \\ \varepsilon_{21} \cos(\Omega t + \zeta_{21}) & \varepsilon_{22} \cos(\Omega t + \zeta_{22}) \end{pmatrix} \right] \begin{pmatrix} q_1 \\ q_2 \end{pmatrix} = \mathbf{0}, \tag{4.16}$$

assuming $k_{11} < k_{22}$ without loss of generality. New are the skew-symmetric circulatory and gyroscopic terms. Without damping, the trivial solution of the underlying $\mathbf{MKN}$ system is assumed to be marginally stable, i.e., the following relation holds

$$\left| \frac{1}{2}(k_{22} - k_{11}) \right| > |n| \,. \tag{4.17}$$

The normal form transformation leads to symbolic expressions which cannot be given here due to their exceeding length. However, the same principal structure can be recognized as in the case of the $\mathbf{MDK} + \mathbf{C}(t)$ system studied before, Eq. (4.2). Nevertheless, the most

important quantity – the largest LCE – can still be sufficiently simplified and is given by

$$\Lambda = \mathrm{Re}\left(\frac{1}{4}(-\delta_{11}-\delta_{22}) + \frac{1}{4}\sqrt{\frac{C_0^2}{C_1} \overset{-}{(+)} \frac{A_\zeta(\varphi)}{C_1\,C_2}}\right) \quad \text{with} \tag{4.18}$$

$$\begin{aligned} A_\zeta(\varphi) =& (k_{11}-k_{22})^2\varepsilon_{12}\varepsilon_{21}\sin(\zeta_{12}-\varphi)\sin(\zeta_{21}-\varphi) \\ & -n(k_{11}-k_{22})\left(\varepsilon_{12}\sin(\zeta_{12}-\varphi)-\varepsilon_{21}\sin(\zeta_{21}-\varphi)\right)\left(\varepsilon_{11}\sin(\varphi)+\varepsilon_{22}\sin(\zeta_{22}-\varphi)\right) \\ & -n^2\left(\left(\varepsilon_{12}\sin(\zeta_{12}-\varphi)+\varepsilon_{21}\sin(\zeta_{21}-\varphi)\right)^2+\left(\varepsilon_{11}\sin(\varphi)+\varepsilon_{22}\sin(\zeta_{22}-\varphi)\right)^2\right) \end{aligned} \tag{4.19}$$

and

$$C_0 = -4n\gamma + (k_{11}-k_{22})(\delta_{11}-\delta_{22}), \tag{4.20a}$$

$$C_1 = (k_{11}-k_{22})^2 - 4n^2, \tag{4.20b}$$

$$C_2 = \sqrt{n^2+k_{11}k_{22}}, \tag{4.20c}$$

while the upper (lower) sign holds for the difference (sum) combination resonance area. The expression for the largest LCE is given as a function of the polar coordinate φ, so that the strongest stabilization and the strongest destabilization can be obtained only for given phase relations ζ_{ij}. It can be shown that the conditions for the coexistence of resonance and anti-resonance are identical to the conditions for the appearance of global effects derived earlier in [40]. It is also easy to see that for $n = 0\,\mathrm{s}^{-2}$, i.e., without circulatory terms, the expression for the largest LCE, Eq. (4.18), is reduced to the already known case treated in section 4.1, Eq. (4.3). The symbolic expressions for the location of the characteristic points cannot be sufficiently simplified for the general case, however, they as well do reveal the same structure as in the case without circulatory terms, compare Eqs. (4.13), (4.15). Yet, another unique feature of an $\mathbf{MDKGN}+\mathbf{C}(t)$ system is clearly seen in Eq. (4.18): In a system featuring both gyroscopic and circulatory terms, anti-resonance as well as coexistence of resonance and anti-resonance are possible also for the case of *uniform* damping as the first term in C_0, Eq. (4.20a), does not vanish.

Obviously, the additional coupling especially through the circulatory terms introduces a high amount of complexity making the analytical approximations less practicable in the general case. Nevertheless, the obtained results can be readily used for analyzing the complex stability behavior of $\mathbf{MDKGN}+\mathbf{C}(t)$ systems with known phase relations. In particular, evaluating only $A_\zeta(\varphi)$, Eq. (4.19), for a given example, quickly shows whether resonance, anti-resonance or coexistence of both take place at each sum and difference

combination resonance frequencies.

In the following, two simple examples are studied. First, the most common type of excitation is studied: synchronous excitation with uniform amplitude, i.e., $\varepsilon_{ij} = \varepsilon$ and $\zeta_{ij} = 0$ with $i, j = 1, 2$. In this case the contribution of parametric excitation $A_\zeta(\varphi)$, Eq. (4.19), is as follows:

$$A_\zeta(\varphi) = \left((k_{11} - k_{22})^2 - 4n^2\right) \varepsilon^2 \sin^2(\varphi) \,. \tag{4.21}$$

With the additional condition given in Eq. (4.17), the whole expression remains positive for all φ and with this also for all Ω. Therefore, considering the signs in front of $A_\zeta(\varphi)$ in Eq. (4.18), synchronous parametric excitation in a $\mathbf{MDGKN} + \mathbf{C}(t)$ system will always have a stabilizing effect for the difference combination resonance frequency (anti-resonance) and destabilizing effects for the sum combination resonance frequency (resonance). No coexistence is possible with this kind of excitation.

In the second case the off-diagonal excitation terms are in antiphase, i.e., $\zeta_{12} = 0$, $\zeta_{21} = \pi$, $\zeta_{22} = 0$ and $\varepsilon_{ij} = \varepsilon$. The contribution of parametric excitation $A_\zeta(\varphi)$ is then evaluated to

$$A_\zeta(\varphi) = -\left(k_{11} - k_{22}\right)^2 \varepsilon^2 \sin^2(\varphi) \,. \tag{4.22}$$

Again, the sign of the whole expression remains negative for all φ. Obviously, the situation is inverse to the previous case: there is resonance at the difference and anti-resonance at the sum combination resonance frequency. In both cases there is no transition point, while the extrema of the LCEs are located at the combination resonance frequencies without a shift.

In this way, the basic stability behavior of a parametrically excited system featuring circulatory terms can be quickly assessed by evaluating one simple expression. In the next section, the characteristic points are given for a significantly more complex special case with phase angles ζ_{ij} identical to those in the minimal brake model with asymmetric bearings [70].

4.2.1 $\mathrm{MDKGN} + \mathrm{C}(t)$ system with given phase relations

The example analyzed in the following is described by Eq. (4.16), while the phase angles are set as follows: $\zeta_{12} = \pi/2$, $\zeta_{21} = \pi/2$, $\zeta_{22} = \pi$. The largest LCE is then given by

$$\Lambda = \mathrm{Re}\left(\frac{1}{4}(-\delta_{11} - \delta_{22}) + \frac{1}{4}\sqrt{\frac{C_0^2}{C_1} \mp \frac{\left((k_{11} - k_{22})^2 \cos^2(\varphi) - 4n^2\right)\varepsilon^2}{C_1\, C_2}}\right), \tag{4.23}$$

while the upper (lower) sign holds for the difference (sum) combination resonance area.From Eq. (4.23) it is already clear that the given asynchronous excitation leads to coexistence of resonance and anti-resonance at combination resonance frequencies. In this system with gyroscopic and circulatory terms the largest LCE of the unperturbed system Λ^0 is not determined by the largest damping coefficient alone, but can still be easily obtained (approximately) from Eq. (4.23) by setting $\varepsilon = 0$. With $\cos^2(\varphi)$ taking values between 0 and 1, the strongest stabilization Λ^s and the strongest destabilization Λ^d read

for the difference:

$$\Lambda^s = \mathrm{Re}\left(\frac{1}{4}(-\delta_{11}-\delta_{22}) + \frac{1}{4}\sqrt{\frac{C_0^2}{C_1} - \frac{\varepsilon^2}{C_2}}\right), \tag{4.24a}$$

$$\Lambda^d = \mathrm{Re}\left(\frac{1}{4}(-\delta_{11}-\delta_{22}) + \frac{1}{4}\sqrt{\frac{C_0^2}{C_1} + \frac{4n^2\varepsilon^2}{C_1 C_2}}\right), \tag{4.24b}$$

for the sum:

$$\Lambda^s = \mathrm{Re}\left(\frac{1}{4}(-\delta_{11}-\delta_{22}) + \frac{1}{4}\sqrt{\frac{C_0^2}{C_1} - \frac{4n^2\varepsilon^2}{C_1\,C_2}}\right), \tag{4.24c}$$

$$\Lambda^d = \mathrm{Re}\left(\frac{1}{4}(-\delta_{11}-\delta_{22}) + \frac{1}{4}\sqrt{\frac{C_0^2}{C_1} + \frac{\varepsilon^2}{C_2}}\right). \tag{4.24d}$$

For this kind of parametric excitation also the locations of the characteristic points can be given in short form:

for the difference:

$$\Omega^s = \omega_2 - \omega_1 + \frac{n\,C_0}{C_1} \quad \text{for } \varepsilon < \varepsilon^*_\Delta, \tag{4.25a}$$

$$\Omega^{*,s} = \omega_2 - \omega_1 + \frac{n\varepsilon^2}{C_0\,C_2} \quad \text{for } \varepsilon > \varepsilon^*_\Delta, \tag{4.25b}$$

$$\Omega^d = \omega_2 - \omega_1 - \frac{C_0}{4n}, \tag{4.25c}$$

$$\Omega^0 = \omega_2 - \omega_1 - \frac{C_0\,(C_1 - 4n^2)}{8\,n\,C_1} + \frac{n\varepsilon^2}{2\,C_0\,C_2}, \tag{4.25d}$$

with

$$\varepsilon_{\Delta}^{*} = \sqrt{\frac{C_0^2\, C_2}{C_1}}; \tag{4.26}$$

for the sum:

$$\Omega^{s} = \omega_2 + \omega_1 - \frac{C_0}{4n} \quad \text{for } \varepsilon < \varepsilon_{\Sigma}^{*}, \tag{4.27a}$$

$$\Omega^{*,s} = \omega_2 + \omega_1 - \frac{n\,\varepsilon^2}{C_0\, C_2} \quad \text{for } \varepsilon > \varepsilon_{\Sigma}^{*}, \tag{4.27b}$$

$$\Omega^{d} = \omega_2 + \omega_1 + \frac{n\, C_0}{C_1}, \tag{4.27c}$$

$$\Omega^{0} = \omega_2 + \omega_1 - \frac{C_0\ (C_1 - 4n^2)}{8\, n\, C_1} - \frac{n\,\varepsilon^2}{2\, C_0\, C_2}. \tag{4.27d}$$

with

$$\varepsilon_{\Sigma}^{*} = \sqrt{\frac{C_0^2\, C_2}{4n^2}}. \tag{4.28}$$

The above expressions allow for a quick qualitative and quantitative insight into the stability behavior of this rather complex system. Additional usability of the derived expressions results from the consistent use of the initial system parameters without intermediate scaling or normalization. Moreover, the symbolic expressions emphasize the importance of accounting for gyroscopic terms in the analysis of parametric stability effects – according to Eq. (4.20a) and Eqs. (4.25), (4.27), depending on the magnitude of the gyroscopic term γ the positions of the stabilized and the destabilized areas can be inverted. At the same time the expressions demonstrate the increased complexity due to the introduction of circulatory and gyroscopic terms and indicate the interpretability limits of such semi-analytical results – a further increase of the model complexity will probably forbid any sensible interpretation of the results.

Figure 4.4 shows the comparison between the analytical approximation and the numerical results (Floquet analysis) for the difference and sum combination resonance of an $\mathbf{MDKN} + \mathbf{C}(t)$ system for a chosen parameter set. In order to exclude superposition of different resonance areas, the parameters are chosen such that the difference combination resonance frequency is sufficiently far away from any other resonance areas. The semi-analytical characteristic points $P^{s}(\Omega^{s}, \Lambda^{(*),s})$, $P^{d}(\Omega^{d}, \Lambda^{d})$ and $P^{0}(\Omega^{0}, \Lambda^{0})$ describing

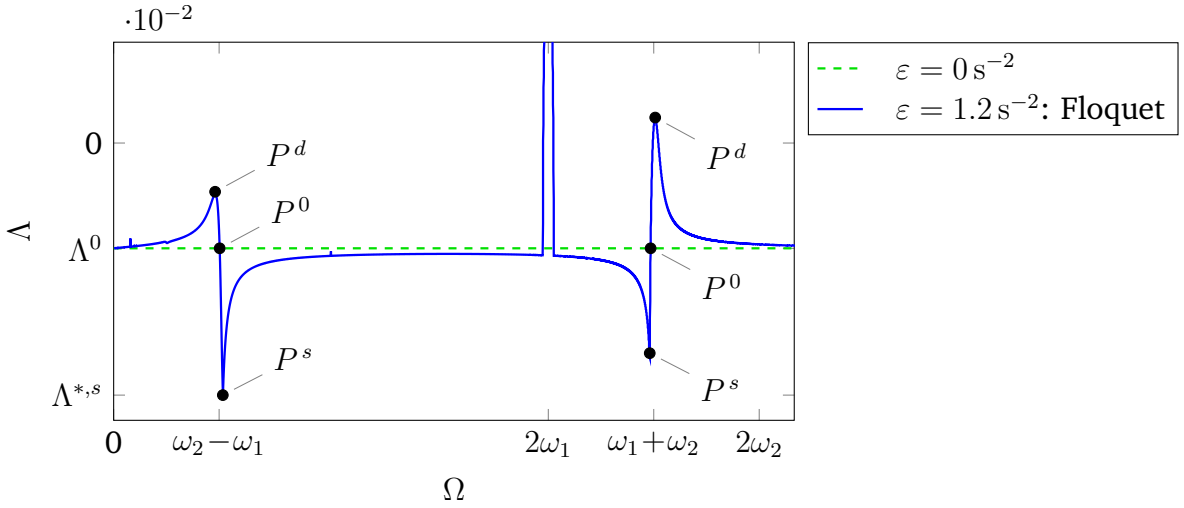

Figure 4.4: The largest LCE and the characteristic points of the $\mathbf{MDKN} + \mathbf{C}(t)$ system under asynchronous parametric excitation, Eq. (4.16), with $k_{11} = 25\,\mathrm{s}^{-2}$, $k_{22} = 64\,\mathrm{s}^{-2}$, $n = 10\,\mathrm{s}^{-2}$, $\delta_{11} = 0.05\,\mathrm{s}^{-1}$, $\delta_{22} = 0.15\,\mathrm{s}^{-1}$, $\delta_c = 0\,\mathrm{s}^{-1}$, $\gamma = 0\,\mathrm{s}^{-1}$, $\varepsilon = 1.2\,\mathrm{s}^{-2}$ and $\zeta_{12} = \pi/2$, $\zeta_{21} = \pi/2$, $\zeta_{22} = \pi$

the location and the magnitude of the strongest stabilization, destabilization and of the transition point, respectively, are obtained according to Eqs. (4.24)-(4.27). The amplitude of excitation with $\varepsilon = 1.2\,\mathrm{s}^{-2}$ is chosen such that the threshold value for the maximum stabilization is exceeded for the difference ($\varepsilon^*_\Delta = 0.75\,\mathrm{s}^{-2}$), but is not exceeded for the sum ($\varepsilon^*_\Sigma = 1.25\,\mathrm{s}^{-2}$) combination resonance frequency, i.e., $\varepsilon^*_\Delta < \varepsilon < \varepsilon^*_\Sigma$. The threshold values are easily calculated from Eqs. (4.26) and (4.28). According to Fig. 4.4, the symbolic expressions derived by the method of normal forms provide a very accurate qualitative and quantitative representation of the stability behavior of an $\mathbf{MDKN} + \mathbf{C}(t)$ system. As indicated by the threshold values ε^*_Δ and ε^*_Σ, for the chosen parameter set, the anti-resonance is stronger at the difference combination resonance frequency than at the sum. This might be different for other system parameters.

Next, the analytical and numerical results are compared for the case of an $\mathbf{MDGKN} + \mathbf{C}(t)$ system, Fig. 4.5. Again, the amplitude of parametric excitation with $\varepsilon = 1.8\,\mathrm{s}^{-2}$ is chosen such that the maximum stabilization through parametric excitation is achieved only for the difference combination resonance area ($\varepsilon^*_\Delta = 1.52\,\mathrm{s}^{-2}$), but not for the sum ($\varepsilon^*_\Sigma = 2.54\,\mathrm{s}^{-2}$), i.e., $\varepsilon^*_\Delta < \varepsilon < \varepsilon^*_\Sigma$. Qualitatively the stability behavior is very similar to the previous case, Fig. 4.4. However, the values of the LCEs are significantly changed even by this rather small gyroscopic term γ. Nevertheless, for the chosen parameter set, the characteristic points obtained by the method of normal forms provide an excellent description of the most important stability features of this complex system.

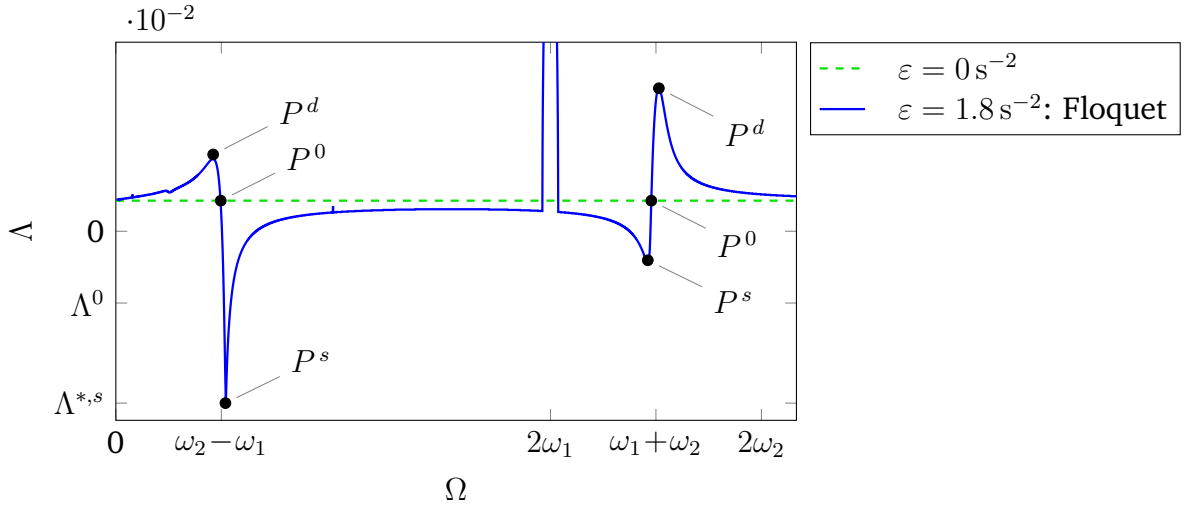

Figure 4.5: The largest LCE and the characteristic points of the $\mathbf{MDGKN} + \mathbf{C}(t)$ system under asynchronous parametric excitation, Eq. (4.16), with $k_{11} = 25\,\mathrm{s}^{-2}$, $k_{22} = 64\,\mathrm{s}^{-2}$, $n = 10\,\mathrm{s}^{-2}$, $\delta_{11} = 0.05\,\mathrm{s}^{-1}$, $\delta_{22} = 0.15\,\mathrm{s}^{-1}$, $\delta_c = 0.1\,\mathrm{s}^{-1}$, $\gamma = -0.1\,\mathrm{s}^{-1}$, $\varepsilon = 1.8\,\mathrm{s}^{-2}$ and $\zeta_{12} = \pi/2$, $\zeta_{21} = \pi/2$, $\zeta_{22} = \pi$

4.2.2 Discussion

Even though the above examples, Figs. 4.4-4.5, show an excellent agreement between the analytical approximation and the numerical results, it is important to keep in mind the assumptions made during the normal form transformation and therefore also the limitations arising from these assumptions. First, the semi-analytical results obtained by the normal form transformation do not account for several interactions of the velocity-proportional terms. In general, even in the absence of parametric excitation, **MDKGN** systems show very complex stability behavior being highly sensitive to particular parameter relations [37]. The LCEs obtained by the method of normal forms provide only an approximation of the actual LCEs: The gyroscopic and the damping terms are only considered for the *approximation* of the LCEs of the unperturbed ($\varepsilon = 0$) system. Furthermore, also possible changes in the circular eigenfrequencies due to the velocity-proportional terms are not accounted for, which might be of importance especially for growing gyroscopic terms. These aspects lead to a limited accuracy of the obtained results from qualitative and quantitative points of view. On the other hand, the results are expected to be more trustful for $\mathbf{MDKN} + \mathbf{C}(t)$ system, i.e., systems without gyroscopic terms.

Another main assumption consists in assuming the amplitude of parametric excitation ε being a small parameter. Therefore, with increasing ε the acucracy of approximation is sure to decrease. Higher order approximations, see e.g. [(]DohnalVerhulst), leading to

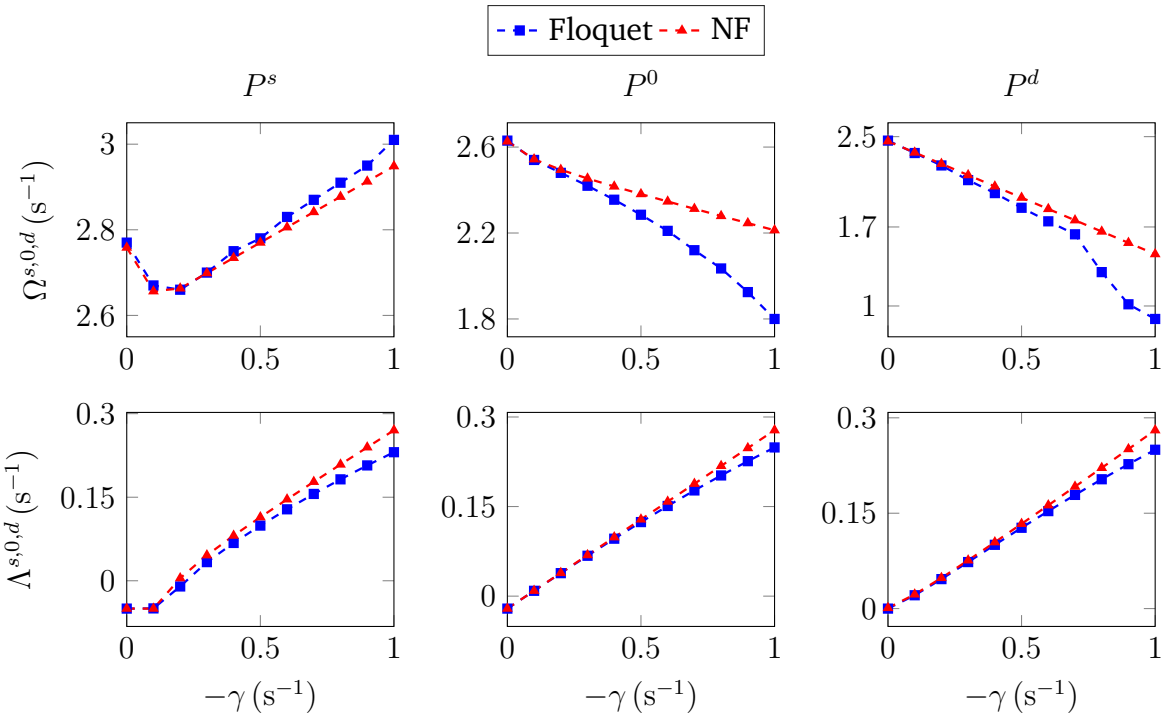

Figure 4.6: Characteristic points for $\Omega \approx |\omega_1 - \omega_2|$ of an $\mathbf{MDGKN} + \mathbf{C}(t)$ system, Eq. (4.16), with $k_{11} = 25\,\mathrm{s}^{-2}$, $k_{22} = 64\,\mathrm{s}^{-2}$, $n = 10\,\mathrm{s}^{-2}$, $\delta_{11} = 0.05\,\mathrm{s}^{-1}$, $\delta_{22} = 0.15\,\mathrm{s}^{-1}$, $\delta_c = 0\,\mathrm{s}^{-1}$, $\varepsilon = 1.8\,\mathrm{s}^{-2}$ and $\zeta_{12} = \pi/2$, $\zeta_{21} = \pi/2$, $\zeta_{22} = \pi$

exceedingly complex expressions not accessible for physical interpretation may alleviate the problem, but do not solve it. Further, each normal form is derived for a particular resonance case, e.g., for the difference combination resonance, so that any possible interferences with other parametric resonance areas are not accounted for.

A parameter study with respect to the gyroscopic term γ is carried out in order to emphasize the limits of the approximation obtained by the semi-analytical method of normal forms. For the growing magnitude of γ, a comparison of the characteristic points obtained by the normal form transformation and by numerical Floquet simulation is presented in Fig. 4.6 and Fig. 4.7 for the difference and the sum combination resonance areas respectively (note the abscissa is taken with negative sign for better representation). The figures show the most significant limitations of the semi-analytical results. First, the general trend of increasing deviation for the growing gyroscopic term γ is obvious for all quantities – for the characteristic LCEs, $\Lambda^{s,0,d}$, as well as for the characteristic frequencies $\Omega^{s,0,d}$. The deviation in the location of the strongest destabilization Ω^d for the case of difference combination resonance, Fig. 4.6, represents the impact of higher order resonances not captured by the normal form analysis. With increasing γ, Ω^d is shifted to lower frequencies towards the second order difference

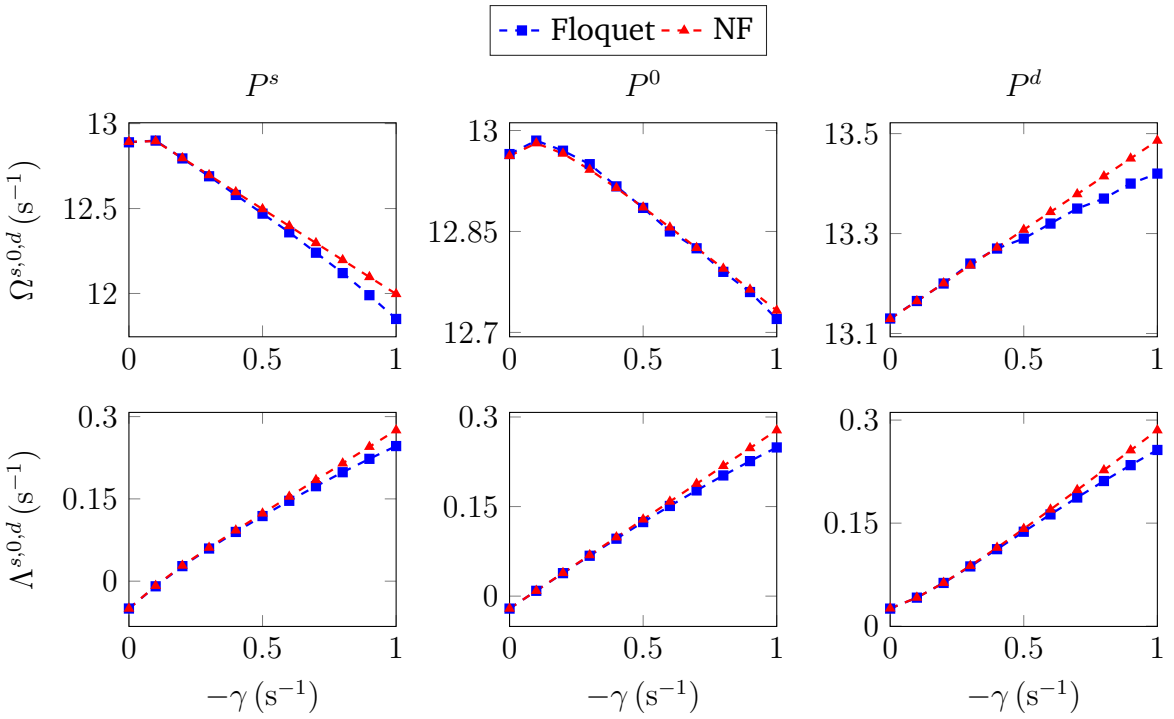

Figure 4.7: Characteristic points for for $\Omega \approx \omega_1 + \omega_2$ of an $\mathbf{MDGKN} + \mathbf{C}(t)$ system, Eq. (4.16), with $k_{11} = 25\,\mathrm{s}^{-2}$, $k_{22} = 64\,\mathrm{s}^{-2}$, $n = 10\,\mathrm{s}^{-2}$, $\delta_{11} = 0.05\,\mathrm{s}^{-1}$, $\delta_{22} = 0.15\,\mathrm{s}^{-1}$, $\delta_c = 0\,\mathrm{s}^{-1}$, $\varepsilon = 1.8\,\mathrm{s}^{-2}$ and $\zeta_{12} = \pi/2$, $\zeta_{21} = \pi/2$, $\zeta_{22} = \pi$

combination resonance ($\Omega \approx 1.4$), which is reached for $\gamma < -0.7$. The area around the difference combination resonance frequency is in general more prone to this kind of error due to an increasing density of higher order resonance frequencies.

Another important kind of error becomes more vivid comparing only the contribution of parametric excitation to the LCEs. The corresponding quantities are introduced as follows: $\Lambda^{s,PE} = \Lambda^s - \Lambda^0$ and $\Lambda^{d,PE} = \Lambda^d - \Lambda^0$. Comparing these quantities, a good agreement can be observed, except for the stabilization contribution $\Lambda^{s,PE}$ in case of difference combination resonance, Fig. 4.8. Here, the stabilization is at first approximated very precisely as long as the strongest stabilization is given by the maximum stabilization possible, $\Lambda^s = \Lambda^{*,s}$. With the growing magnitude of γ, as soon as the maximum stabilization does not apply, there is a significant deviation compared to the numerical results. A higher order normal form approximation, not given here, does provide better results, but is not practicable due to high complexity. This kind of error affects $\mathbf{MDGKN} + \mathbf{C}(t)$ as well as simpler $\mathbf{MDKN} + \mathbf{C}(t)$ systems, more so for growing amplitude of variation ε.

The above parameter study emphasizes the limitations of the semi-analytical normal form analysis which relies on the assumption of *small parameters*. As in other perturbation

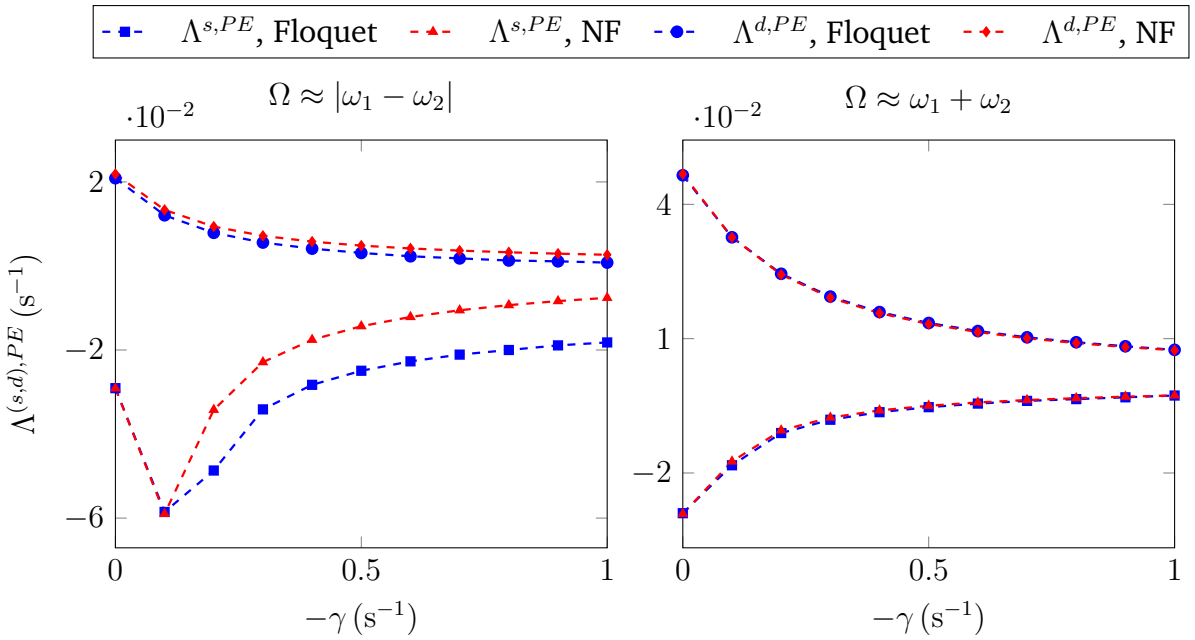

Figure 4.8: Stability contribution of parametric excitation in $\mathbf{MDGKN} + \mathbf{C}(t)$ system, Eq. (4.16), with $k_{11} = 25\,\mathrm{s}^{-2}$, $k_{22} = 64\,\mathrm{s}^{-2}$, $n = 10\,\mathrm{s}^{-2}$, $\delta_{11} = 0.05\,\mathrm{s}^{-1}$, $\delta_{22} = 0.15\,\mathrm{s}^{-1}$, $\delta_c = 0\,\mathrm{s}^{-1}$, $\varepsilon = 1.8\,\mathrm{s}^{-2}$ and $\zeta_{12} = \pi/2$, $\zeta_{21} = \pi/2$, $\zeta_{22} = \pi$

methods, it is not clear when the parameter can still be assumed as small so that it is difficult to estimate the region in which the results can be trusted, especially concerning their quantitative accuracy. Nevertheless, the symbolic expressions do provide deep insight and accurate qualitative representation of the stability behavior. The quantitative accuracy, however, has to be first assessed by a comparison to the more accurate numerical results evaluating whether the parameter values are in the trusted region.

4.3 Velocity-proportional excitation: $\mathrm{MDK} + \mathrm{B}(t)$ system

Also in the case of velocity-proportional asynchronous parametric excitation, the most significant effects take place around combination resonance areas. Therefore, the area around combination resonances is analyzed in detail by deriving corresponding normal forms for $\Omega \approx |\omega_1 \mp \omega_2|$. The case of synchronous harmonic velocity-proportional parametric excitation has been studied by Dohnal in [15], while only the impact on stability boundaries was investigated. Here the focus is on both stabilizing and destabilizing effects due to asynchronous excitation expressed in terms of LCEs.

For this purpose an $\mathrm{MDK} + \mathrm{B}(t)$ system with variable phase relations in the velocity-

proportional parametric excitation is considered

$$\begin{pmatrix}\ddot{q}_1\\ \ddot{q}_2\end{pmatrix}+\left[\begin{pmatrix}\delta_{11} & \delta_c\\ \delta_c & \delta_{22}\end{pmatrix}+\begin{pmatrix}\varepsilon_{\delta,11}\cos(\Omega t) & \varepsilon_{\delta,12}\cos(\Omega t+\psi_{12})\\ \varepsilon_{\delta,21}\cos(\Omega t+\psi_{21}) & \varepsilon_{\delta,22}\cos(\Omega t+\psi_{22})\end{pmatrix}\right]\begin{pmatrix}\dot{q}_1\\ \dot{q}_2\end{pmatrix}+\begin{pmatrix}\omega_1^2 & 0\\ 0 & \omega_2^2\end{pmatrix}\begin{pmatrix}q_1\\ q_2\end{pmatrix}=\mathbf{0}. \tag{4.29}$$

The corresponding normal form for $\Omega \approx |\omega_1 \mp \omega_2|$ is derived according to the procedure described in [40] and is given by

$$\dot{r}_1 = -\frac{\delta_{11}}{2}\, r_1 - \frac{\varepsilon_{\delta,12}}{4}\cos(\varphi)\, r_2, \tag{4.30a}$$

$$\dot{r}_2 = -\frac{\delta_{22}}{2}\, r_2 - \frac{\varepsilon_{\delta,21}}{4}\cos(\varphi-\psi_c)\, r_1, \tag{4.30b}$$

$$\dot{\varphi} = \omega_{2\ (\mp)}\,\omega_1 - \Omega + \frac{\varepsilon_{\delta,12}\sin(\varphi)\, r_2^2 + \varepsilon_{\delta,21}\sin(\varphi-\psi_c)\, r_1^2}{4\, r_1 r_2}, \tag{4.30c}$$

while the upper (lower) sign applies for difference (sum) combination resonance. As only the off-diagonal excitation terms are involved, the phase angles ψ_{12} and ψ_{21} are replaced by $\psi_{21} = \psi_c$, $\psi_{12} = 0$. Similar to the case of displacement-proportional excitation, the normal form provides an autonomous approximation, while all three equations are nonlinear and coupled. For this reason in order to solve for the LCEs further linearization and transformations are required, so that the eventual analytical expression is way too complex to be sensibly interpreted. The most important features are extracted from the extrema of the LCEs, analogously to the case with displacement proportional excitation.The eigenvalues for difference and sum combination resonance are given by

$$\nu_{1,2} = -\frac{\delta_{11}+\delta_{22}}{4} \mp \frac{1}{4}\sqrt{(\delta_{11}-\delta_{22})^2 + \varepsilon_{\delta,12}\varepsilon_{\delta,21}\cos(\varphi_0)\cos(\varphi_0-\psi_c)}. \tag{4.31}$$

Again, the product of the variation coefficients $\varepsilon_{\delta,ij}$ will be further denoted by ε_δ^2, keeping in mind that both off-diagonal excitation terms are involved.For $\varepsilon_\delta^2 = 0$ the approximated eigenvalues of the original autonomous system with $\nu_i = -\frac{1}{2}\delta_{ii}$, $i = 1, 2$, are obtained. For $\varepsilon_\delta^2 > 0$ and $\delta_{11} \neq \delta_{22}$, $\delta_{ii} \neq 0$, stabilizing (anti-resonance) as well as destabilizing (resonance) action of parametric excitation can be observed. Whether the area around $\Omega \approx |\omega_1 \mp \omega_2|$ is stabilized or destabilized, or even both at the same time, depends primarily on the phase angle ψ_c, but also on the relation of the damping terms, i.e., $\delta_{11} \gtrless \delta_{22}$. Eq. (4.31) shows that the effects, in contrast to displacement-proportional excitation, are identical (and not opposite!) at both combination resonance frequencies. Again, three representative cases

are treated: $\psi_c = 0$, $\psi_c = \pi$ and $\psi_c \neq \pi z$, $z \in \mathbb{Z}$. Further, as the largest LCE is the one decisive for stability, only the real part of the eigenvalue with the plus sign before the root in Eq. (4.31) will be considered.

4.3.1 Parametric anti-resonance

In the first case with $\psi_c = \pi$ the largest LCE reads

$$\Lambda = \mathrm{Re}\left(-\frac{\delta_{11}+\delta_{22}}{4} + \frac{1}{4}\sqrt{\left(\delta_{11}-\delta_{22}\right)^2 - \varepsilon_\delta^2 \cos^2\left(\varphi_0\right)}\right). \tag{4.32}$$

Assuming $\delta_{11} \neq \delta_{22}$ and with $\cos^2\left(\varphi_0\right) \geq 0$ for all φ_0, the radicand is reduced for all $\varepsilon_\delta^2 > 0$ compared to the unperturbed case with $\varepsilon_\delta^2 = 0$. This leads to a lower Λ and thus to an increased stability of the trivial solution compared to the unperturbed autonomous case. Obviously, this effect of anti-resonance disappears in case of uniform damping with $\delta_{11} = \delta_{22} = \delta_u$, as the radicand instantly becomes negative and the root expression becomes imaginary so that parametric excitation does not contribute to a change of the largest LCE. The highest stabilization through anti-resonance is achieved for vanishing or negative radicand in Eq. (4.32) and is equal to the highest stabilization $\Lambda^{*,s}$ given by

$$\Lambda^{*,s} = -\frac{1}{4}(\delta_{11}+\delta_{22}), \tag{4.33}$$

which is identical to the case of displacement-proportional parametric excitation, Eq. (4.5). In order to achieve $\Lambda^{*,s}$ at the point of the strongest stabilization with $\cos^2\left(\varphi_0\right) = 1$, the minimum amplitude of variation

$$\varepsilon_\delta^{2,*} = \left(\delta_{11}-\delta_{22}\right)^2 \tag{4.34}$$

is required.

4.3.2 Parametric resonance

In the second case with $\psi_c = 0$ the largest LCE reads

$$\Lambda = \mathrm{Re}\left(-\frac{\delta_{11}+\delta_{22}}{4} + \frac{1}{4}\sqrt{\left(\delta_{11}-\delta_{22}\right)^2 + \varepsilon_\delta^2 \cos^2\left(\varphi_0\right)}\right). \tag{4.35}$$

Due to the summation of two positive terms, the radicand will remain positive for all ε_δ^2 and φ_0, so that for $\psi_c = 0$ the area around the difference combination resonance is always destabilized. Unlike for the anti-resonance, there is no upper limit for the destabilization – an increasing amplitude of excitation ε_δ^2 will always lead to a stronger destabilization. For the same reason, the destabilizing effect persists also for the case of uniform damping, while the stabilizing effect disappears. These two first cases represent the current perception with resonance and anti-resonance appearing separately either at the sum or at the difference combination resonance frequencies.

4.3.3 Simultaneous parametric resonance and anti-resonance

In a general case with $\psi_c \neq \pi z$, $z \in \mathbb{Z}$, as described by Eq. (4.31), the sign of the parametric contribution term depends on φ_0, which, as shown in Eq. (4.30c), depends on Ω. In this way, there will be both stabilizing and destabilizing effects in the vicinity of the combination resonance depending on the excitation frequency. Though the analytical expression for φ_0 and therefore for Λ can be obtained in a lengthy transformation process from Eq. (4.30c), the result is a very complex expression which does not provide any insight. However, important information considering the location and the amplitude of the strongest stabilization and destabilization can be extracted considering only the extrema of $\cos(\varphi_0)\cos(\varphi_0 - \psi_c)$ with respect to φ_0.

First, the amplitudes of the highest stabilization and destabilization in terms of the corresponding LCEs are considered. With the maxima and minima of the term $\cos(\varphi_0)\cos(\varphi_0 - \psi_c)$ given as follows

$$\varphi_{0,max} = \frac{\psi_c}{2}, \tag{4.36a}$$

$$\varphi_{0,min} = \frac{\psi_c + \pi}{2}, \tag{4.36b}$$

the LCEs describing the highest stabilization Λ^s and destabilization Λ^d points in the vicinity of a combination resonance read

$$\Lambda^{s,d} = \mathrm{Re}\left(-\frac{\delta_{11}+\delta_{22}}{4} + \frac{1}{4}\sqrt{(\delta_{11}-\delta_{22})^2 + \frac{\varepsilon_\delta^2}{2}(\cos(\psi_c) \mp 1)}\right), \tag{4.37}$$

while the upper sign in the radicand corresponds to the stabilization effect. The above equation vividly demonstrates the influence of the phase shift ψ_c, describing the emergence

and decay of resonance and anti-resonance. From Eq. (4.37) it is also obvious that the separate appearance of resonance and anti-resonance is only a special case for $\psi_c = \pi z$, while, in general, for $\psi_c \neq \pi z$, $z \in \mathbb{Z}$, and $\delta_{11} \neq \delta_{22}$ both effects are present. Apparently, the conditions for the global stability effects as well as for simultaneous resonance and anti-resonance are the same. The most significant difference to the case of displacement-proportional excitation is that the magnitude of contribution of parametric excitation does not depend on the eigenfrequencies of the system – it depends solely on the parametric excitation parameters ε_δ^2 and Ω. Though, it has to be noted that the damping terms, and with this also the variation of damping ε_δ^2, are, in general, several orders of magnitude smaller than the stiffness terms. Further, Eq. (4.37) can be easily solved for the threshold value of the excitation amplitude leading to instability. Setting $\Lambda^d = 0$, the threshold value is given by

$$\varepsilon_{\delta,th}^2 = \frac{8\delta_{11}\delta_{22}}{1 + \cos(\psi_c)}, \tag{4.38}$$

which is, again, equal for the sum and the difference combination resonance areas.

Figure 4.9 depicts $\Lambda^{s,d}$ for different values of ψ_c with $\varepsilon_\delta^2 > \varepsilon_\delta^{2,*}$. Compared to the unperturbed case, $\varepsilon_\delta^2 = 0$, parametric excitation introduces resonance and anti-resonance depending on ψ_c. It can be seen that the highest stabilization is limited to $\Lambda^s = \Lambda^{*,s}$ due to the negative radicand in Eq. (4.37). The results of the semi-analytical approximation, Eq. (4.37), are also compared to numerical Floquet analysis of the original system showing excellent agreement. However, while the semi-analytical results are given by a compact and meaningful expression, the numerical results are obtained from a sweep over Ω for each specified ψ_c and a constant ε_δ^2 requiring considerable computational effort.

Of great importance is also the location of the stabilizing and destabilizing effects, Ω^s and Ω^d respectively, which depends on the phase angle ψ_c as well as on the relation of the damping coefficients δ_{11} and δ_{22}. The approximate analytical expression can be obtained by substituting Eq. (4.36) into Eq. (4.30c) and solving for Ω. The location of the strongest stabilization and destabilization is given by

$$\Omega^s = \omega_2 \,\overline{(+)}\, \omega_1 + \frac{1}{2}(\delta_{11} - \delta_{22}) \cot\left(\frac{\psi_c}{2}\right) \quad \text{for } \varepsilon_\delta^2 < \varepsilon_\delta^{2,*}, \tag{4.39a}$$

$$\Omega^{*,s} = \omega_2 \,\overline{(+)}\, \omega_1 + \frac{\varepsilon_\delta^2 \sin(\psi_c)}{4(\delta_{11} - \delta_{22})} \quad \text{for } \varepsilon_\delta^2 > \varepsilon_\delta^{2,*}, \tag{4.39b}$$

$$\Omega^d = \omega_2 \,\overline{(+)}\, \omega_1 - \frac{1}{2}(\delta_{11} - \delta_{22}) \tan\left(\frac{\psi_c}{2}\right), \tag{4.39c}$$

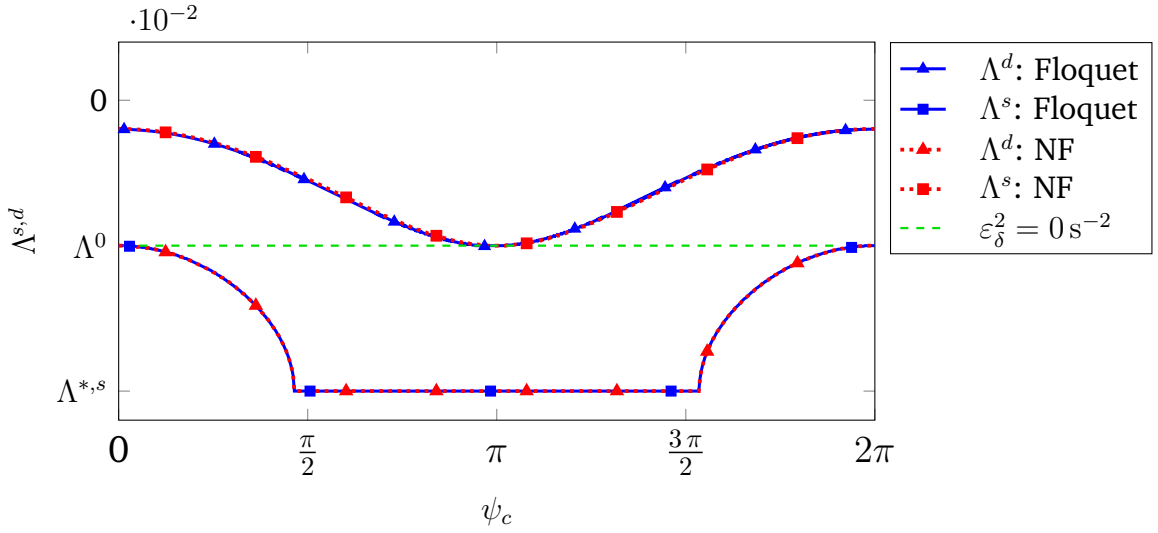

Figure 4.9: Amplitude of highest stabilization Λ^s and highest destabilization Λ^d in system (4.29) with $\Omega \approx |\omega_1 - \omega_2|$, $\varepsilon_\delta^2 = (0.15\,\mathrm{s}^{-2})^2$, $\omega_1 = 1\,\mathrm{s}^{-1}$, $\omega_2 = \sqrt{3}\,\mathrm{s}^{-1}$, $\delta_{11} = 0.05\,\mathrm{s}^{-1}$, $\delta_{22} = 0.15\,\mathrm{s}^{-1}$, $\delta_c = 0\,\mathrm{s}^{-1}$, $\psi_{12} = 0$, $\psi_{21} = \psi_c$, $\psi_{22} = 0$

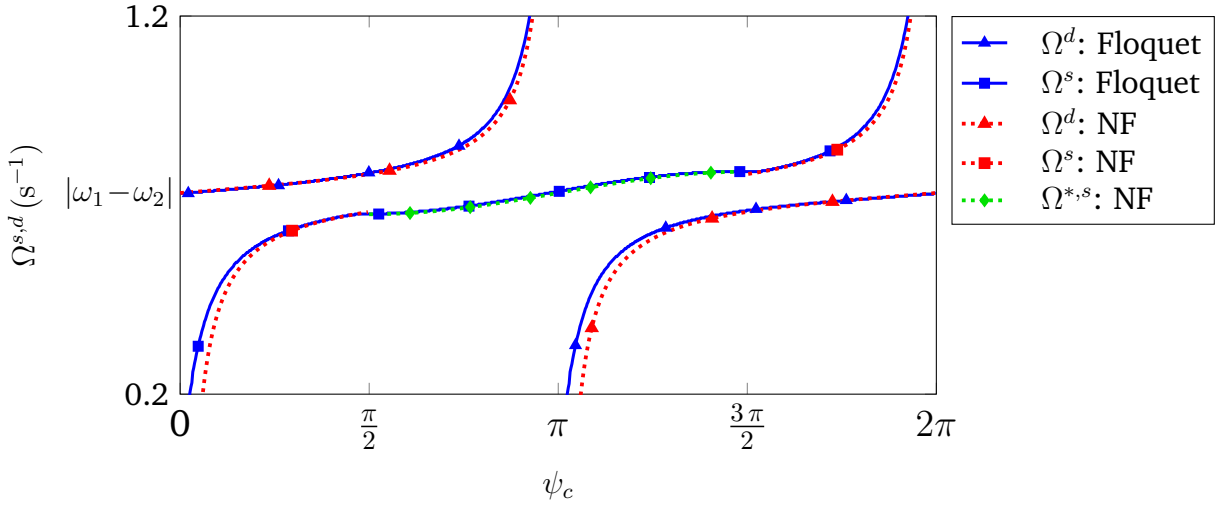

Figure 4.10: Location of the highest stabilization Ω^s and the highest destabilization Ω^d in system (4.29) with $\Omega \approx |\omega_1 - \omega_2|$, $\varepsilon_\delta^2 = (0.15\,\mathrm{s}^{-2})^2$, $\omega_1 = 1\,\mathrm{s}^{-1}$, $\omega_2 = \sqrt{3}\,\mathrm{s}^{-1}$, $\delta_{11} = 0.0\,\mathrm{s}^{-1}5$, $\delta_{22} = 0.15\,\mathrm{s}^{-1}$, $\delta_c = 0\,\mathrm{s}^{-1}$, $\psi_{12} = 0$, $\psi_{21} = \psi_c$, $\psi_{22} = 0$

with

$$\varepsilon_{\delta}^{2,*} = \frac{2(\delta_{11} - \delta_{22})^2}{1 - \cos(\psi_c)}, \tag{4.40}$$

while the upper (lower) sign holds for the difference (sum) combination resonance area. Again, the expressions are very compact and clear and do not depend on ε_{δ}^2, except the maximum stabilization $\Lambda^{*,s}$ is reached. Though, it has to be kept in mind that these results are obtained from an approximation up to the first power of ε_{δ}^2 derived for $\Omega \approx |\omega_2 \mp \omega_1|$. There might be effects of higher orders or due to superposition of different resonance effects.

Figure 4.10 clearly demonstrates the changing positions of stabilized and destabilized areas depending on the phase angle ψ_c. For $\frac{\pi}{2} < \psi_c < \frac{3\pi}{2}$ the limit of the highest stabilization $\Lambda^{*,s}$ is active, Fig. 4.9. Therefore, in this frequency region the location of the strongest stabilization is defined by Eq. (4.39b), otherwise Eq. (4.39a) holds. Figure 4.10 also shows that resonance and anti-resonance come closest for $\psi_c = \frac{\pi}{2}$ and $\psi_c = \frac{3\pi}{2}$. The agreement between the numerical Floquet analysis and the semi-analytical results is very good. These findings also agree with findings reported in [40] for the case of non-resonant velocity-proportional excitation.

Of interest is also the transition point Ω^0 between the stabilizing and the destabilizing behavior. It can be obtained from the zero solution of the parametric contribution term in Eq. (4.31) and the subsequent solving of the linearized Eq. (4.30c) for Ω:

$$\Omega^0 = \omega_2 \,{}_{(\bar{+})}\, \omega_1 + \frac{1}{2}\left(\delta_{11} - \delta_{22}\right)\cot(\psi_c) + \frac{\varepsilon_{\delta}^2 \sin(\psi_c)}{8(\delta_{11} - \delta_{22})}, \tag{4.41a}$$

while the upper (lower) sign holds for the difference (sum) combination resonance. The characteristic points $P^s(\Omega^s, \Lambda^{(*),s})$, $P^d(\Omega^d, \Lambda^d)$ and $P^0(\Omega^0, \Lambda^0)$ describing the location and the magnitude of the strongest stabilization and destabilization as well as of the transition point are presented in Table 4.2.

The above analysis provides a deep insight into the stability behavior of an $\mathbf{MDK} + \mathbf{B}(t)$ system around the combination resonance frequencies, completing the findings obtained from the non-resonant parametric excitation. The derived compact expressions can also be used as a tool for designing a system with desired properties concerning the location and the magnitude of resonance and anti-resonance. In particular, the influence of the off-diagonal phase shift parameter ψ_c, dramatically affecting the stability behavior, is described clearly and precisely.

The most significant difference to the case with displacement-proportional excitation is

Combination resonance $\Omega \approx \lvert\omega_1 \mp \omega_2\rvert$	
Λ^s	$\mathrm{Re}\left(-\frac{\delta_{11}+\delta_{22}}{4}+\frac{1}{4}\sqrt{(\delta_{11}-\delta_{22})^2+\frac{\varepsilon_\delta^2}{2}\left(\cos\left(\psi_c\right)-1\right)}\right)$
Λ^d	$\mathrm{Re}\left(-\frac{\delta_{11}+\delta_{22}}{4}+\frac{1}{4}\sqrt{(\delta_{11}-\delta_{22})^2+\frac{\varepsilon_\delta^2}{2}\left(\cos\left(\psi_c\right)+1\right)}\right)$
Ω^s, $\varepsilon_\delta^2 < \varepsilon_\delta^{2,*}$	$\omega_2 \mp \omega_1 + \frac{1}{2}\left(\delta_{11}-\delta_{22}\right)\cot\left(\frac{\psi_c}{2}\right)$
Ω^s, $\varepsilon_\delta^2 > \varepsilon_\delta^{2,*}$	$\omega_2 \mp \omega_1 + \frac{\varepsilon_\delta^2 \sin(\psi_c)}{4(\delta_{11}-\delta_{22})}$
Ω^d	$\omega_2 \mp \omega_1 - \frac{1}{2}\left(\delta_{11}-\delta_{22}\right)\tan\left(\frac{\psi_c}{2}\right)$
Ω^0	$\omega_2 \mp \omega_1 + \frac{1}{2}\left(\delta_{11}-\delta_{22}\right)\cot(\psi_c) + \frac{\varepsilon_\delta^2 \sin(\psi_c)}{8(\delta_{11}-\delta_{22})}$
$\varepsilon_\delta^{2,*}$	$\frac{2(\delta_{11}-\delta_{22})^2}{1-\cos(\psi_c)}$
$\varepsilon_{\delta,th}^2$	$\frac{8\delta_{11}\delta_{22}}{1+\cos(\psi_c)}$
with $\Lambda^{*,s} = -\frac{1}{4}(\delta_{11}+\delta_{22})$ the strongest stabilization for $\varepsilon_\delta^2 > \varepsilon_\delta^{2,*}$	

Table 4.2: Coordinates of the characteristic points $P^s(\Omega^s, \Lambda^s)$, $P^d(\Omega^d, \Lambda^d)$, $P^0(\Omega^0, \Lambda^0)$ for asynchronous parametric excitation in $\mathbf{MDK} + \mathbf{B}(t)$ system (4.29) with $\varepsilon_{\delta,ij} = \varepsilon_\delta$, $i, j = 1, 2$.

that the stability contribution of parametric excitation does not depend on the magnitude of the circular eigenfrequencies. While for displacement-proportional excitation, the impact of PE diminishes with increasing eigenfrequencies, for velocity-proportional excitation, the contribution of PE remains the same, Eqs. (4.37), (4.11). This relation may be of particular importance for systems with high eigenfrequencies, in particular MEMS, where displacement-proportional PE would require very high amplitudes of variation. At the same time it has to be kept in mind that velocity-proportional, i.e., damping, terms are, in mechanical systems, naturally of a much smaller magnitude than the displacement-proportional, i.e., stiffness, terms.

4.4 Simultaneous displacement- and velocity-proportional excitation

The characteristic features of simultaneous displacement- and velocity-proportional excitation can be derived in the same way, however, the obtained approximate analytical expressions are increasingly complex and cannot provide as much insight as in the case of single displacement- or velocity-proportional excitation. Nevertheless, certain characteristic features can still be recognized. The following system is analyzed by the method of normal forms in order to obtain its approximate autonomous representation in the vicinity of combination resonances:

$$\begin{pmatrix} 1 & 0 \\ 0 & 1 \end{pmatrix} \begin{pmatrix} \ddot{q}_1 \\ \ddot{q}_2 \end{pmatrix} + \left[\begin{pmatrix} \delta_{11} & \delta_c \\ \delta_c & \delta_{22} \end{pmatrix} + \begin{pmatrix} \varepsilon_{\delta,11} \cos(\Omega t) & \varepsilon_{\delta,12} \cos(\Omega t + \psi_{12}) \\ \varepsilon_{\delta,21} \cos(\Omega t + \psi_{21}) & \varepsilon_{\delta,22} \cos(\Omega t + \psi_{22}) \end{pmatrix} \right] \begin{pmatrix} \dot{q}_1 \\ \dot{q}_2 \end{pmatrix} + \left[\begin{pmatrix} \omega_1^2 & 0 \\ 0 & \omega_2^2 \end{pmatrix} + \begin{pmatrix} \varepsilon_{\kappa,11} \cos(\Omega t + \zeta_{11}) & \varepsilon_{\kappa,12} \cos(\Omega t + \zeta_{12}) \\ \varepsilon_{\kappa,21} \cos(\Omega t + \zeta_{21}) & \varepsilon_{\kappa,22} \cos(\Omega t + \zeta_{22}) \end{pmatrix} \right] \begin{pmatrix} q_1 \\ q_2 \end{pmatrix} = \mathbf{0}. \tag{4.42}$$

The corresponding normal form for $\Omega \approx |\omega_1 \mp \omega_2|$ is then given by

$$\dot{r}_1 = -\frac{\delta_{11}}{2}\, r_1 - \frac{1}{4}\left(\varepsilon_{\delta,12}\cos\left(\varphi-\psi_{12}\right) + \frac{\varepsilon_{\kappa,12}}{\omega_2}\sin\left(\varphi-\zeta_{12}\right)\right) r_2, \tag{4.43a}$$

$$\dot{r}_2 = -\frac{\delta_{22}}{2}\, r_2 - \frac{1}{4}\left(\varepsilon_{\delta,21}\cos\left(\varphi-\psi_{21}\right) \mathbin{\overline{(+)}} \frac{\varepsilon_{\kappa,21}}{\omega_1}\sin\left(\varphi-\zeta_{21}\right)\right) r_1, \tag{4.43b}$$

$$\begin{aligned}\dot{\varphi} = \omega_2 \mathbin{(\overline{+})} \omega_1 - \Omega + \frac{\varepsilon_{\delta,12}\sin(\varphi-\psi_{12})\, r_2^2 + \varepsilon_{\delta,21}\sin(\varphi-\psi_{21})\, r_1^2}{4\, r_1 r_2} \\ - \frac{\varepsilon_{\kappa,12}\cos(\varphi-\zeta_{12})\omega_1\, r_2^2 \mathbin{(\overline{+})} \varepsilon_{\kappa,21}\cos(\varphi-\zeta_{21})\omega_2\, r_1^2}{4\,\omega_1\omega_2\, r_1 r_2},\end{aligned} \tag{4.43c}$$

while the upper (lower) sign applies for difference (sum) combination resonance. It is easy to see that the terms attributed to parametric excitation are simply composed of individual terms associated with single displacement- and velocity-proportional excitation, Eqs. (4.2), (4.30). However, when considering the LCEs, the impact of simultaneous parametric excitation is not simply a combination of single excitations; instead, there are additional multiplicative interaction terms:

$$\Lambda = \mathrm{Re}\left(-\frac{\delta_{11}+\delta_{22}}{4} + \frac{1}{4}\sqrt{\left(\delta_{11}-\delta_{22}\right)^2 + \varepsilon_\delta^2 E_\delta + \varepsilon_\delta\varepsilon_\kappa E_{\delta\kappa} \mathbin{\overline{(+)}} \varepsilon_\kappa^2 E_\kappa}\right) \tag{4.44}$$

with

$$E_\delta = \cos\left(\varphi_0-\psi_{12}\right)\cos\left(\varphi_0-\psi_{21}\right), \tag{4.45a}$$

$$E_{\delta\kappa} = \mathbin{\overline{(+)}}\frac{\cos(\varphi_0-\psi_{12})\sin(\varphi_0-\zeta_{21})}{\omega_1} + \frac{\sin(\varphi_0-\zeta_{12})\cos(\varphi_0-\psi_{21})}{\omega_2}, \tag{4.45b}$$

$$E_\kappa = \frac{\sin\left(\varphi_0-\zeta_{12}\right)\sin\left(\varphi_0-\zeta_{21}\right)}{\omega_1\omega_2}, \tag{4.45c}$$

while the upper (lower) sign applies for difference (sum) combination resonance and assuming $\varepsilon_{\delta,ij} = \varepsilon_\delta$ and $\varepsilon_{\kappa,ij} = \varepsilon_\kappa$ with $i,j = 1,2$. Due to the many parameters involved and due to the considerably increased complexity, it is not possible to extract concise symbolic expressions for the characteristic points. It is nevertheless clear that in this case there are in general both resonance and anti-resonance at each combination resonance frequency, except for the one special case already outlined by means of the non-resonant normal form. This special case is given by displacement- and velocity-proportional excitations being both synchronous, but shifted by $\pi/2$ with respect to each other, i.e., $\psi_{kl} - \zeta_{lk} = \frac{\pi}{2}(2z+1)$ with $k,l = 1,2$, $k \neq l$ and $z \in \mathbb{Z}$.

4.5 Conclusions

In this chapter the semi-analytical method of normal forms was applied to various dynamical systems under asynchronous parametric excitation in order to derive analytical approximations for the characteristic points. The characteristic points, describing the most important stability features in terms of the Lyapunov characteristic exponents, provide a simple yet powerful tool for studying the coexistence of resonance and anti-resonance.

Starting with the most common case of an $\mathbf{MDK} + \mathbf{C}(t)$ system, the characteristic points are eventually obtained also for a complex $\mathbf{MDGKN} + \mathbf{C}(t)$ system. The results show that resonance and anti-resonance coexist at each combination resonance frequency for the general case of asynchronous parametric excitation. Using the concise symbolical expressions for the characteristic points, the assessment of what kind of resonance to expect (resonance, anti-resonance or both) can now be easily made for a circulatory system based on the equations of motion alone.

Furthermore, also velocity-proportional asynchronous parametric excitation ($\mathbf{MDK}+\mathbf{B}(t)$ system) is studied establishing a direct comparison to the displacement-proportional case. The most apparent difference is identified in the strength of parametric resonance effects not being dependent on the eigenfrequencies of the system. In this way, a certain level of parametric velocity-proportional variation leads to the same resonance impact in systems with low and with high eigenfrequencies. On the other hand, in order to keep the resonance effect at the same level in case of displacement-proportional excitation, the amplitude of variation has to grow proportionally to the eigenfrequencies.

Eventually, the $\mathbf{MDGKN} + \mathbf{C}(t)$ system is also used to discuss the limitations of the derived approximate expressions. The implications of different assumptions made during the normal form analysis, e.g., assumption of small parameters or neglecting higher order terms, are vividly demonstrated. It is emphasized that the symbolic expressions cannot fully substitute numerical calculations, in particular in increasingly complex systems. However, the symbolic are essential for the profound understanding of the stability phenomena and, keeping in mind the assumptions, can still be used for quantitative analysis and design.

5 Simulation-based validation of coexistence

A validation of recent theoretical results on the stability effects of asynchronous parametric excitation is presented. In particular, the coexistence of both resonance and anti-resonance at each combination resonance frequency is to be confirmed on a close-to-experiment simulation model. The simulation model reproduces the experimental setup developed by Schmieg in 1976, remaining the only experimental study on asynchronous excitation to this day. The model consists of two oscillating electronic circuits with feedback-free coupling through parametric excitation. In contrast to a mechanical system, the phase relations of the parametric excitation terms in an electronic system can be easily adjusted. The implementation of the simulation model is performed in the electronic circuit simulation software LTspice. The electronic model itself is first validated against the experimental results obtained by Schmieg and is then used to confirm the theoretical findings. The results of the electronic circuit simulation show excellent qualitative and quantitative agreement with analytical approximations confirming the coexistence of resonance and anti-resonance effects near a combination resonance frequency.

5.1 Introduction

The theoretical results concerning these newly discovered stabilizing effects of asynchronous excitation have to be verified and validated in order to acquire credibility. The semi-analytical results obtained by the method of normal forms, e.g., as shown in Table 4.1, have already been verified by comparison with numerical integration, i.e., Floquet analysis, in section 4.1.3. However, while the unstable behavior has been validated by Schmieg by conducting experimental studies on an electronic circuit system, the stable behavior has yet to be validated on a physical system. The purpose of the present section is to *validate* the stabilizing effects and, in particular, the coexistence of resonance and anti-resonance at a

combination resonance frequency. As indicated by the previous analytical investigations in chapters 3 and 4, specific phase relations, depending on the structure of system matrices, are required for the coexistence of resonance and anti-resonance. For systems with purely symmetric system matrices, i.e., systems without circulatory terms, only the phase shift in the off-diagonal terms leads to such effects. For more complex systems featuring skew-symmetric coupling through circulatory terms, there are several additional phase relations possible, which are not limited to the phase shift in the antidiagonal. Considering mechanical systems, the practical realization of the seemingly more simple case appears to be impossible – there are no mechanical systems known featuring phase-shifted off-diagonal parametric excitation terms. On the other hand, the more complex case with skew-symmetric system matrices and necessary phase relations of parametric excitation terms is more likely to appear in mechanical systems. For example, the minimal model of a disk brake with asymmetric bearing, as treated in [70, 40], does indeed fulfill all necessary conditions for the coexistence of resonance and anti-resonance. However, as to the question of validation, such a complex system featuring also gyroscopic terms along with circulatory terms is rather inadequate for this purpose – the interaction and superposition of different effects make it impossible to study the implications of individual system parameters. For this reason, the validation of the newly discovered stability effects is performed using a close-to-experiment simulation setup of an electronic system based on the real experiment conducted by Schmieg [68].

According to the IEEE Standard for Validation of Computational Electromagnetics Computer Modeling and Simulations, suitable validation references are not limited to measurements, i.e., "silicon data". Another suitable reference for validation may be also obtained from comparison of two different modeling techniques [35]. If the used techniques are different enough, then high confidence in the results can be obtained [23]. For this purpose, additionally to the solution of differential equations, a detailed electronic system is implemented in the electronic circuit simulation software LTspice XVII, which is based on SPICE electronic circuit simulator [1]. SPICE, standing for *Simulation Program with Integrated Circuit Emphasis*, is the worldwide standard integrated circuit simulator widely used in education, research and industry. The invention of SPICE in 1970 was recognized as a significant technical achievement and awarded an IEEE Milestone in 2011 [36]. With the simulation results being very close to real silicon data, SPICE is considered as a "golden reference" in industry and is also used for validation [60]. In the present chapter, the electronic simulation model itself is first validated by means of the existing experimental data. Based on this validated model, the theoretical findings concerning the coexistence of

resonance and anti-resonance are to be confirmed. In this way, a simulation-based validation is performed due to the missing real world experimental data.

5.2 Electronic system design

SCHMIEG used an electronic system for the validation of the theoretical findings concerning the instability in case of asynchronous parametric excitation [68]. The stabilization effects could have been studied by the same experimental setup, but were not in the scope of interest and remained concealed by stability. In the present contribution, the same experimental setup is reproduced in detail in the electronic circuit simulation program LTspice. In order for the LTspice simulation model to provide a suitable validation reference in compliance with the IEEE standard [35], it has to be different enough from the other method used for analysis. This is ensured by constructing a detailed electronic model containing various components like operational amplifiers and amplitude modulators, while the numerical and the semi-analytical results are based on abstract differential equations representing the conceptual model of the underlying system. The close-to-experiment simulation model itself will be first validated against the available experimental data in order to establish confidence in the model and later it will be used to confirm the theoretical results concerning the stabilizing effects of parametric excitation.

Analogously to mechanical oscillators, oscillating circuits can as well be realized using electronic components. An RLC electronic circuit consists of three main components: resistor (R), inductor (L) and capacitor (C). The behavior of an RLC circuit is analogous to a one-dimensional damped mechanical oscillator, while resistance corresponds to damping, inductance to mass and capacitance to the inverse of stiffness (compliance) [6]. The electronic system analyzed in the following consists of two RLC circuits (RLC1 and RLC2) coupled through parametric excitation without feedback. The voltage from one RLC circuit is transferred and amplified by means of a buffer amplifier enabling feedback-free coupling. The voltage signal is multiplied with cosine or sine signal (realized as amplitude modulation) introducing parametric excitation. After integration, the signal is then introduced to the second RLC circuit through a voltage-controlled current source. The simulation schematic is presented in Fig. 5.1.

The governing equations of the above system in terms of voltage u_i, with $i = 1, 2$, are obtained applying the KIRCHHOFF's current law. After differentiation, the equations are

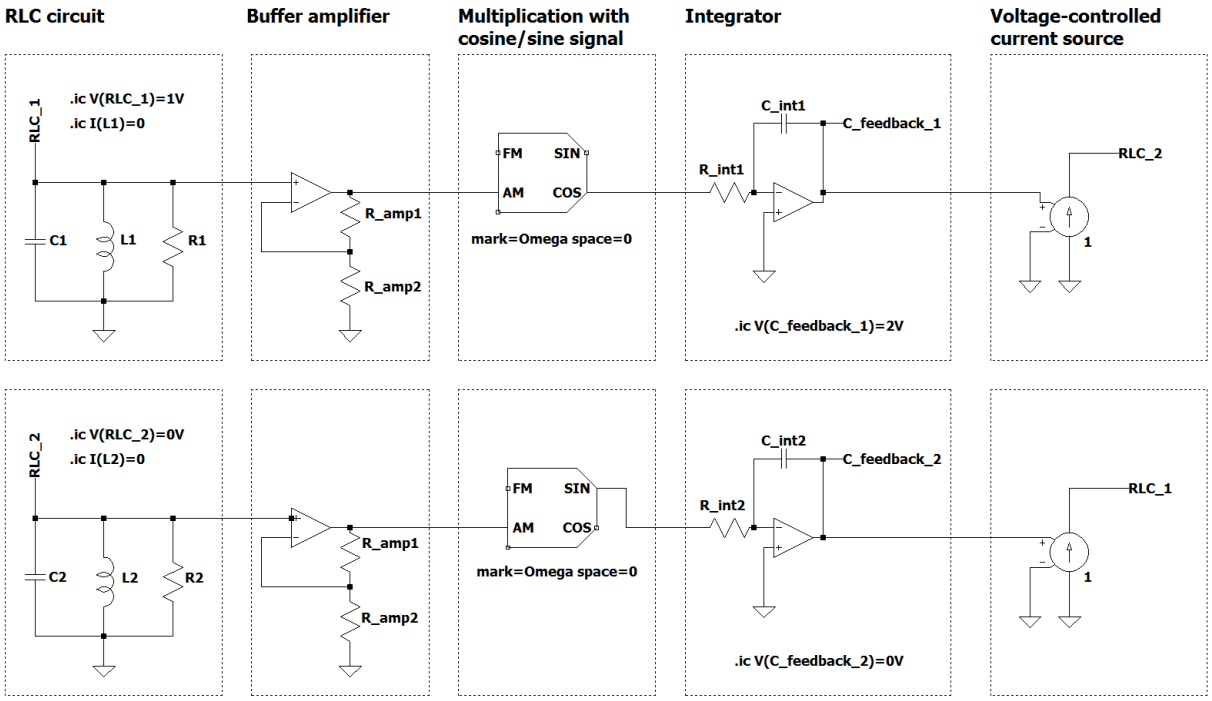

Figure 5.1: Simulation schematic: two RLC circuits with feedback-free coupling through asynchronous parametric excitation

given as follows

$$\begin{pmatrix} 1 & 0 \\ 0 & 1 \end{pmatrix} \begin{pmatrix} \ddot{u}_1 \\ \ddot{u}_2 \end{pmatrix} + \begin{pmatrix} \frac{1}{C_1 R_1} & 0 \\ 0 & \frac{1}{C_2 R_2} \end{pmatrix} \begin{pmatrix} \dot{u}_1 \\ \dot{u}_2 \end{pmatrix} + \left[\begin{pmatrix} \frac{1}{C_1 L_1} & 0 \\ 0 & \frac{1}{C_2 L_2} \end{pmatrix} + \begin{pmatrix} 0 & -\frac{1}{C_1 R_{int,1}} \cos(\Omega t) \\ -\frac{1}{C_2 R_{int,2}} \cos(\Omega t + \zeta_c) & 0 \end{pmatrix} \right] \begin{pmatrix} u_1 \\ u_2 \end{pmatrix} = \mathbf{0}, \tag{5.1}$$

where C_i, R_i and L_i are the capacitance, resistance and inductance values of the RLC circuits respectively. $R_{int,i}$ represents the resistance in the integration block through which the amplitude of parametric excitation will be controlled. Obviously, Eqs. (4.1) and (5.1) have the same structure. According to the mechanical–electrical analogy, the following equivalence is given: The damping coefficients δ_{ii} correspond to $\frac{1}{C_i R_i}$, the squared natural frequencies ω_i^2 correspond to $\frac{1}{C_i L_i}$, and the amplitude of variation ε is given by $-\frac{1}{C_i R_{int,i}}$. In the following, the notation used in the general formulation in Eq. (4.1) will be used for the electrical system as well. In order to obtain the same natural eigenfrequencies and damping values as in the experiments done by Schmieg, the parameters of the RLC circuits are set

Notation symbol	Expression	Numerical value	Unit	Parameter description
C_1	-	330	μF	capacitance RLC1
C_2	-	330	μF	capacitance RLC2
R_1	$\frac{1}{\delta_{11}C_1}$	-	Ω	resistance RLC1
R_2	$\frac{1}{\delta_{22}C_2}$	-	Ω	resistance RLC2
L_1	$\frac{1}{C_1\omega_1^2}$	130.138	μH	inductance RLC1
L_2	$\frac{1}{C_2\omega_2^2}$	43.721	μH	inductance RLC2

Table 5.1: Parameters of the RLC circuits with $\omega_1 = 2\pi \cdot 768\,\mathrm{s}^{-1}$, $\omega_2 = 2\pi \cdot 1325\,\mathrm{s}^{-1}$ and variable damping coefficients δ_{ii}

according to Table 5.1.

The stability maps, such as those in Fig. 5.2, identify the transition between the stable and the unstable region and represent a common tool in the analysis of parametrically excited systems. However, they miss a great deal of information about what exactly is happening inside each of the regions. In particular, any potential stabilizing effects cannot be recognized. Therefore, a deeper insight requires the analysis of the Lyapunov characteristic exponents (LCEs). Schmieg investigated only the unstable region and determined the LCEs from the rate of exponential growth of the signals. While this is easily done in the case of an exponentially unstable trivial solution with monotonously growing amplitudes, determining the LCEs from the signals' time history in the stable case is rather complicated and unreliable. The reason is that in the stable case the amplitudes are quickly decaying beating waves, so that an envelope function accounting for the beat effects has to be constructed. Here, the simulation approach in LTspice offers a significant advantage over the real experimental setup: instead of analyzing the time histories, a proper Floquet analysis can be performed on the electronic system providing reliable LCE values. With the ability to precisely define the initial conditions of the simulations and to know the solution at any instant of time, the monodromy matrix, and with this the LCEs, can be calculated with high precision.

In order to perform the Floquet analysis of the electronic system in LTspice for different parameters and to efficiently process the results, a MATLAB script is written (ver. R2018a) [51]. The script coordinates the LTspice runs starting each simulation with appropriate parameters, including the amplitude of parametric excitation $\tilde{\varepsilon}$, the excitation frequency Ω, the damping

coefficients δ_{ii} as well as the phase angle ζ_c. For the post-processing, the results of the LTspice simulation are imported to MATLAB using *LTspice2Matlab* function.

5.3 Validation of the theoretical findings

The electronic LTspice model itself is first validated with respect to its ability to identify the stability boundaries for different excitation frequencies Ω and amplitudes of variation ε. In particular, the ability of the model to represent the shift of the stability boundaries in case of asynchronous excitation is demonstrated. Further, a more detailed investigation of the stability effects in terms of the largest LCE is performed. Here, the electronic model is validated against the experimental data available for the unstable region. The validated model is then used to confirm the stability effects identified by analytical and numerical methods.

In the first step, the data from SCHMIEG's experiments, available only in printed version, are extracted using the software *WebPlotDigitizer* [66]. However, SCHMIEG provides only scarce information on parameter values giving only the eigenfrequencies and the damping coefficients, while other parameters of the electronic circuit such as those defining the amplitude of variation are unknown. Instead, the amplitude is represented by an effective voltage U_{eff} scaled with an unknown factor. Therefore, the amplitude of variation ε has to be determined, which is done by matching the stability boundaries between the experiment and the numerical Floquet analysis for one single value of variation $U_{eff} = 6\,V$ for the uniformly damped system without a phase shift. The following relation is found and used for all subsequent calculations:

$$U_{eff} = 362500\,V \cdot \mathrm{s}^2\ \varepsilon. \tag{5.2}$$

For a better representation, a new amplitude parameter $\tilde{\varepsilon}$ is introduced, which is of the same magnitude as U_{eff}, i.e., $\tilde{\varepsilon} = \varepsilon/362500$.

Fig. 5.2 shows the stability boundaries for a uniformly damped system with $\delta_{11} = \delta_{22} = 70\,\mathrm{s}^{-1}$ and varying phase angle ζ_c. For each case, $\zeta_c = 0$ and $\zeta_c = \pi/2$, four sets of data are compared: SCHMIEG's analytical and experimental data, numerical FLOQUET analysis and electronic circuit simulation with LTspice, denoted further as "analytical", "experiment", "Floquet", and "LTspice" respectively. The comparison shows reasonable qualitative and quantitative agreement between all four data sets, while only for the case of $\zeta_c = \pi/2$ a noticeable deviation can be seen in the lower excitation frequencies Ω. Partially, the

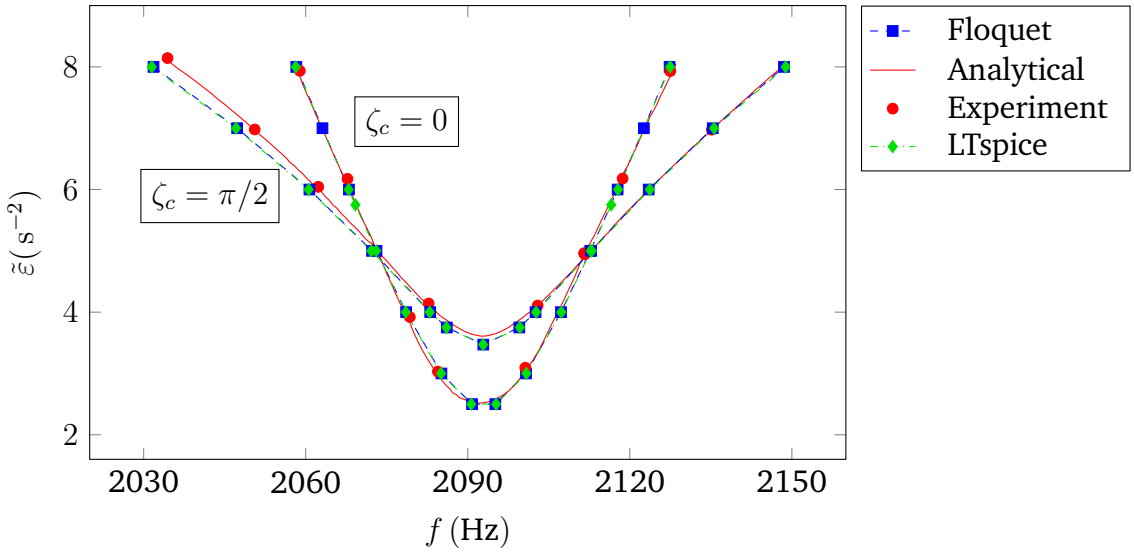

Figure 5.2: Stability boundary: $\delta_{11} = \delta_{22} = 70\,\mathrm{s}^{-1}$, variable phase shift ζ_c

deviation may be explained by errors during the data extraction process from the printed media. This is confirmed by comparing the analytical data obtained from the expressions derived by SCHMIEG against the same analytical data obtained from the digitized plot. Nevertheless, Fig. 5.2 shows that the reconstructed electronic LTspice model is performing well in predicting the stability boundary for synchronous and asynchronous parametric excitation over wide regions of ε and Ω.

Of greater importance is, however, the ability of the LTspice electronic model to reliably reproduce the LCEs of the underlying physical system. SCHMIEG's experiments provide data for the unstable behavior, which are used for the validation of the LTspice model. Figure 5.3 shows the largest LCE of a non-uniformly damped system under parametric excitation with variable phase shift ζ_c. Again, four data sets are presented: analytical, experimental, Floquet and LTspice. A remarkable qualitative and quantitative agreement can be identified between all four data sets in the unstable region with $\Lambda > 0$. In particular, the electronic model predicts the experimental data with great accuracy.

So far, the close-to-experiment LTspice model has been validated with respect to its ability to predict the stability boundaries as well as the LCEs in the unstable region confirming the physical accuracy of the model. The validation domain includes the variation of the phase angle with $\zeta_c = 0, \pi/2$, the variation of the damping ratio with $\delta_{11}/\delta_{22} = 1, 10$ and the variation of the excitation frequency in the frequency range $\Omega = [2030, 2150]$ Hz. The intended application domain of the electronic simulation model lies completely within the validation domain, which additionally increases the confidence in prediction based on this

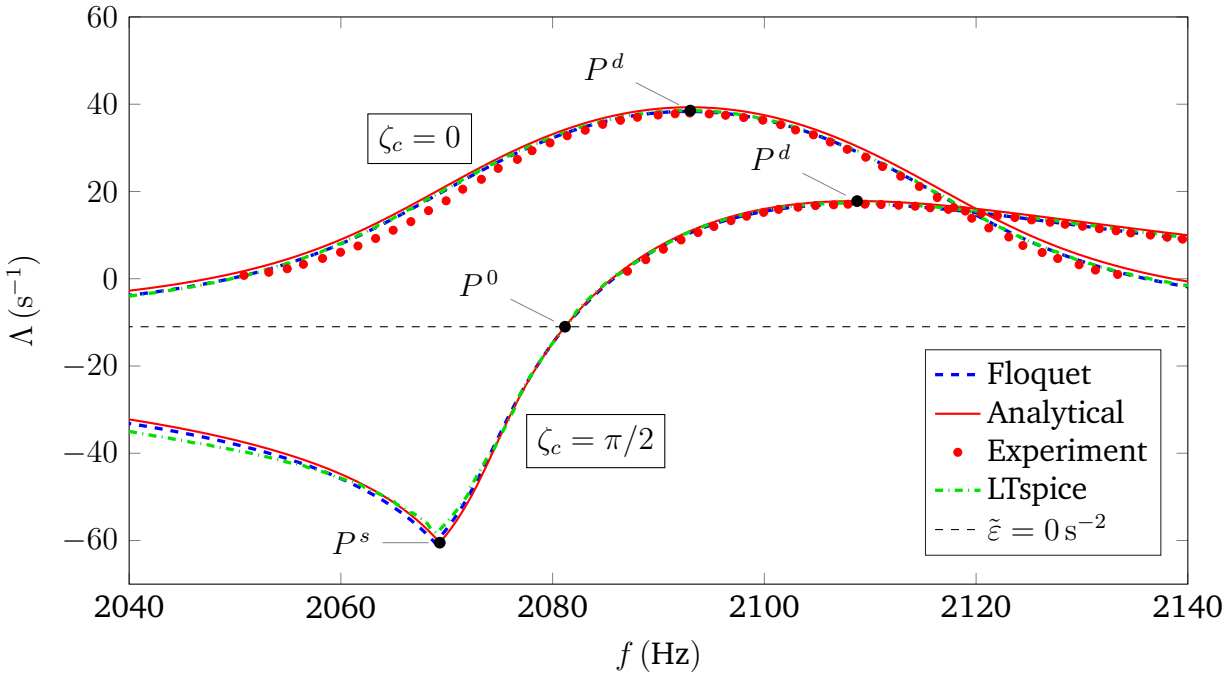

Figure 5.3: Stabilizing and destabilizing effects of asynchronous parametric excitation: $\delta_{11} = 220\,\mathrm{s}^{-1}$, $\delta_{22} = 22\,\mathrm{s}^{-1}$, $\tilde{\varepsilon} = 6\,\mathrm{s}^{-2}$, variable phase shift ζ_c

model. Therefore, it is further assumed that the electronic model represents a suitable validation reference and reliably reproduces the stability behavior of the underlying physical system.

Further comparison between the LTspice electronic circuit simulation, Floquet and analytical results in the stable region is performed in order to prove the physical significance of the predicted stabilizing effects of asynchronous parametric excitation. Figure 5.3 shows, that also in the stable region there is good agreement between the three data sets. Also the analytically derived expressions for the characteristic points P^s, P^d and P^0 match very well with the results of the electronic circuit simulation. In this way, the predicted coexistence of resonance and anti-resonance is confirmed by simulation of a physical system represented by the electronic circuit.

Fig. 5.3 provides a comprehensive insight into the impact of asynchronous excitation covering both the stabilizing and the destabilizing behavior. In the studies performed by Schmieg [68], the impact was characterized as a mere shift of the stability boundaries, while the actual reason – merging of resonance and anti-resonance – was not recognized. In the same manner, Dohnal [15] studied the shifts of the stability boundaries in case of anti-resonance, where particular attention has to be paid to the adjacent resonance area with a sharp transition to possible instability.

5.4 Conclusions

An electronic simulation model was used to validate new theoretical findings on asynchronous parametric excitation. Recent studies revealed coexistence of resonance and anti-resonance at each combination resonance frequency for general phase relations between the excitation terms. While the effects of asynchronous excitation in case of instability were explored and validated by Schmieg in 1976, the more general behavior, including the coexistence of resonance and anti-resonance, remained unrecognized for a long time. The close-to-experiment simulation using the electronic circuit simulation software LTspice confirmed the recent theoretical findings. The use of a simulation model offers significant advantages over an experimental setup and enables a thorough study of stability phenomena in terms of stability boundaries, but also, more importantly, in terms of Lyapunov characteristic exponents, providing deeper insight into all possible stabilizing and destabilizing effects. Further, the simulation also confirmed the usefulness of the more practical characteristic points describing the most prominent stability features like the location and the magnitude of the strongest stabilization and destabilization. Understanding such new stability phenomena might be of importance in the growing field of applications of parametric excitation, in particular in the field of microelectromechanical systems.

6 Fundamental resonances

While the various effects of asynchronous parametric excitation on combination resonances have been extensively discussed in the previous chapters, the impact on the fundamental resonances needs to be studied as well. To the best of the author's knowledge, there are currently no studies on fundamental resonances under asynchronous parametric excitation. Further, with the existing studies on fundamental resonances focusing on the stability boundaries [14, 74, 57], characteristic exponents providing different qualitative insight deserve particular attention: It is important to know how strong instability is or whether a stable region is close to potential instability and threatens to become unstable due to uncertain parameters. This kind of information can only be provided by the LCEs. As the previous chapters proved, circulatory terms might be particularly important in case of asynchronous parametric excitation. Therefore, this chapter presents the analysis of first order fundamental resonance areas for asynchronously excited systems which cannot be decoupled applying modal transformation due to the constant skew-symmetric components in the equations of motion. The systems are studied based on the (approximate) LCEs obtained by means of the normal form transformation. The analysis shows that circulatory terms do not only affect the magnitude of fundamental resonances, but also their occurrence, while the resulting effect is highly sensitive to the phase relations in the parametric excitation terms.

6.1 $\mathrm{MDK} + \mathrm{C}(t)$ system

First, an asynchronously excited system featuring neither circulatory nor gyroscopic terms is investigated:

$$\begin{pmatrix} \ddot{q}_1 \\ \ddot{q}_2 \end{pmatrix} + \begin{pmatrix} \delta_{11} & \delta_c \\ \delta_c & \delta_{22} \end{pmatrix} \begin{pmatrix} \dot{q}_1 \\ \dot{q}_2 \end{pmatrix} + \left[\begin{pmatrix} \omega_1^2 & 0 \\ 0 & \omega_2^2 \end{pmatrix} + \begin{pmatrix} \varepsilon_{11}\cos(\Omega t + \zeta_{11}) & \varepsilon_{12}\cos(\Omega t + \zeta_{12}) \\ \varepsilon_{21}\cos(\Omega t + \zeta_{21}) & \varepsilon_{22}\cos(\Omega t + \zeta_{22}) \end{pmatrix} \right] \begin{pmatrix} q_1 \\ q_2 \end{pmatrix} = \mathbf{0}. \tag{6.1}$$

The corresponding second order normal form accounting for linear ε_{ij} terms for the fundamental resonance area $\Omega \approx 2\omega_i$ is given by

$$\dot{r}_i = \left(-\frac{1}{2}\delta_{ii} + \frac{\varepsilon_{ii}\sin(\zeta_{ii} - 2\varphi_i)}{4\omega_i} \right) r_i, \tag{6.2a}$$

$$\dot{r}_j = -\frac{1}{2}\delta_{jj} r_j, \tag{6.2b}$$

$$\dot{\varphi}_i = \omega_i - \frac{\Omega}{2} - \frac{\varepsilon_{ii}\cos(\zeta_{ii} - 2\varphi_i)}{4\omega_i}, \tag{6.2c}$$

$$\dot{\varphi}_j = \omega_j - \frac{\Omega}{2} \tag{6.2d}$$

with $i, j = 1, 2$ and $i \neq j$. It can be clearly seen that the two degrees of freedom are decoupled and neither the off-diagonal damping terms, nor the off-diagonal excitation terms play a role. Further, unlike in the case of combination resonances, the equations are linear in the amplitude coordinates $r_{i,j}$. In this case the LCEs are given by the coefficients of $r_{i,j}$. After solving Eq. (6.2c) with $\dot{\varphi}_i = 0$ for φ_i and substituting into Eq. (6.2a), the largest LCE is simply given by

$$\Lambda = \max\left\{ \mathrm{Re}\left(-\frac{1}{2}\delta_{ii} + \frac{1}{4}\sqrt{\frac{\varepsilon_{ii}^2}{\omega_i^2} - 4\left(\Omega - 2\omega_i\right)^2} \right), -\frac{1}{2}\delta_{jj} \right\}. \tag{6.3}$$

Remarkably, the approximate expression for the largest LCE Λ over the excitation frequency Ω can be given just as a function of a few system parameters, while all phase angles can be eliminated. The maximum of the resonance is exactly at the resonances frequency and is given by

$$\Lambda^* = \max\left\{ -\frac{1}{2}\delta_{ii} + \frac{\varepsilon_{ii}}{4\omega_i}, -\frac{1}{2}\delta_{jj} \right\}. \tag{6.4}$$

Further, also the expression for the stability boundaries can be easily derived by setting $\Lambda = 0$ and solving for ε_{ii}:

$$\varepsilon_{ii} = 2\omega_1 \sqrt{\delta_{ii}^2 + \left(\Omega - 2\omega_i\right)^2}. \tag{6.5}$$

While the stability boundaries of such asynchronously excited systems have been extensively studied before [25, 67, 45], the symbolic expression for the largest LCE of a fundamental resonance is new.

A comparison of the largest LCE from Eq. (6.3) with numerical Floquet analysis for two

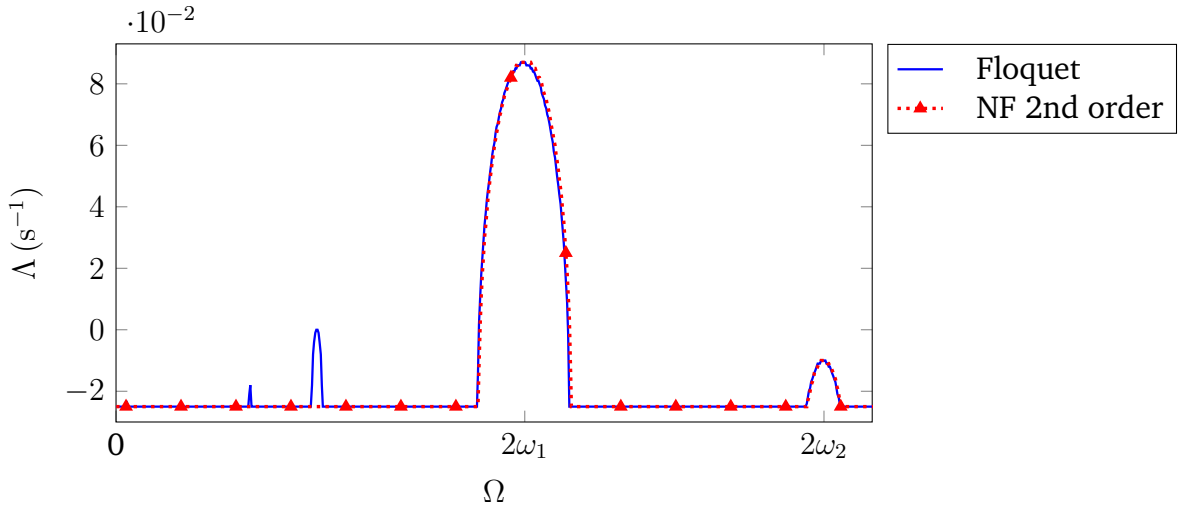

Figure 6.1: Fundamental resonances of system (6.1) with $\varepsilon_{11} = \varepsilon_{22} = 0.45\,\mathrm{s}^{-2}$, $\varepsilon_{12} = \varepsilon_{21} = 0\,\mathrm{s}^{-2}$, $\omega_1 = 1\,\mathrm{s}^{-1}$, $\omega_2 = \sqrt{3}\,\mathrm{s}^{-1}$, $\delta_{11} = 0.05\,\mathrm{s}^{-1}$, $\delta_{22} = 0.15\,\mathrm{s}^{-1}$, $\delta_c = 0\,\mathrm{s}^{-1}$, $\zeta_{11} = \zeta_{12} = \zeta_{21} = \zeta_{22} = 0$

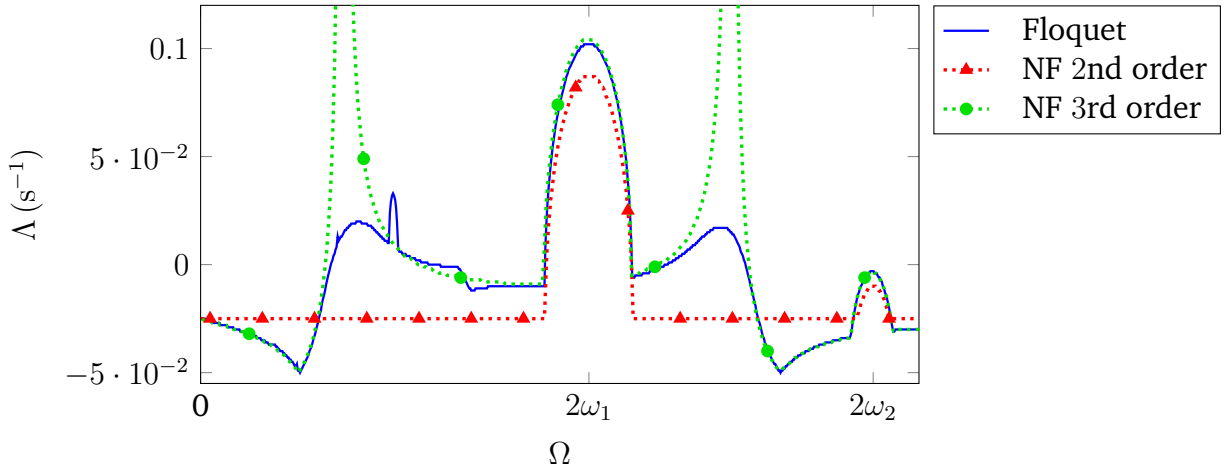

Figure 6.2: Fundamental resonances of system (6.1) with $\varepsilon_{11} = \varepsilon_{12} = \varepsilon_{21} = \varepsilon_{22} = 0.45\,\mathrm{s}^{-2}$, $\omega_1 = 1\,\mathrm{s}^{-1}$, $\omega_2 = \sqrt{3}\,\mathrm{s}^{-1}$, $\delta_{11} = 0.05\,\mathrm{s}^{-1}$, $\delta_{22} = 0.15\,\mathrm{s}^{-1}$, $\delta_c = 0\,\mathrm{s}^{-1}$, $\zeta_{11} = \zeta_{12} = \zeta_{22} = 0$, $\zeta_{21} = -\pi/2$

different parameter sets shows rather different results, Figs. 6.1-6.2. While there is an excellent agreement in the first case with synchronous excitation, Eq. (6.3) does not capture all of the effects in case of asynchronous excitation with a phase shift in the off-diagonal terms. However, the deviation is obviously caused by the appearance of the "global effect", which is rather strong in this example due to the proximity to a combination resonance area. Although, the deviation seems to be substantial, the qualitative behavior at the resonance areas themselves is still captured quite well, while merely the amplitudes are underestimated.

The main source of error in the approximation by means of the normal forms originates from the truncation of higher order terms. In an attempt to obtain a better understanding, the normal form transformation has to be continued to higher order terms. The third order normal form accounting for quadratic ε_{ij} terms for $\Omega \approx 2\omega_i$ is given by

$$\dot{r}_i = \left(-\frac{1}{2}\delta_{ii} + \frac{\varepsilon_{ii}\sin(\zeta_{ii}-2\varphi_i)}{4\omega_i} + \frac{\varepsilon_{ij}\varepsilon_{ji}\Omega\sin(\zeta_{ji}-\zeta_{ij})}{2\left[\Omega^2-(\omega_i-\omega_j)^2\right]\left[\Omega^2-(\omega_i+\omega_j)^2\right]} + \frac{\delta_{ii}\varepsilon_{ii}(2\omega_i+\Omega)\cos(\zeta_{ii}-2\varphi_i)}{16\omega_i^2\Omega} \right) r_i, \tag{6.6a}$$

$$\dot{r}_j = \left(-\frac{1}{2}\delta_{jj} - \frac{\varepsilon_{ij}\varepsilon_{ji}\Omega\sin(\zeta_{ji}-\zeta_{ij})}{2\left[\Omega^2-(\omega_i-\omega_j)^2\right]\left[\Omega^2-(\omega_i+\omega_j)^2\right]} \right) r_j, \tag{6.6b}$$

$$\dot{\varphi}_i = \omega_i - \frac{\Omega}{2} - \frac{\varepsilon_{ii}\cos(\zeta_{ii}-2\varphi_i)}{4\omega_i} + \frac{\varepsilon_{ij}\varepsilon_{ji}(\Omega^2+(\omega_i^2-\omega_j^2))\cos(\zeta_{ji}-\zeta_{ij})}{4\omega_i\left[\Omega^2-(\omega_i-\omega_j)^2\right]\left[\Omega^2-(\omega_i+\omega_j)^2\right]} - \frac{\varepsilon_{ii}^2}{16\omega_i^2\left(\Omega+2\omega_i\right)} + \frac{\delta_{ii}\varepsilon_{ii}(\Omega+2\omega_i)\sin(\zeta_{ii}-2\varphi_i)}{16\omega_i^2\Omega} - \frac{\delta_{ii}^2}{8\omega_i}, \tag{6.6c}$$

$$\dot{\varphi}_j = \omega_j - \frac{\Omega}{2} + \frac{\varepsilon_{ij}\varepsilon_{ji}(\Omega^2-(\omega_i^2-\omega_j^2))\cos(\zeta_{ji}-\zeta_{ij})}{4\omega_j\left[\Omega^2-(\omega_i-\omega_j)^2\right]\left[\Omega^2-(\omega_i+\omega_j)^2\right]} + \frac{\varepsilon_{jj}^2}{4\omega_j\left(\Omega-2\omega_j\right)\left(\Omega+2\omega_j\right)} - \frac{\delta_{jj}^2}{8\omega_j}. \tag{6.6d}$$

The degrees of freedom are still decoupled and the equations are linear in the amplitude coordinates $r_{i,j}$. However, due to the increased complexity of the phase equations, the LCEs with eliminated $\varphi_{i,j}$ cannot be given in short form. Nevertheless, the LCEs, given again as coefficients of $r_{i,j}$ in Eqs. (6.6a)-(6.6b), can be studied qualitatively. By considering the higher order terms, the impact of the off-diagonal excitation terms and phase angles becomes vivid. In fact, the terms proportional to the product $\varepsilon_{ij}\varepsilon_{ji}$ are identical to those from the non-resonant normal form, Eq. (3.13), and describe the contribution of the global effect in the vicinity of the fundamental resonance areas. A further quadratic term in Eq. (6.6a) featuring $\delta_{ii}\varepsilon_{ii}$ involves again only the main-diagonal terms. A comparison to the numerical values provides now a much better agreement, Fig. 6.2.

The above analysis demonstrates that, apart from the global effect, the fundamental

resonances in an $\mathbf{MDK}+\mathbf{C}(t)$ system depend exclusively on the corresponding main-diagonal terms. With global effects being in general rather small, the concise symbolic expressions derived from the second order approximation are yet expected to provide sufficiently precise results.

6.2 $\mathbf{MDGKN}+\mathbf{C}(t)$ system

All of the previous results cannot be applied as soon as there are skew-symmetric velocity- or displacement-proportional terms. Even though the presence of the skew-symmetric terms is not expected to dramatically change the appearance of the fundamental resonances, their contribution to the magnitude of the effects might be substantial. The analyzed system is now extended by introducing gyroscopic and circulatory terms:

$$\begin{pmatrix}\ddot{q}_1\\ \ddot{q}_2\end{pmatrix}+\begin{pmatrix}\delta_{11} & \delta_c+\gamma\\ \delta_c-\gamma & \delta_{22}\end{pmatrix}\begin{pmatrix}\dot{q}_1\\ \dot{q}_2\end{pmatrix}+\left[\begin{pmatrix}k_{11} & n\\ -n & k_{22}\end{pmatrix}+\begin{pmatrix}\varepsilon_{11}\cos(\Omega t+\zeta_{11}) & \varepsilon_{12}\cos(\Omega t+\zeta_{12})\\ \varepsilon_{21}\cos(\Omega t+\zeta_{21}) & \varepsilon_{22}\cos(\Omega t+\zeta_{22})\end{pmatrix}\right]\begin{pmatrix}q_1\\ q_2\end{pmatrix}=\mathbf{0}. \tag{6.7}$$

Without loss of generality it is further assumed $k_{22}>k_{11}$. With the approximate circular eigenfrequencies neglecting the velocity-proportional terms given as

$$\omega_{1,2}=\sqrt{\frac{1}{2}\left(k_{11}\mp\sqrt{\left(k_{11}-k_{22}\right)^2-4n^2}+k_{22}\right)}, \tag{6.8}$$

the second order normal form for the fundamental resonance area $\Omega\approx 2\omega_i$ reads:

$$\begin{aligned}\dot{r}_i=&\left(-\frac{1}{4}\left(\delta_{ii}+\delta_{jj}\right)+A_0-A_1\varepsilon_{ii}\sin\left(\zeta_{ii}-2\varphi_i\right)+A_2\varepsilon_{jj}\sin\left(\zeta_{jj}-2\varphi_i\right)\right.\\ &\left.+A_3\left(\varepsilon_{ij}\sin\left(\zeta_{ij}-2\varphi_i\right)-\varepsilon_{ji}\sin\left(\zeta_{ji}-2\varphi_i\right)\right)\right)r_i, &\text{(6.9a)}\\ \dot{r}_j=&\left(-\frac{1}{4}\left(\delta_{ii}+\delta_{jj}\right)-A_0\right)r_j, &\text{(6.9b)}\\ \dot{\varphi}_i=&\omega_i-\frac{\Omega}{2}+A_1\varepsilon_{ii}\cos\left(\zeta_{ii}-2\varphi_i\right)-A_2\varepsilon_{jj}\cos\left(\zeta_{jj}-2\varphi_i\right)\\ &-A_3\left(\varepsilon_{ij}\cos\left(\zeta_{ij}-2\varphi_i\right)-\varepsilon_{ji}\cos\left(\zeta_{ji}-2\varphi_i\right)\right), &\text{(6.9c)}\\ \dot{\varphi}_j=&\omega_j-\frac{\Omega}{2} &\text{(6.9d)}\end{aligned}$$

with the coefficients

$$A_0 = \frac{(k_{11}-k_{22})(\delta_{ii}-\delta_{jj}) - 4n\gamma(3-2i)}{4\sqrt{(k_{11}-k_{22})^2 - 4n^2}}, \tag{6.10a}$$

$$A_1 = \frac{\left(k_{11} - \sqrt{(k_{11}-k_{22})^2 - 4n^2} - k_{22}\right)}{8\sqrt{(k_{11}-k_{22})^2 - 4n^2}\,\omega_i}, \tag{6.10b}$$

$$A_2 = \frac{\left(k_{11} + \sqrt{(k_{11}-k_{22})^2 - 4n^2} - k_{22}\right)}{8\sqrt{(k_{11}-k_{22})^2 - 4n^2}\,\omega_i}, \tag{6.10c}$$

$$A_3 = \frac{n}{4\sqrt{(k_{11}-k_{22})^2 - 4n^2}\,\omega_i} \tag{6.10d}$$

and $i, j = 1, 2$ and $i \neq j$. Due to the additional coupling even the second order normal form is already too complex to derive explicit expressions for the LCEs depending on the system parameters only. However, as the equations are still linear and decoupled with respect to the amplitude coordinates $r_{i,j}$, the above expressions vividly demonstrate the impact of different parameters on the fundamental resonances. The first two terms in Eqs. (6.9a)-(6.9b) represent the approximate LCEs for the unperturbed system taking into account the circulatory and the gyroscopic terms. The next term in Eq. (6.9a) proportional to ε_{ii} accounts for the contribution of the i-th main-diagonal excitation term and represents the main contribution to the resonance area. With $n = 0\,\mathrm{s}^{-2}$ it is equivalent to the second term in Eq. (6.2a). Due to the coupling through circulatory terms, also the j-th main-diagonal excitation term contributes to the resonance around the i-th eigenfrequency through the ε_{jj}-proportional term. Finally, the last term in Eq. (6.9a) describes the contribution of the off-diagonal excitation terms to the fundamental resonances. The contribution vanishes for in-phase off-diagonal terms of equal amplitude, i.e., with $\varepsilon_{ij} = \varepsilon_{ji}$ and $\zeta_{ij} = \zeta_{ji}$. It has to be kept in mind that this second order normal form does not account for possible contribution of global stability effects, as shown in section 6.1. These are treated separately in section 3.2. Moreover, due to the procedure of the normal form transformation, the impact of the gyroscopic terms is considered only in terms of their contribution to the LCEs of the unperturbed system, i.e., no direct impact in context of parametric excitation is included in the analysis.

Even though the general case can be analyzed only qualitatively, for a system with given parametric excitation, i.e., defined amplitudes and phase relations, Eqs. (6.9a)-(6.9d) can

be solved for LCEs depending on a few system parameters only, e.g., stiffness, damping, gyroscopic and circulatory terms. In particular, for some representative cases, two of which will be presented in the following, the LCEs can be given in concise form. First, for the case of synchronous excitation, i.e., $\zeta_{ij} = 0$ with $i, j = 1, 2$, the approximate LCEs for system (6.7) are given as follows:

$$\lambda_i = -\frac{1}{4}(\delta_{ii} + \delta_{jj}) + A_0 + \frac{1}{8}\sqrt{\frac{\left(\sqrt{(k_{11}-k_{22})^2-4n^2}\,(\varepsilon_{ii}+\varepsilon_{jj})-(k_{11}-k_{22})(\varepsilon_{ii}-\varepsilon_{jj})+2n(\varepsilon_{ij}-\varepsilon_{ji})\right)^2}{\left((k_{11}-k_{22})^2-4n^2\right)\omega_i^2} - 16(\Omega-2\omega_i)^2}, \tag{6.11a}$$

$$\lambda_j = -\frac{1}{4}(\delta_{ii} + \delta_{jj}) - A_0, \tag{6.11b}$$

while the largest LCE deciding upon the stability of the trivial solution is defined as $\Lambda = \max\{\lambda_i, \lambda_j\}$. In the second case the excitation is synchronous except for the off-diagonal terms being in anti-phase, i.e., $\zeta_{11} = \zeta_{22} = \zeta_{12} = 0$ and $\zeta_{21} = \pi$. The LCEs are very similar to the previous case except for the considerably stronger contribution of the off-diagonal excitation terms:

$$\lambda_i = -\frac{1}{4}(\delta_{ii} + \delta_{jj}) + A_0 + \frac{1}{8}\sqrt{\frac{\left(\sqrt{(k_{11}-k_{22})^2-4n^2}\,(\varepsilon_{ii}+\varepsilon_{jj})-(k_{11}-k_{22})(\varepsilon_{ii}-\varepsilon_{jj})+2n(\varepsilon_{ij}+\varepsilon_{ji})\right)^2}{\left((k_{11}-k_{22})^2-4n^2\right)\omega_i^2} - 16\,(\Omega-2\omega_i)^2}, \tag{6.12a}$$

$$\lambda_j = -\frac{1}{4}(\delta_{ii} + \delta_{jj}) - A_0. \tag{6.12b}$$

Keeping the variable amplitudes of variation provides clear insight into the contribution of different excitation terms. Of special importance is the additional coupling though circulatory terms which leads to the contribution of the off-diagonal excitation terms to the fundamental resonances. These may not only increase of decrease the fundamental resonances induced by the main-diagonal excitation terms, but may also create fundamental resonances on their own even in the absence of main-diagonal excitation.

Figures 6.3-6.4 show a comparison between the largest LCE obtained by means of

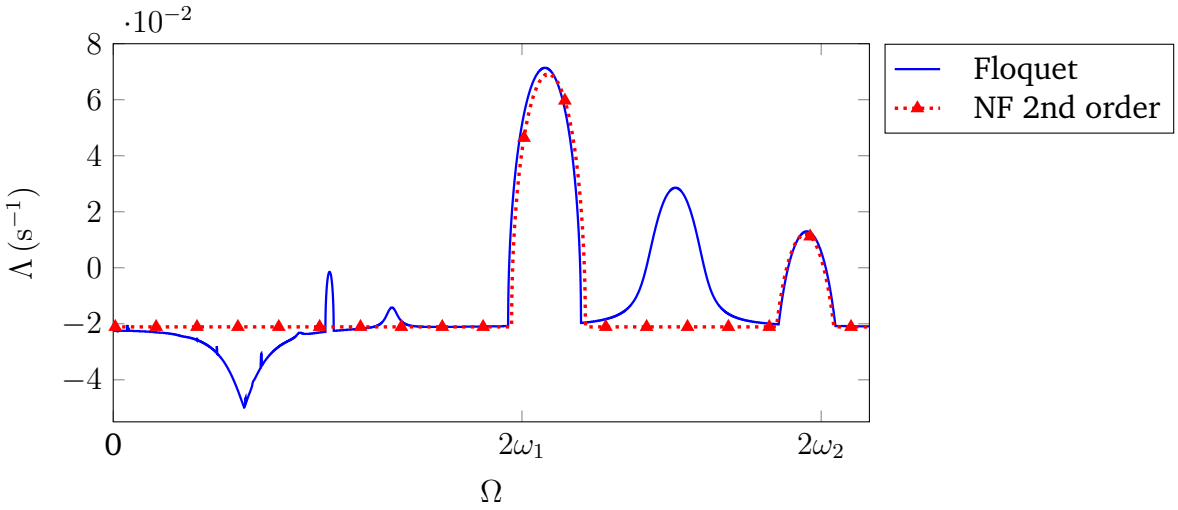

Figure 6.3: Fundamental resonances of system (6.7) with $\varepsilon_{11} = \varepsilon_{12} = \varepsilon_{21} = 0.4\,\mathrm{s}^{-2}$, $\varepsilon_{22} = 0.6\,\mathrm{s}^{-2}$, $k_{11} = 1\,\mathrm{s}^{-2}$, $k_{22} = 3\,\mathrm{s}^{-2}$, $n = 0.5\,\mathrm{s}^{-2}$, $\gamma = 0\,\mathrm{s}^{-1}$, $\delta_{11} = 0.05\,\mathrm{s}^{-1}$, $\delta_{22} = 0.15\,\mathrm{s}^{-1}$, $\delta_c = 0\,\mathrm{s}^{-1}$, $\zeta_{11} = \zeta_{12} = \zeta_{21} = \zeta_{22} = 0$

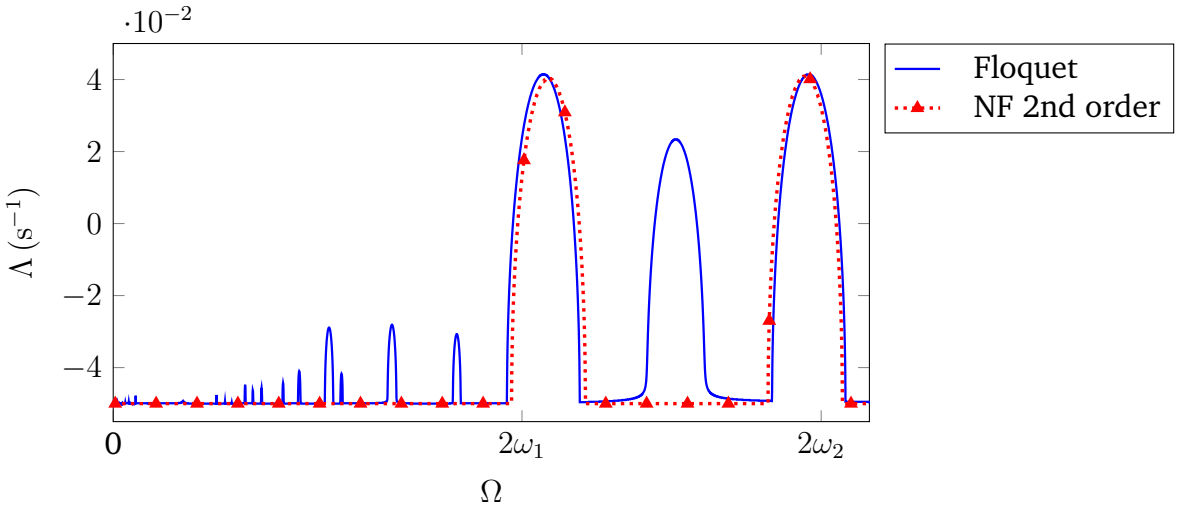

Figure 6.4: Fundamental resonances of system (6.7) with $\varepsilon_{11} = \varepsilon_{12} = \varepsilon_{21} = 0.4\,\mathrm{s}^{-2}$, $\varepsilon_{22} = 0.6\,\mathrm{s}^{-2}$, $k_{11} = 1\,\mathrm{s}^{-2}$, $k_{22} = 3\,\mathrm{s}^{-2}$, $n = 0.5\,\mathrm{s}^{-2}$, $\gamma = 0.1\,\mathrm{s}^{-1}$, $\delta_{11} = 0.05\,\mathrm{s}^{-1}$, $\delta_{22} = 0.15\,\mathrm{s}^{-1}$, $\delta_c = 0\,\mathrm{s}^{-1}$, $\zeta_{11} = \zeta_{12} = \zeta_{21} = \zeta_{22} = 0$

the symbolic expression in Eqs. (6.11a)-(6.11b) and numerical Floquet analysis for an $\mathbf{MDKN} + \mathbf{C}(t)$ and an $\mathbf{MDGKN} + \mathbf{C}(t)$ system respectively. In both cases there is an excellent qualitative and quantitative agreement. In this way, the approximate symbolic expressions obtained from the normal form are not only useful for qualitative understanding, but can also be used as a tool for quick analysis or design of systems with desired stability behavior.

6.3 Conclusions

The behavior of parametric fundamental resonances in an $\mathbf{MDGKN} + \mathbf{C}(t)$ system has been studied for the first time providing important insight on the impact of circulatory terms. It was found found out that circulatory terms may significantly affect the fundamental resonances in terms of their magnitude or even occurrence, while the particular effect is highly sensitive to the specific parameters of parametric excitation, e.g., phase relations and magnitudes of variation. Using the method of normal forms, approximate symbolic expressions were derived describing qualitatively the diverse effects. For some specific cases, e.g., $\mathbf{MDK} + \mathbf{C}(t)$ system or $\mathbf{MDGKN} + \mathbf{C}(t)$ systems with given phase relations, explicit symbolic expressions for the LCEs could be derived representing a powerful tool in the analysis and design of fundamental resonances in a parametrically excited system.

7 Asynchronous parametric excitation in nonlinear systems

The previous chapters show various impacts of asynchronous parametric excitation on the stability of the trivial solution in a linear system. As parametric excitation may easily lead to an unstable trivial solution or even to total instability, it may also be of interest to investigate the impact of asynchronous parametric excitation on the limit cycles of a nonlinear system. A nonlinear system with cubic stiffness and asynchronous off-diagonal parametric excitation has been studied by Schmieg for the area around the sum combination resonance frequency [68]. In the present contribution the nonlinear behavior of a similar system extended by cubic damping is studied for the whole frequency range by deriving normal forms for both resonant and non-resonant parametric excitation. The impact of phase shift and damping is presented in terms of the amplitude curves. A comparison between the semi-analytical normal form results and purely numerical analysis shows good agreement.

7.1 Analyzed system

The following simple $\mathbf{MDK} + \mathbf{C}(t)$ system with uniform linear damping extended by cubic stiffness and damping is investigated:

$$\begin{pmatrix} \ddot{q}_1 \\ \ddot{q}_2 \end{pmatrix} + \begin{pmatrix} \delta & 0 \\ 0 & \delta \end{pmatrix} \begin{pmatrix} \dot{q}_1 \\ \dot{q}_2 \end{pmatrix} + \left[\begin{pmatrix} \omega_1^2 & 0 \\ 0 & \omega_2^2 \end{pmatrix} + \varepsilon \begin{pmatrix} 0 & \cos(\Omega t) \\ \cos(\Omega t + \zeta_c) & 0 \end{pmatrix} \right] \begin{pmatrix} q_1 \\ q_2 \end{pmatrix} + \xi \begin{pmatrix} \dot{q}_1^3 \\ \dot{q}_2^3 \end{pmatrix} + \kappa \begin{pmatrix} q_1^3 \\ q_2^3 \end{pmatrix} = \mathbf{0}. \tag{7.1}$$

As in the study of limit cycles the areas with unstable trivial solution are of the main interest, uniform damping is considered so that there is no parametric anti-resonance, i.e., stabilization. This nonlinear parametrically excited system will be studied applying the normal form theory. The additional cubic nonlinearities do not change the procedure applied before to systems with parametric excitation only, as the parametric excitation terms were already

treated as nonlinearities. As seen in the previous sections, the asynchronous parametric excitation affects the stability behavior for the whole range of excitation frequencies. For this reason, the limit cycles of the above system are studied deriving both the non-resonant normal form as well as the normal form for sum and difference combination resonances. In order to study different effects individually, first an undamped system is studied highlighting the effects of the phase shift alone. Further, the impact of damping on the fixed points, i.e., limit cycles, in a asynchronously excited system is studied.

7.2 Non-resonant parametric excitation

First the normal form is derived for the non-resonant parametric excitation:

$$\dot{r}_1 = \left[-\frac{1}{2}\delta + \frac{\varepsilon^2\Omega\sin(\zeta_c)}{2[\Omega^2-(\omega_1+\omega_2)^2][\Omega^2-(\omega_1-\omega_2)^2]}\right] r_1 - \frac{3}{8}\xi\omega_1^2 r_1^3, \tag{7.2a}$$

$$\dot{r}_2 = \left[-\frac{1}{2}\delta - \frac{\varepsilon^2\Omega\sin(\zeta_c)}{2[\Omega^2-(\omega_1+\omega_2)^2][\Omega^2-(\omega_1-\omega_2)^2]}\right] r_2 - \frac{3}{8}\xi\omega_2^2 r_2^3, \tag{7.2b}$$

$$\dot{\varphi}_1 = \omega_1 - \frac{\Omega}{2} - \frac{\delta^2}{8\,\omega_1} + \frac{\varepsilon^2(\Omega^2+\omega_1^2-\omega_2^2)\cos(\zeta_c)}{4\omega_1[\Omega^2-(\omega_1+\omega_2)^2][\Omega^2-(\omega_1-\omega_2)^2]} + \frac{3}{8}\frac{\kappa}{\omega_1}r_1^2, \tag{7.2c}$$

$$\dot{\varphi}_2 = \omega_2 - \frac{\delta^2}{8\,\omega_2} + \frac{\varepsilon^2(\Omega^2-\omega_1^2+\omega_2^2)\cos(\zeta_c)}{4\omega_2[\Omega^2-(\omega_1+\omega_2)^2][\Omega^2-(\omega_1-\omega_2)^2]} + \frac{3}{8}\frac{\kappa}{\omega_2}r_2^2. \tag{7.2d}$$

The expressions are identical to the previously derived non-resonant normal form, Eq. (3.15), except for the additional stiffness and damping nonlinearities. It can be seen from Eq. (7.2) that for $\delta = 0$ and $\zeta_c \neq z\pi$, $z \in \mathbb{N}$ the trivial solution is unstable in the sense of Lyapunov for all $\varepsilon \neq 0$, especially for all non-resonant frequencies Ω of the parametric excitation: as the coefficients of r_1 and r_2 are equal except for the opposite sign, at least one of them will always be positive. In this case the positive cubic damping leads to limit cycle oscillations, since there is a fixed point approximately given by

$$r_i = \sqrt{\pm\frac{4}{3}\frac{\varepsilon^2\Omega\sin(\zeta_c)}{\xi\omega_i^2[\Omega^2-(\omega_1+\omega_2)^2][\Omega^2-(\omega_1-\omega_2)^2]}}, \quad i = 1 \text{ or } 2, \tag{7.3}$$

where the upper (lower) sign applies for $i=1$ ($i=2$). It depends on the sign of the coefficients of linear terms in r_1 and r_2 in (7.2), if $i=1$ or $i=2$ holds. These coefficients are of same absolute value, opposite in sign and change sign at $\Omega^2=(\omega_1\pm\omega_2)^2$, i.e., at the combination resonance frequencies. Therefore the frequency of limit cycle oscillation in coordinates of the normal form is ω_1 for $\Omega^2<(\omega_1-\omega_2)^2$ or $\Omega^2>(\omega_1+\omega_2)^2$ and is ω_2 for $(\omega_1-\omega_2)^2<\Omega^2<(\omega_1+\omega_2)^2$.

7.3 Combination resonances

In the case of combination resonances the normal form can be written as

$$\dot{r}_1 = -\frac{\delta}{2} r_1 - \frac{\varepsilon}{4\,\omega_2} \sin(\varphi)\, r_2 + \delta\varepsilon A_1 \cos(\varphi) r_2 + \varepsilon^2 B \sin(\psi)\, r_1 - \frac{3}{8}\xi\omega_1^2 r_1^3, \tag{7.4a}$$

$$\dot{r}_2 = -\frac{\delta}{2} r_2 \pm \frac{\varepsilon}{4\,\omega_2} \sin(\varphi - \zeta_c)\, r_1 + \delta\varepsilon A_2 \cos(\varphi - \zeta_c) r_1 \mp \varepsilon^2 B \sin(\psi)\, r_2 - \frac{3}{8}\xi\omega_2^2 r_2^3, \tag{7.4b}$$

$$\dot{\varphi} = \omega_2 \mp \omega_1 - \Omega \pm \frac{\varepsilon \cos(\varphi - \zeta_c)}{4\,\omega_1} \frac{r_1}{r_2} - \frac{\varepsilon \cos(\varphi)}{4\,\omega_2} \frac{r_2}{r_1} + \delta\varepsilon \left(C_1 \sin(\zeta_c - \varphi) \frac{r_1}{r_2} - C_2 \sin(\varphi) \frac{r_2}{r_1} \right) \tag{7.4c}$$

$$\pm \delta^2 D \pm \frac{\varepsilon^2}{8\,\omega_1\omega_2(\Omega + \omega_2 \mp \omega_1)} \cos(\zeta_c) \mp \frac{3\kappa}{8\,\omega_1} r_1^2 + \frac{3\kappa}{8\,\omega_2} r_2^2 \tag{7.4d}$$

with the coefficients given by

$$A_1 = \frac{\Omega + \omega_2 \mp \omega_1}{16\,\omega_2^2(\,\Omega - (\omega_2 \pm \omega_1))}, \qquad A_2 = \frac{\Omega + \omega_2 \mp \omega_1}{16\,\omega_1^2(\,\Omega + \omega_2 \pm \omega_1)}, \tag{7.5a}$$

$$B = \frac{\Omega^2 + 2\Omega(\omega_2 \mp \omega_1) + (\omega_2 \pm \omega_1)^2}{16\,\omega_1\omega_2\,(\Omega^2 - (\omega_2 \pm \omega_1)^2)\,(\Omega + \omega_2 \mp \omega_1)}, \tag{7.5b}$$

$$C_1 = \frac{\Omega + \omega_2 \mp \omega_1}{16\,\omega_1^2(\Omega + \omega_2 \pm \omega_1)}, \qquad C_2 = \frac{\Omega + \omega_2 \mp \omega_1}{16\,\omega_2^2(\Omega - (\omega_2 \pm \omega_1))}, \tag{7.5c}$$

$$D = \frac{\omega_1^2 \mp 6\omega_1\omega_2 + \omega_2^2}{8\,\omega_1\omega_2(\omega_2 \mp \omega_1)}, \tag{7.5d}$$

where the upper (lower) signs apply for difference (sum) combination resonance. In order to account for the cubic nonlinearities, the normal form is continued up to the third order terms, revealing also the higher order terms associated with parametric excitation. Compared to the second order normal form with only linear ε, Eq. (4.2), the expressions have become substantially more complex forbidding any deeper analytical investigations. The fixed points of (7.4) can be calculated numerically for a given set of parameters. The results for the combination resonance $\Omega \approx \omega_1 + \omega_2$ and $\zeta_c = 0$ are identical to those obtained in [29] by the method of slowly varying phase and amplitude.

Figs. 7.1-7.2 show the fixed points of Eq. (7.4) for a given set of parameters and varying phase angle ζ_c. These fixed points correspond to periodic solutions of the original system (7.1) with $\delta = 0$. The periodic solutions can be calculated applying the reverse transformation from the normal form coordinates to the original coordinates. A comparison of the amplitudes of the periodic solutions obtained by the normal form theory and numerical integration of the original equations is shown in Figs. 7.3, 7.4. The numerical and the semi-analytical results

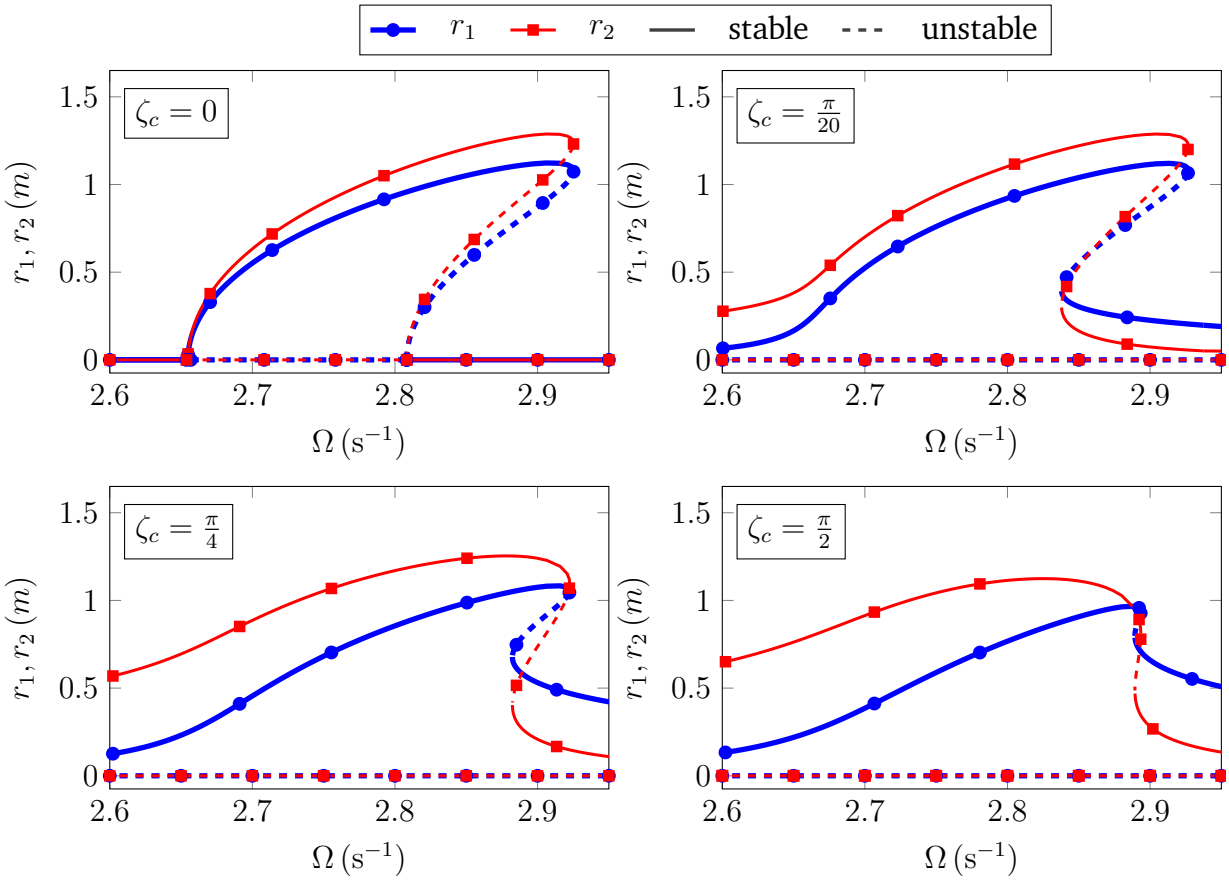

Figure 7.1: Fixed points r_1, r_2 near the combination resonance $\Omega \approx \omega_1 + \omega_2$ for $\zeta_c = [0, \pi/20, \pi/4, \pi/2]$. Parameter values: $\omega_1 = 1\,\mathrm{s}^{-1}$, $\omega_2 = \sqrt{3}\,\mathrm{s}^{-1}$, $\xi = 0.07\,\mathrm{s\,m}^{-2}$, $\kappa = 0.3\,\mathrm{m}^{-2}\,\mathrm{s}^{-2}$, $\varepsilon = 0.2\,\mathrm{s}^{-2}$, $\delta = 0\,\mathrm{s}^{-1}$

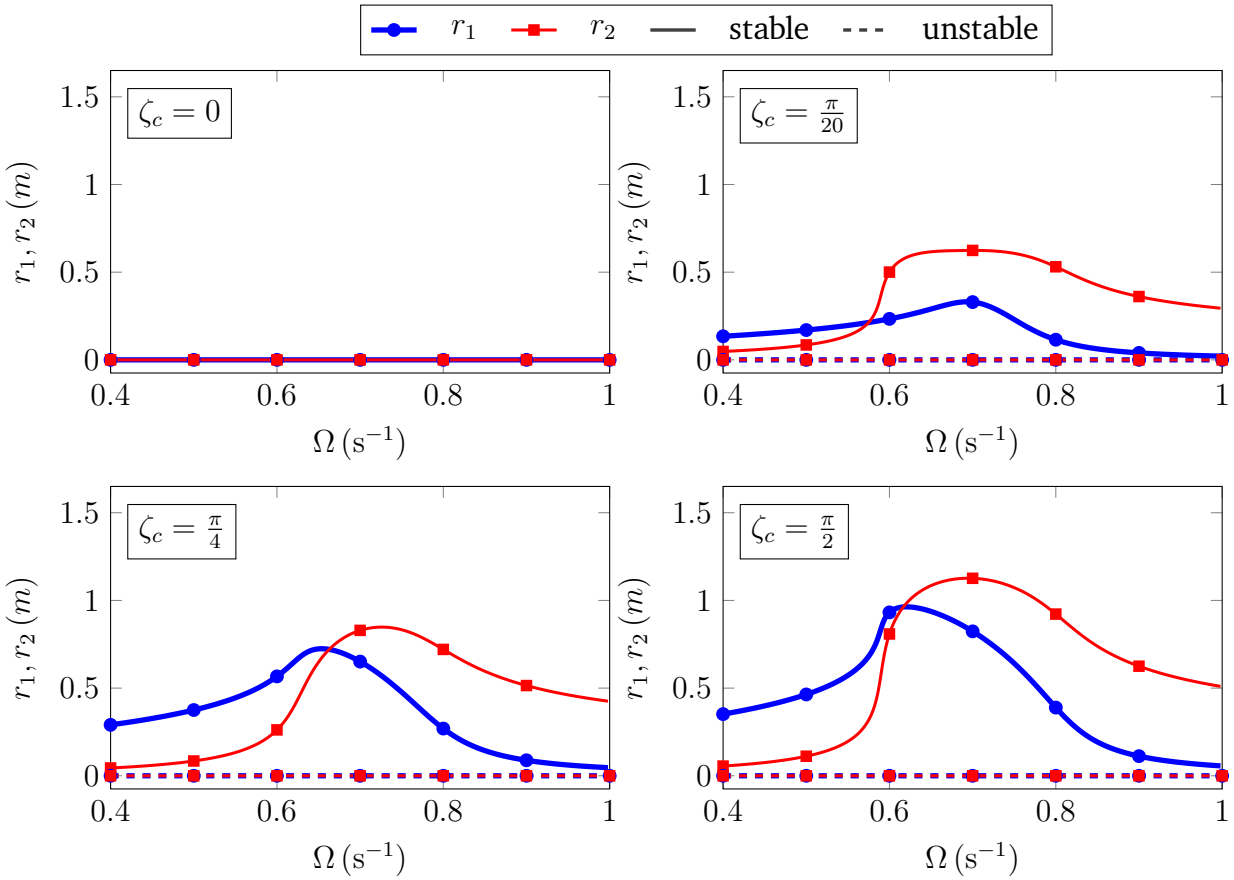

Figure 7.2: Fixed points r_1, r_2 near the combination resonance $\Omega \approx \omega_2 - \omega_1$ for $\zeta_c = [0, \pi/20, \pi/4, \pi/2]$. Parameter values: $\omega_1 = 1\,\mathrm{s}^{-1}$, $\omega_2 = \sqrt{3}\,\mathrm{s}^{-1}$, $\xi = 0.07\,\mathrm{s\,m}^{-2}$, $\kappa = 0.3\,\mathrm{m}^{-2}\,\mathrm{s}^{-2}$, $\varepsilon = 0.2\,\mathrm{s}^{-2}$, $\delta = 0\,\mathrm{s}^{-1}$

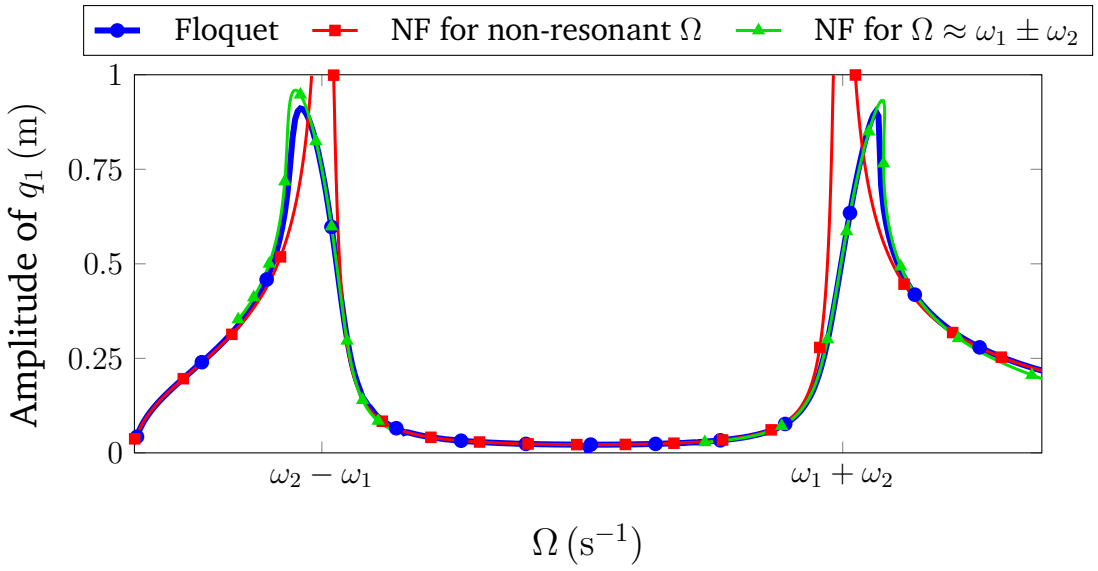

Figure 7.3: Limit cycle amplitudes of system (7.1): q_1 for $\zeta_c = \pi/2$ and $\omega_1 = 1\,\mathrm{s}^{-1}$, $\omega_2 = \sqrt{3}\,\mathrm{s}^{-1}$, $\xi = 0.07\,\mathrm{s\,m}^{-2}$, $\kappa = 0.3\,\mathrm{m}^{-2}\,\mathrm{s}^{-2}$, $\varepsilon = 0.2\,\mathrm{s}^{-2}$, $\delta = 0\,\mathrm{s}^{-1}$

are in a good agreement: While the non-resonant normal form performs well in the wide frequency region, except for the combination resonance areas, the resonant normal forms provide a fair approximation for this missing parts.

Further, the impact of damping on the fixed points of Eq. (7.4) is visualized. Figure 7.5 shows the fixed points of a synchronously and of an asynchronously excited system for increasing uniform damping. As the resonance in case of asynchronous excitation is weaker for the same amplitude of variation, the fixed points and with this also the amplitudes of the limit cycles are expectedly lower as well. Further, the bifurcation points appear to be much more sensitive to the damping in case of asynchronous excitation – the width of the region with unstable trivial solution is decreasing quickly with increasing damping. Another qualitative difference to the case with synchronous excitation, is that the curves are generally “flattened” and the amplitudes grow more slowly, especially in the vicinity of the bifurcation points, which means that the amplitudes of the limit cycles do not become abruptly very large, but increase more steadily. To a certain extent, this agrees with the behavior of the LCEs of the underlying linear system: in case of synchronous excitation with uniform damping, the impact of the parametric combination resonance occurs “suddenly”, i.e., there is no continuous increase of the largest LCE in the vicinity of the resonance area, but just a kink at a certain excitation frequency. This is different for the case of uniform damping and asynchronous excitation or, in general, for the case of non-uniform damping.

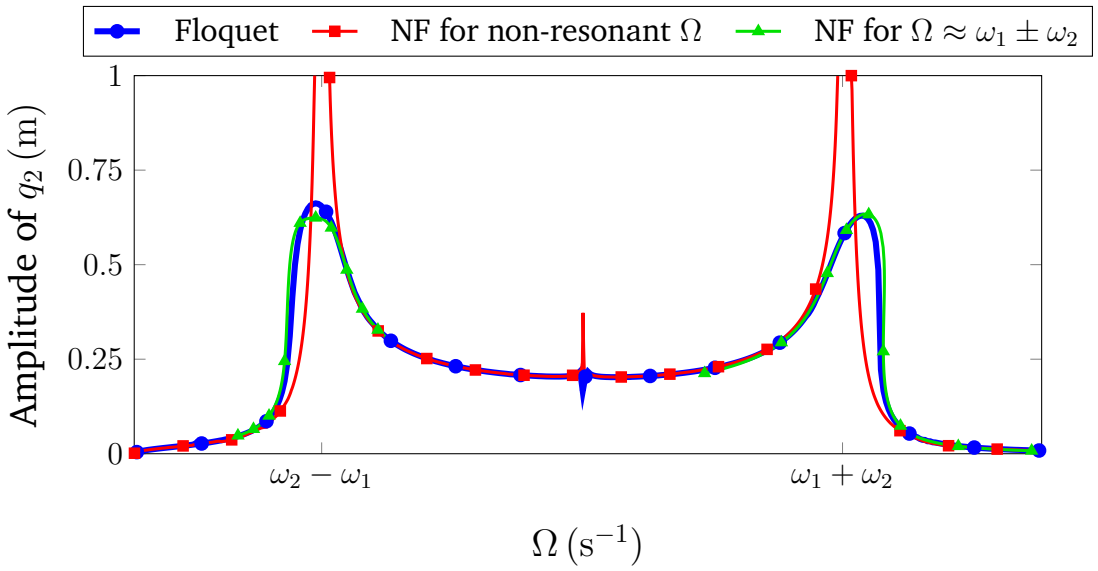

Figure 7.4: Limit cycle amplitudes of system (7.1): q_2 for $\zeta_c = \pi/2$ and $\omega_1 = 1\,\mathrm{m}^{-1}$, $\omega_2 = \sqrt{3}\,\mathrm{m}^{-1}$, $\xi = 0.07\,\mathrm{s\,m}^{-2}$, $\kappa = 0.3\,\mathrm{m}^{-2}\,\mathrm{s}^{-2}$, $\varepsilon = 0.2\,\mathrm{s}^{-2}$, $\delta = 0\,\mathrm{s}^{-1}$

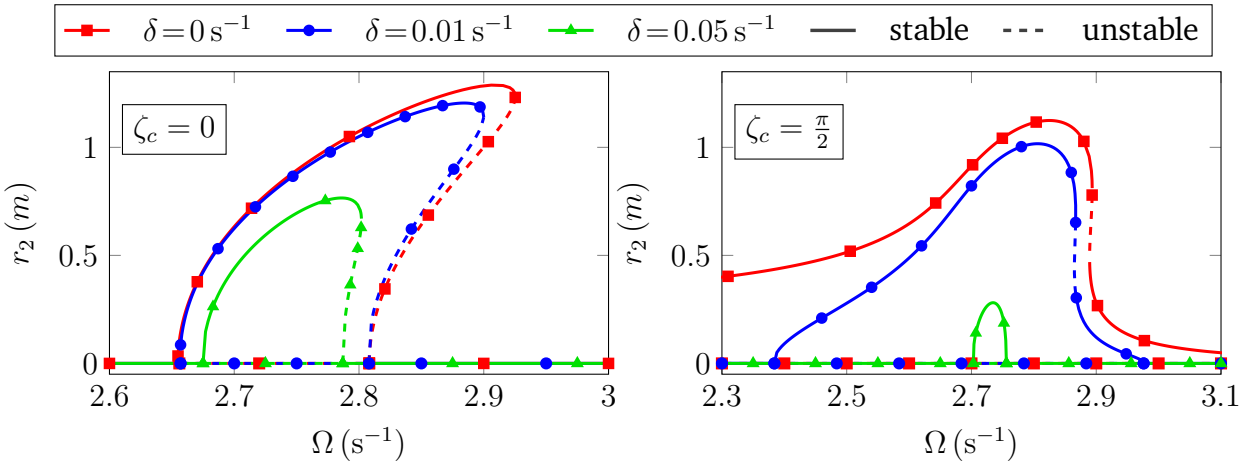

Figure 7.5: Parameter values: $\omega_1 = 1\,\mathrm{s}^{-1}$, $\omega_2 = \sqrt{3}\,\mathrm{s}^{-1}$, $\xi = 0.07\,\mathrm{s\,m}^{-2}$, $\kappa = 0.3\,\mathrm{m}^{-2}\,\mathrm{s}^{-2}$, $\varepsilon = 0.2\,\mathrm{s}^{-2}$

7.4 Conclusions

The above examples emphasize the impact of asynchronous parametric excitation on the behavior of a nonlinear system with cubic stiffness and damping. The semi-analytical analysis by means of the normal form continued up to the third order terms leads to symbolic expressions which complexity does not allow much insight, but the expressions can still be used for quick numerical computation of the fixed points. A comparison with purely numerical results obtained from integration of the original system showed a good agreement.

8 Mechanical examples

The results of the analytical investigations are applied to mechanical examples with the purpose of demonstrating the applicability of the symbolic expressions derived with the method of normal forms. In particular the characteristic points are used for understanding the complex stability behavior of asynchronously excited systems featuring circulatory terms.

8.1 Rotating Disk

The first mechanical example is given by a simple two-degrees-of-freedom system featuring circulatory terms and asynchronous parametric excitation in the main diagonal. The original system [30], aimed at demonstrating various aspects of Coulomb friction, is extended by introducing harmonically varying stiffness coefficients. Due to the presence of circulatory terms in the equations of motion, the appearance of different parametric resonances, in particular combination resonances, is not obvious. The results from sections 4.2 and 6.2 are to be applied in order to quickly obtain profound understanding of the overall stability behavior including fundamental and combination resonances.

8.1.1 Problem definition

The system consists of a particle P (mass m) which is in frictional contact with a rotating disk (angular velocity ν, friction coefficient μ, normal force N), Fig. 8.1. The particle is held by two springs with time-periodic stiffness coefficients

$$k_1(t) = k_1 + \varepsilon_{11}\cos(\Omega t), \tag{8.1a}$$

$$k_2(t) = k_2 + \varepsilon_{22}\cos(\Omega t + \zeta_{22}), \tag{8.1b}$$

where ε_{ii}, $i = 1, 2$, is the amplitude of parametric excitation, Ω is the excitation frequency and ζ_{22} stands for the phase shift.

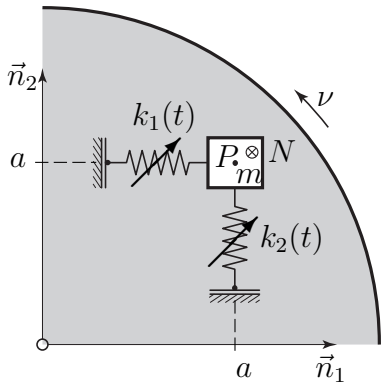

Figure 8.1: Rotating disk; parameter values: $a = 0.2\,\mathrm{m}$, $m = 1\,\mathrm{kg}$, $\mu = 0.3$, $N = 1\,\mathrm{N}$, $\nu = 100\,\mathrm{rad/s}$, $k_1 = 1\,\mathrm{N\,m}$, $k_2 = 3\,\mathrm{N\,m}$

The system can be described by the linearized equations of motion:

$$\mathbf{M}\,\ddot{\mathbf{q}}(t) + \mathbf{D}\,\dot{\mathbf{q}}(t) + [\mathbf{K}_0 + \varepsilon\mathbf{K}_1(t) + \mathbf{N}_0]\;\mathbf{q}(t) = \mathbf{0} \quad \text{with} \tag{8.2}$$

$$\mathbf{M} = \begin{pmatrix} m & 0 \\ 0 & m \end{pmatrix},\; \mathbf{D} = \frac{\mu N}{2\sqrt{2}a\nu}\begin{pmatrix} 1 & 1 \\ 1 & 1 \end{pmatrix}, \tag{8.3a}$$

$$\mathbf{K}_0 = \begin{pmatrix} k_1 - \frac{\mu N}{2\sqrt{2}a} & 0 \\ 0 & k_2 + \frac{\mu N}{2\sqrt{2}a} \end{pmatrix},\; \mathbf{K}_1(t) = \begin{pmatrix} \varepsilon_{11}\cos(\Omega t) & 0 \\ 0 & \varepsilon_{22}\cos(\Omega t + \zeta_{22}) \end{pmatrix}, \tag{8.3b}$$

$$\mathbf{N}_0 = \begin{pmatrix} 0 & \frac{\mu N}{2\sqrt{2}a} \\ -\frac{\mu N}{2\sqrt{2}a} & 0 \end{pmatrix}, \tag{8.3c}$$

where dot denotes time differentiation and $\mathbf{q} \in \mathbb{R}^n$, $n = 2$, is the column vector of coordinates. The real matrices $\mathbf{M} = \mathbf{M}^T$, $\mathbf{D} = \mathbf{D}^T$, $\mathbf{K}_0 = \mathbf{K}_0^T$, $\mathbf{K}_1(t) = \mathbf{K}_1^T(t)$, $\mathbf{N}_0 = -\mathbf{N}_0^T$ are related to inertia, damping, constant potential, time-periodic potential, and circulatory forces respectively. The circulatory terms as well as the linear damping originate both from the linearization of friction forces.

Due to the presence of circulatory terms, the equations of motion cannot be transformed to generalized coordinates with diagonal system matrices. Therefore, the question of what kinds of resonances are to be expected, is not trivial even for this rather simple system. Until recently, the appearance of different parametric resonances was well studied only for $\mathbf{MDK} + \mathbf{C}(t)$ systems, i.e., for systems without circulatory or gyroscopic forces. However, applying the recent results of the normal form analysis from section 4.2 and 6.2, potential

combination and fundamental resonances can be easily studied.

8.1.2 Stability analysis

First, combination resonances are discussed. As there is only main-diagonal parametric excitation, no combination resonances are expected coming from the stiffness terms. However, the additional coupling through the circulatory terms might yet cause combination resonances. Evaluating Eqs. (4.18)-(4.20c) for the example at hand, the largest LCE for $\Omega \approx |\omega_1 \mp \omega_2|$ is given as

$$\Lambda = \mathrm{Re}\left(\frac{1}{4}(-\delta_{11}-\delta_{22}) + \frac{1}{4}\sqrt{\pm\frac{n^2(\varepsilon_{11}\sin(\varphi)+\varepsilon_{22}\sin(\zeta_{22}-\varphi))^2}{((k_{11}-k_{22})^2-4n^2)\sqrt{n^2+k_{11}k_{22}}}}\right) \tag{8.4}$$

with

$$\begin{aligned} k_{11} &= \frac{k_1}{m} - \frac{\mu N}{2\sqrt{2}m\,a}, & k_{22} &= \frac{k_2}{m} + \frac{\mu N}{2\sqrt{2}m\,a}, \\ n &= \frac{\mu N}{2\sqrt{2}m\,a}, & \delta_{11} &= \delta_{22} = \frac{\mu N}{2\sqrt{2}m\,a\nu} = \delta, \end{aligned} \tag{8.5}$$

where the upper (lower) sign holds for the difference (sum) combination resonance area. From Eq. (8.4) it is apparent that for this kind of excitation the combination resonances are solely on the account of the circulatory terms. Further, the sign of the radicand remains constant independently of φ, so that potentially only resonance at the difference and anti-resonance at the sum frequency are possible. In the considered example, however, no anti-resonance is possible due to uniform damping. Therefore, there is no stability effect for the sum combination resonance frequency at all. On the other hand, for $\zeta_{22} \neq 0$ there is a destabilizing effect near the difference combination resonance frequency, which becomes maximal for $\zeta_{22} = \pi$. For the case of uniform amplitude of variation $\varepsilon_{11} = \varepsilon_{22} = \varepsilon$ and phase shift $\zeta_{22} = \pi$, the maximum destabilizing effect is given by:

$$\Lambda^d = \mathrm{Re}\left(-\frac{\delta}{2} + \frac{1}{2}\sqrt{\frac{n^2\varepsilon^2}{((k_{11}-k_{22})^2-4n^2)\sqrt{n^2+k_{11}k_{22}}}}\right) \tag{8.6}$$

As there is no coexistence of resonance and anti-resonance, the maximum of the destabilizing effect is at the difference combination resonance frequency without a shift, that is $\Omega^d = |\omega_1 - \omega_2|$.

In the next step fundamental resonances are discussed. Due to the absence of the off-

diagonal excitation, the circulatory terms are not expected to have a strong effect, however, the magnitude of the LCEs in the resonance areas might still be affected. Evaluating the normal form for $\Omega = 2\omega_i$, Eqs. (6.9a)-(6.10d), for the given excitation, it is obvious that the presence of circulatory terms leads to both diagonal excitation terms $\varepsilon_{ii}, \varepsilon_{jj}$ contributing to each fundamental resonance:

$$\dot{r}_i = \left(-\frac{1}{2}\delta - A_1 \varepsilon_{ii} \sin\left(\zeta_{ii} - 2\varphi_i\right) + A_2 \varepsilon_{jj} \sin\left(\zeta_{jj} - 2\varphi_i\right) \right) r_i, \tag{8.7a}$$

$$\dot{r}_j = -\frac{1}{2}\delta r_j, \tag{8.7b}$$

$$\dot{\varphi}_i = \omega_i - \frac{\Omega}{2} + A_1 \varepsilon_{ii} \cos\left(\zeta_{ii} - 2\varphi_i\right) - A_2 \varepsilon_{jj} \cos\left(\zeta_{jj} - 2\varphi_i\right), \tag{8.7c}$$

$$\dot{\varphi}_j = \omega_j - \frac{\Omega}{2} \tag{8.7d}$$

with $i, j = 1, 2$, the coefficients

$$A_1 = \frac{\left(k_{11} - \sqrt{\left(k_{11} - k_{22}\right)^2 - 4n^2} - k_{22} \right)}{8\sqrt{\left(k_{11} - k_{22}\right)^2 - 4n^2}\,\omega_i}, \quad A_2 = \frac{\left(k_{11} + \sqrt{\left(k_{11} - k_{22}\right)^2 - 4n^2} - k_{22} \right)}{8\sqrt{\left(k_{11} - k_{22}\right)^2 - 4n^2}\,\omega_i} \tag{8.8a}$$

and the approximate eigenfrequencies

$$\omega_{1,2} = \sqrt{\frac{1}{2}\left(k_{11} \mp \sqrt{\left(k_{11} - k_{22}\right)^2 - 4n^2} + k_{22} \right)}. \tag{8.9}$$

An explicit expression for the largest LCE can be easily derived for given phase shift ζ_{22}. Assuming uniform amplitude of excitation and a phase shift of $\zeta_{22} = \pi$, the largest LCE for the fundamental resonances $\Omega \approx 2\omega_{1,2}$ reads:

$$\Lambda_{1,2} = \mathrm{Re}\left(-\frac{\delta}{2} + \frac{1}{4}\sqrt{\frac{\left(k_{11} - k_{22}\right)^2}{\left(\left(k_{11} - k_{22}\right)^2 - 4n^2\right)}\frac{\varepsilon^2}{\omega_{1,2}^2} - 4\left(\Omega - 2\omega_{1,2}\right)^2} \right) \tag{8.10}$$

with parameters defined according to Eq. (8.5). The contribution of the circulatory terms is twofold. First, the minor contribution is given by the change in the eigenfrequencies, Eq. (8.9). However, the major contribution is through the additional factor increasing the contribution of parametric excitation in Eq. (8.10). Therefore, for the given phase relation, the presence of the circulatory terms contributes to stronger fundamental parametric

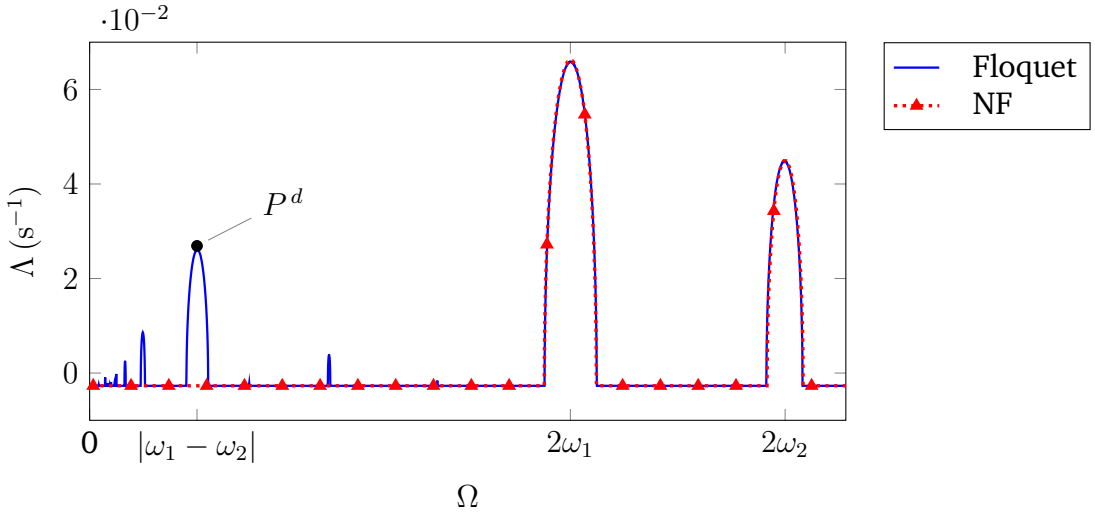

Figure 8.2: Stability impact of parametric excitation in system (8.2): numerical results (Floquet) versus analytical results (NF) for $\Omega \approx |\omega_1 - \omega_2|$, Eq. (8.6), and for $\Omega \approx 2\omega_{1,2}$, Eq. (8.10) with $a = 0.2\,\mathrm{m}$, $m = 1\,\mathrm{kg}$, $\mu = 0.3$, $N = 1\,\mathrm{N}$, $\nu = 100\,\mathrm{rad/s}$, $k_1 = 1\,\mathrm{N\,m}$, $k_2 = 3\,\mathrm{N\,m}$

resonances.

In this way, a qualitative assessment of the stability behavior of an $\mathbf{MDKN} + \mathbf{C}(t)$ system can be easily performed. Furthermore, for given parametric excitation, even quantitative description can be derived for both combination and fundamental resonances, Eqs. (8.6), (8.10) respectively. Figure 8.2 shows the stability impact of parametric excitation in terms of the largest LCE comparing the analytical and numerical (Floquet) results. For the chosen parameter set, there is an excellent agreement for both first order fundamental resonance areas. Also the strongest destabilization in the difference combination resonance area is captured with only slight deviation.

8.1.3 Conclusions

The above example demonstrates the usability of the approximate symbolic expressions for the stability analysis of a parametrically excited $\mathbf{MDKN} + \mathbf{C}(t)$ system. With the expressions derived for both fundamental and combination resonances, the various stability phenomena of a system featuring circulatory terms could be quickly assessed in qualitative and also quantitative concern. It was shown that purely main-diagonal excitation can surprisingly lead to difference combination resonances. Further, the impact of the circulatory terms on the magnitude of the fundamental resonances was clearly demonstrated. Therefore, it is important to consider the contribution of the circulatory terms to parametric resonance

effects, as they may lead to unexpected resonance areas through the additional coupling.

8.2 Minimal model of a disk brake with asymmetric mounting

A mechanical example of a system featuring circulatory and gyroscopic terms subject to asynchronous parametric excitation is given by the minimal model of a disk brake with asymmetric mounting as presented in [71] and [70], Fig. 8.3. This is a highly complex system the stability behavior of which could not be full understood so far. The newly obtained general understanding of such systems and the approximate symbolic expressions describing the characteristic points obtained from the analysis of a general $\mathbf{MDGKN} + \mathbf{C}(t)$ system in section 4.2 are to be applied to this system in order to explain the stability impact of the asymmetry. The focus is on the low frequency region with difference combination resonances being the only significant parametric stability effects. The results presented resume and extend prior investigations originally published in [38].

8.2.1 Problem definition

The original model with symmetric mounting was introduced in [75] in order to demonstrate the excitation mechanism of brake squeal. It was further extended in [71] and [70] by introducing asymmetry in the mounting leading to time-periodic coefficients in the equations of motion. The model consists of a rigid disk (thickness h, radius r) which is in frictional contact with idealized brake pads (preload N_0, stiffness k, damping d). The central inertia tensor $\mathbf{\Theta}$ in the body fixed frame $\vec{d}_i$, $i = 1, 2, 3$ is given by

$$\mathbf{\Theta} = \begin{pmatrix} \Theta & 0 & 0 \\ 0 & \Theta & 0 \\ 0 & 0 & \Phi \end{pmatrix}. \tag{8.11}$$

In the inertial Cartesian coordinate system defined by the unit vectors $\vec{n}_i$, $i = 1, 2, 3$, the disk rotates around the axis $\vec{n}_3$ at a constant angular velocity $\hat{\Omega}$ and is free to tilt with respect to the $\vec{n}_1, \vec{n}_2$-plane. The disk is hinged in its center of mass and is viscoelastically supported by asymmetric rotational springs and dampers (stiffness k_{t1}, k_{t2}, damping d_{t1}, d_{t2}) with the torque $\mathbf{M}_t$. The introduced asymmetry is sought to account for possible asymmetries in the real disk brakes appearing due to ventilation channels and mounting by bolts.

This two-degrees-of-freedom model, described in an inertial frame by Eqs. (8.12)-(8.13),

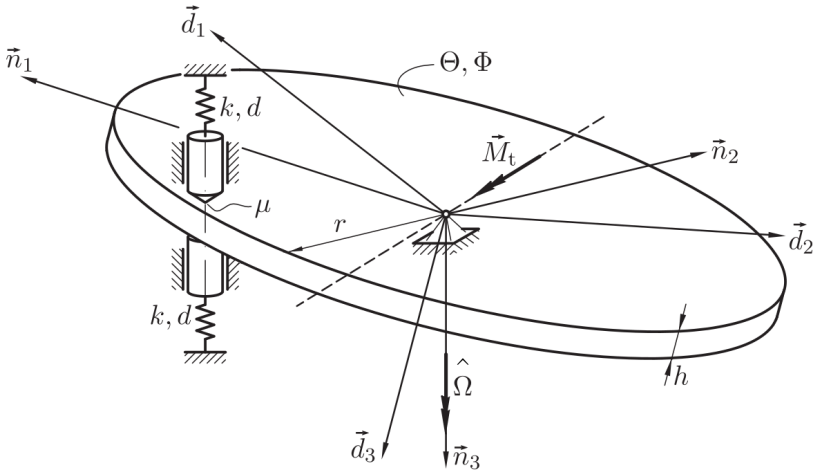

Figure 8.3: Minimal model of a disk brake [70]

contains asynchronous parametric excitation. The linearized equations of motion are

$$\mathbf{M}\ddot{\mathbf{q}}(t) + (\mathbf{D} + \mathbf{G} + \mathbf{B}(t))\,\dot{\mathbf{q}}(t) + (\mathbf{K} + \mathbf{N} + \mathbf{C}(t))\,\mathbf{q}(t) = \mathbf{0} \tag{8.12}$$

with

$$\mathbf{M} = \begin{pmatrix} \Theta & 0 \\ 0 & \Theta \end{pmatrix}, \tag{8.13a}$$

$$\mathbf{D} = \begin{pmatrix} \frac{1}{2}(d_{t1}+d_{t2}) + 2dr^2 + \frac{1}{2}\mu N_0 \frac{h^2}{r\hat{\Omega}} & -\frac{1}{2}dh\mu r \\ -\frac{1}{2}dh\mu r & \frac{1}{2}(d_{t1}+d_{t2}) \end{pmatrix}, \tag{8.13b}$$

$$\mathbf{G} = \begin{pmatrix} 0 & \frac{1}{2}dh\mu r + \Phi\hat{\Omega} \\ -\frac{1}{2}dh\mu r - \Phi\hat{\Omega} & 0 \end{pmatrix}, \tag{8.13c}$$

$$\mathbf{B}(t) = \frac{1}{2}d_{t2}\,(\delta - 1) \begin{pmatrix} \cos 2\hat{\Omega}t & \sin 2\hat{\Omega}t \\ \sin 2\hat{\Omega}t & -\cos 2\hat{\Omega}t \end{pmatrix}, \tag{8.13d}$$

$$\mathbf{K} = \begin{pmatrix} \frac{1}{2}(k_{t1}+k_{t2}) + 2kr^2 + N_0 h & \frac{1}{4}\mu N_0 \frac{h^2}{r} - \frac{1}{2}\mu(khr + 2N_0 r) \\ \frac{1}{4}\mu N_0 \frac{h^2}{r} - \frac{1}{2}\mu(khr + 2N_0 r) & \frac{1}{2}(k_{t1}+k_{t2}) + (1+\mu^2)N_0 h \end{pmatrix}, \tag{8.13e}$$

$$\mathbf{N} = \begin{pmatrix} 0 & \frac{1}{4}\mu N_0 \frac{h^2}{r} + \frac{1}{2}\mu(khr + 2N_0 r) \\ -\frac{1}{4}\mu N_0 \frac{h^2}{r} - \frac{1}{2}\mu(khr + 2N_0 r) & 0 \end{pmatrix}, \tag{8.13f}$$

$$\mathbf{C}(t) = \varepsilon\frac{1}{2}k_{t2}\,(\kappa - 1) \begin{pmatrix} \cos 2\hat{\Omega}t & \sin 2\hat{\Omega}t \\ \sin 2\hat{\Omega}t & -\cos 2\hat{\Omega}t \end{pmatrix}, \tag{8.13g}$$

where $\delta = \frac{d_{t1}}{d_{t2}}$ and $\kappa = \frac{k_{t1}}{k_{t2}}$ are the asymmetry parameters, while $\delta = 1$ and $\kappa = 1$ corresponds to the symmetric mounting. The linearized equations (8.12)-(8.13) describe a complex system with gyroscopic and circulatory terms as well as with periodic coefficients in the velocity- and displacement-proportional terms. According to Eqs. (8.13d) and (8.13g), the parametric excitation is asynchronous, its amplitude is proportional to the asymmetry of the mounting, while the frequency is twice the angular velocity of the disk. An additional switch in order to deliberately disable only the displacement-proportional parametric excitation retaining all other asymmetry related terms is introduced through ε. By default the parametric excitation is active with $\varepsilon = 1$, except stated otherwise. The parameter values of the system are taken according to the original work by VON WAGNER et al. [75]. In [75], realistic parameter values for the reference angular velocity $\hat{\Omega} = 5\,\pi\,\mathrm{s}^{-1}$ are identified as follows

$$\begin{aligned} h &= 0.02\,\mathrm{m}, & r &= 0.13\,\mathrm{m}, \\ k_{t2} &= 1.88 \cdot 10^7\,\mathrm{Nm}, & k &= 6.00 \cdot 10^6\,\mathrm{N/m}, \\ d &= 5\,\mathrm{N\,s/m} & d_{t2} &= 0.1\,\mathrm{N\,m\,s}, \\ \Theta &= 0.16\,\mathrm{kg/m^2}, & \Phi &= 2\Theta, \\ N_0 &= 3.00\,\mathrm{kN}, & \mu &= 0.6. \end{aligned} \tag{8.14}$$

The angular velocity $\hat{\Omega}$ is one of the main parameters to be varied during the analysis of the stability behavior, while, according to the equations of motion, $\hat{\Omega}$ is supposed to be greater than zero. Therefore, for the subsequent analysis, a minimum value of $\hat{\Omega} > 0.5\,\mathrm{rad/s}$ is assumed.

8.2.2 Stability analysis

In the following, stability analysis is performed with the aim to assess the squealing behavior of the brake – an unstable trivial solution would indicate the brake's tendency to squeal. Due to the presence of periodic coefficients, the stability behavior is expressed in terms of the largest LCE obtained from numerical analysis. For further analysis only asymmetry in the elastic restoring torque is considered, while the damping coefficients are assumed equal, i.e., $\kappa \neq 1$ and $\delta = 1$ respectively. The stability of the trivial solution in terms of the largest LCE obtained via the direct integration method (Floquet) for different values of κ is depicted in Fig. 8.4. The region of interest for the angular velocity is limited to low values due to the brake squeal appearing primarily at lower speeds. In the case of symmetric mounting

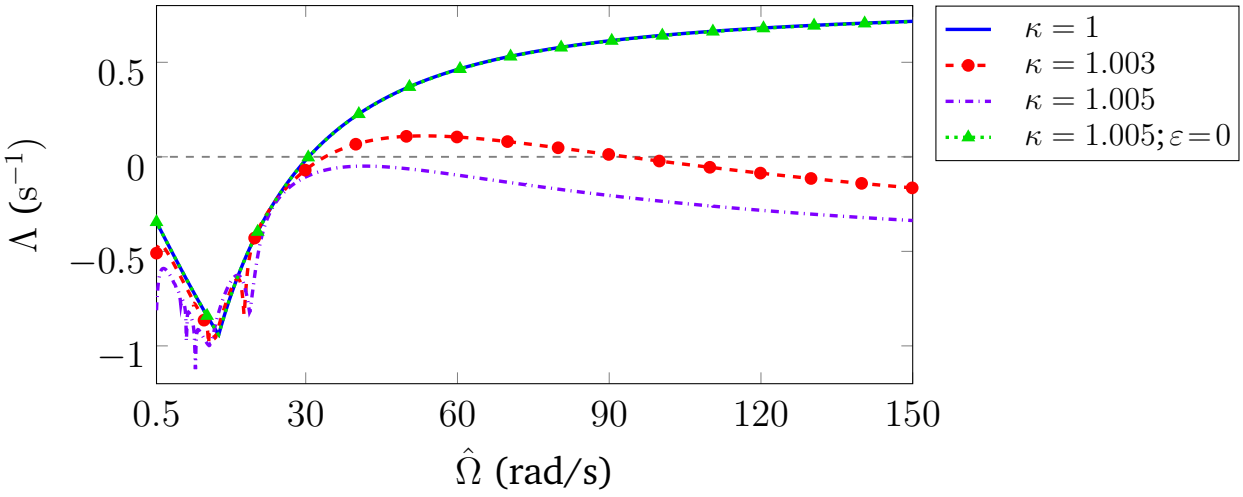

Figure 8.4: The largest LCE Λ versus angular velocity $\hat{\Omega}$ for the minimal brake model (8.12) with symmetric damping ($\delta = 1$) and varying stiffness asymmetry κ

($\kappa = 1$), the trivial solution becomes unstable for all angular velocities exceeding some critical value $\hat{\Omega}_{crit}$. Rather unexpectedly, with increasing asymmetry, and thus the amplitude of parametric excitation, the trivial solution becomes more and more stable, especially for $\hat{\Omega} > 25\,\mathrm{rad/s}$, so that for sufficiently large κ, e.g., $\kappa = 1.005$, it may stay stable for all angular velocities, i.e., excitation frequencies.

Although this stabilizing effect was also observed in [71], its mechanism and relation to parametric excitation could not be fully understood. There, assuming an asymmetry induced splitting of the eigenfrequencies, reported to have a beneficial effect on stability [69], it was concluded that the stabilization is due to the increased gap between the eigenfrequencies. However, in this particular example the splitting of the eigenfrequencies cannot be the decisive factor, since, contrary to expectations, the difference of the eigenfrequencies, $\Delta = |\omega_1 - \omega_2|$, is shrinking for $\kappa > 1$ and growing only for $\kappa < 1$, while the stability is increased in both directions, judged on the critical angular velocity $\hat{\Omega}_{crit}$ for which the trivial solution of system (8.12) becomes unstable, as shown in Fig. 8.5. Apart from that, the variation of the gap of less than $0.2\,\mathrm{s}^{-1}$ in the analyzed region is rather negligible compared to the eigenfrequencies of about $10.000\,\mathrm{s}^{-1}$. At the same time, the amplitude of parametric excitation is growing for both $\kappa > 1$ and $\kappa < 1$, which allows the assumption that the parametric excitation must be primarily responsible for the observed behavior. That the changes in the stability behavior are solely due to the parametric excitation, and not due the splitting of the eigenfrequencies, is obvious for the case with rather strong asymmetry, $\kappa = 1.005$, and turned off parametric excitation, $\varepsilon = 0$, Fig. 8.4.

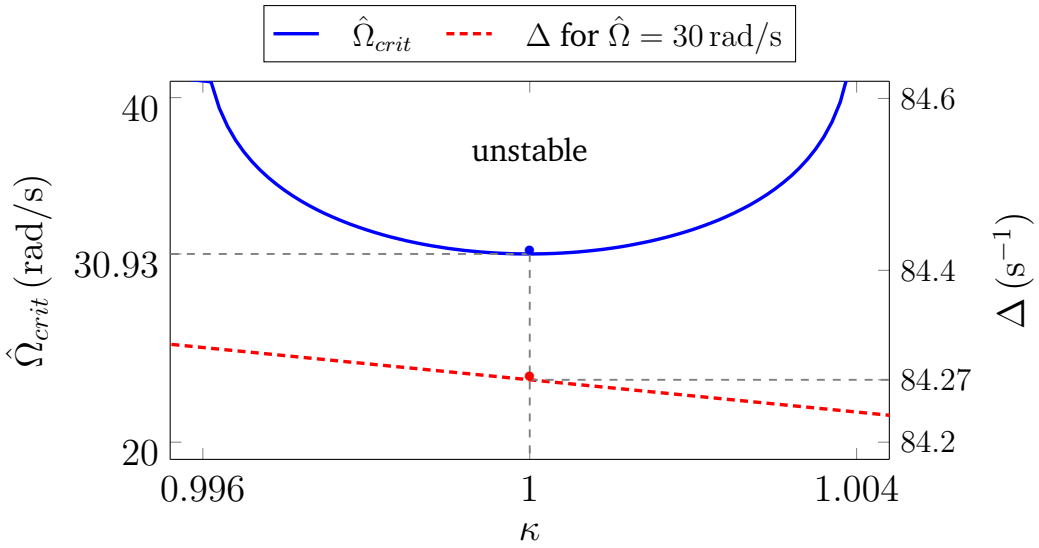

Figure 8.5: Critical angular velocity $\hat{\Omega}_{crit}$ and the difference of the eigenfrequencies Δ (of the unperturbed autonomous system) for varying stiffness asymmetry κ with symmetric damping ($\delta = 1$)

In order to understand the stabilization and the destabilization patterns, it is necessary to know the position of the current parametric excitation frequency with respect to the characteristic frequencies. On the one hand, this knowledge can be obtained using the approximate symbolic expressions derived by the method of normal forms for an $\mathbf{MDGKN} + \mathbf{C}(t)$ system in section 4.2. These have shown to be highly useful in obtaining a general understanding of such complex systems. Though due to the limitations discussed in section 4.2.2, they may not capture all of the effects taking place in this particular system, e.g., higher order resonances. Further, in contrast to the system analyzed in section 4.2, in the considered minimal disk brake model (8.12), the stiffness matrix is not strictly diagonal, but contains off-diagonal entries. These, however, are several orders of magnitude smaller than the diagonal terms and will be neglected when applying the semi-analytical results. On the other hand, more precise information can be obtained applying the numerical Floquet method. Even though it provides only a snapshot of the system's behavior for certain parameter values, with the general understanding obtained before, it is nevertheless possible to interpret the observed stability behavior.

However, the high complexity of this $\mathbf{MDGKN} + \mathbf{C}(t)$ system makes the understanding of the parametric resonance effects and establishing a connection to the previous results a challenging task. A rather unusual pattern of alternating stabilized and destabilized behavior can be observed for low angular velocities: A detailed view presented in Fig. 8.6 shows a destabilizing behavior for $12.5 < \hat{\Omega} < 23\,\mathrm{rad/s}$ and stabilizing behavior outside of this

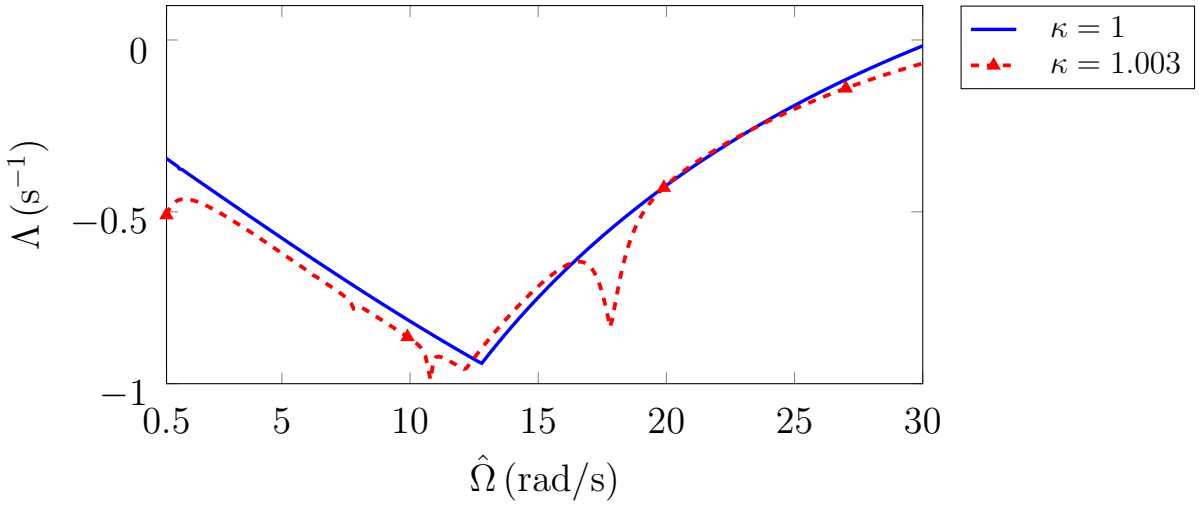

Figure 8.6: Alternating stabilizing and destabilizing effects of parametric excitation in terms of the largest LCE Λ for the minimal brake model (8.12) with symmetric damping ($\delta = 1$) and varying stiffness asymmetry κ

interval (note that the interval is overlaid by a higher order anti-resonance). Further, apart from the presence of circulatory and gyroscopic terms, an additional complexity of the system originates from the coupling between the excitation frequency Ω and the angular velocity given by $\Omega = 2\hat{\Omega}$. The angular velocity $\hat{\Omega}$ has a strong impact on the gyroscopic terms, Eq. (8.13c), which, in turn, exert a considerable impact on the eigenfrequencies of the underlying unperturbed system. This impact is shown in Fig. 8.7 in terms of difference of the eigenfrequencies, $\Delta = |\omega_1 - \omega_2|$, representing the first order difference combination resonance frequency, and the parametric excitation frequency Ω. While such a strong impact of the angular velocity is not typical for a real disk brake, this is nevertheless an important characteristic of the present model. At the same time, the eigenfrequencies used during the normal form analysis are approximated neglecting the velocity proportional terms, i.e., damping and gyroscopic terms. In this way, the approximated difference of the eigenfrequencies agrees well with the real eigenfrequencies only for low values of the excitation frequency, while the deviation quickly becomes substantial for increasing Ω, Fig. 8.7. Obviously, when using these poorly approximated values, no sensible results can be expected from the symbolic expressions derived by the normal form analysis. This kind of error directly affects the characteristic frequencies Ω^0, Ω^s and Ω^d, but can be easily alleviated by simply using the numerically calculated "true" eigenfrequencies in Eqs. (4.25a)-(4.25d).

As already mentioned, the gyroscopic terms, which strongly affect the location of the characteristic frequencies, Eqs. (4.20a)-(4.20c) and Eqs. (4.25a)-(4.25d), are also coupled

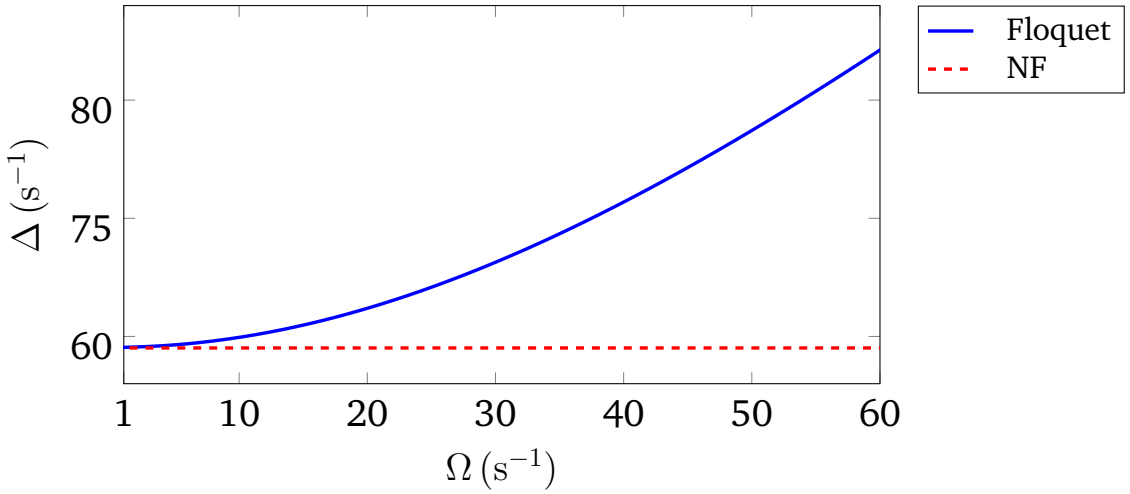

Figure 8.7: First order difference combination resonance frequency Δ versus excitation frequency Ω: numerical results (Floquet) and approximation neglecting velocity-proportional terms used in the method of normal forms (NF)

to the parametric excitation frequency Ω, Eq. (8.13g). In this way, a "standard" sweep over the excitation frequency, as in Fig. 8.6, will not provide information about the relative position of the excitation frequency with respect to the characteristic frequencies. Instead, a sweep over the excitation frequency for each value of angular velocity, i.e., with gyroscopic terms held constant, has to be calculated. With this approach the characteristic frequencies can be obtained numerically (Floquet), though at high computational costs. Figure 8.8 demonstrates two exemplary cases of such sweeps performed with fixed gyroscopic terms corresponding to angular velocities of 5 and $15\,\mathrm{rad/s}$. The results are presented in terms of the largest LCE Λ versus parametric excitation frequency Ω, which is twice the angular velocity of the disk $\hat{\Omega}$, i.e., $\Omega = 2\hat{\Omega}$. Figure 8.8 vividly shows different relations between the current excitation frequency and the characteristic frequencies. In the first case with $\hat{\Omega} = 5$ rad/s, the corresponding excitation frequency $\Omega = 10\,\mathrm{s}^{-1}$ lies within the parametrically stabilized region with the transition to the destabilized area occurring at $\Omega = 80\,\mathrm{s}^{-1}$. On the other hand, the increase in the angular velocity to $\hat{\Omega} = 15\,\mathrm{rad/s}$, changes the whole pattern substantially: The corresponding excitation frequency $\Omega = 30\,\mathrm{s}^{-1}$ rad/s is now in the destabilized region, while the transition to the stabilized behavior occurs at $\Omega = 70\,\mathrm{s}^{-1}$. Obviously, in this particular example, the sequence of stabilizing and destabilizing action of parametric excitation is highly sensitive to the magnitude of the gyroscopic terms. Further, Fig. 8.8 indicates potential interference with higher order difference combination resonances.

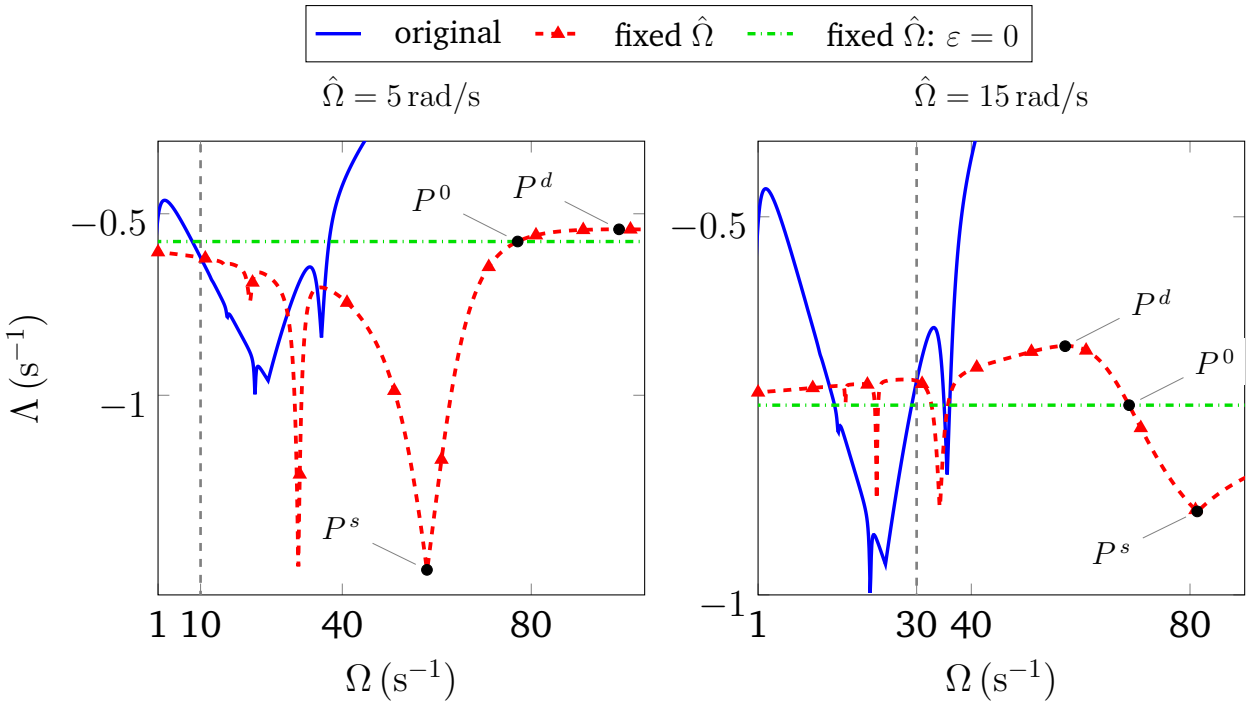

Figure 8.8: Sweep over the parametric excitation frequency Ω for system (8.12): fixed angular velocity $\hat{\Omega}$ compared to original model with $\delta = 0$, $\kappa = 1.003$

Characteristic frequencies

Now the approximate symbolic expressions for the characteristic frequencies are evaluated in order to understand the alternating stabilizing and destabilizing action of parametric excitation. As mentioned above, the circular eigenfrequencies $\omega_{1,2}$ in Eqs. (4.25a)-(4.25d) are evaluated numerically taking into account the complete system without parametric excitation, i.e., including the velocity-proportional terms as well. Figure 8.9 shows the location of the strongest stabilization Ω^s, strongest destabilization Ω^d, but most importantly also the location of the transition point Ω^0 separating the stabilized and destabilized areas. It can be seen that the excitation frequency is in the area of stabilizing effect of parametric excitation for $\Omega < 25\,\mathrm{s}^{-1}$, i.e., for $\hat{\Omega} = 12.5\,\mathrm{rad/s}$. This corresponds exactly to the behavior observed in Fig. 8.6. For greater values, Ω crosses the line of strongest destabilization and is approaching the transition point again. However, the transition point is reached only at $\Omega = 64.4\,\mathrm{s}^{-1}$, while, according to Fig. 8.6, the transition to the stabilized area was expected at $\Omega = 46\,\mathrm{s}^{-1}$.

In the next step, the characteristic frequencies are calculated numerically in order to assess the quality of the normal form results from qualitative and quantitative points of view. Accounting for all stability effects, the numerical results are obtained at high computational

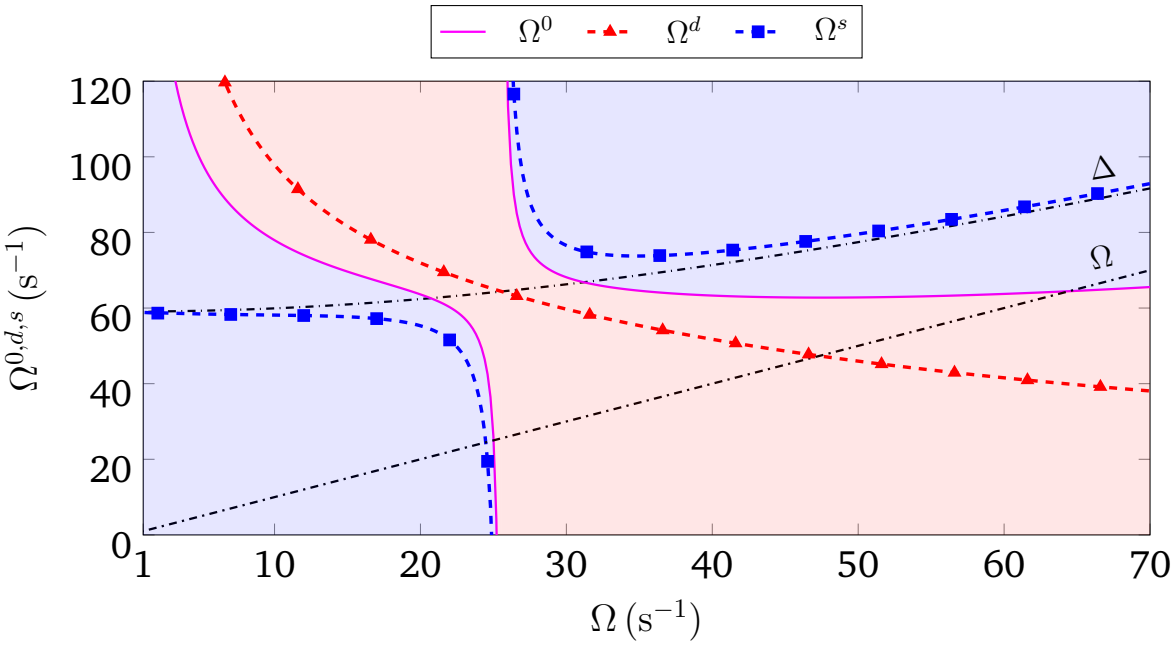

Figure 8.9: Characteristic frequencies for system (8.12) using symbolic expressions derived with the method of normal forms, Eqs. (4.25a)-(4.25d), with $\delta = 0$, $\kappa = 1.003$; destabilizing, stabilizing effect of parametric excitation

costs. Figure 8.10 shows the comparison of semi-analytical and numerical results. An excellent qualitative and quantitative agreement for all characteristic frequencies can be observed for $\Omega < 30\,\mathrm{s}^{-1}$. It is remarkable that the concise symbolic expressions accounting for gyroscopic terms in a simple way are perfectly able to capture the abrupt switch in the sequence of stabilized and destabilized areas occurring at $\Omega = 25\,\mathrm{s}^{-1}$. While the approximation of Ω^s (location of the strongest stabilization) is very good also for $\Omega > 30\,\mathrm{s}^{-1}$, Ω^d and Ω^0 reveal increasing deviation for $\Omega > 30\,\mathrm{s}^{-1}$ with abrupt jumps occurring at $\Omega = 42\,\mathrm{s}^{-1}$ and $\Omega = 46\,\mathrm{s}^{-1}$, respectively. At these excitation frequencies, Ω^d and Ω^0 both approach the same value of about $46\,\mathrm{s}^{-1}$. This increasing deviation and in particular the jump in the course of Ω^0 lead to a much sooner transition back to the stabilized region, than predicted by the symbolic expressions, Figure 8.9. The transition happens exactly at the jump with $\Omega = 46\,\mathrm{s}^{-1}$, i.e., $\hat{\Omega} = 23\,\mathrm{rad/s}$, with Ω crossing Ω^0. This corresponds to the previous observation in Figure 8.6.

Keeping in mind the assumptions made during the derivation of the symbolic expressions, section 4.2.2, and observing numerical results, the deviations and the jumps themselves can be easily explained. Figure 8.10 shows that exactly at the jumps both Ω^d and Ω^0 cross the higher order difference resonance frequency $\Delta/2$, which has a stabilizing anti-resonance effect. For Ω^0 even a further jump at the intersection with the third order difference

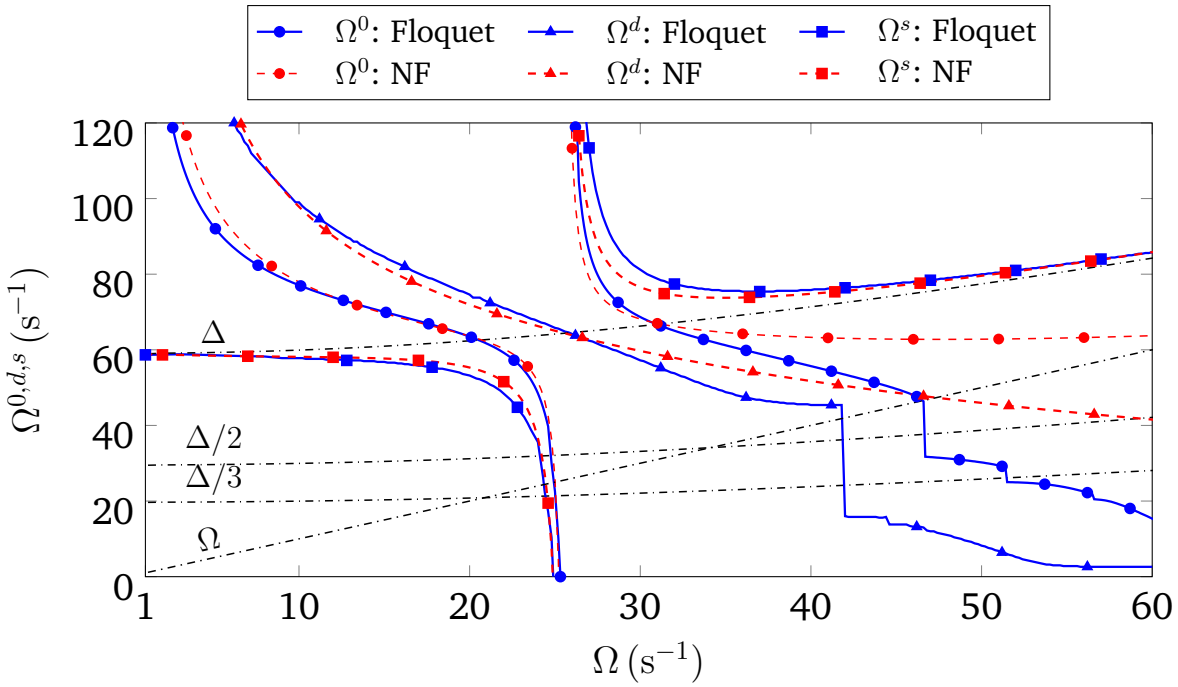

Figure 8.10: Characteristic frequencies for system (8.12): symbolic expressions (NF), Eqs. (4.25a)-(4.25d), versus numerical computations (Floquet) with $\delta = 0$, $\kappa = 1.003$

combination resonance frequency can be observed. Therefore, the increasing deviation and, in particular, the jumps of $\Omega^{0,d}$ are caused by the interference with higher order resonances, while the normal form, on which the symbolic expressions are based, was derived to account for the first order difference combination resonance only. At the same time, no obvious deviation due to the increasing gyroscopic terms (proportional to the excitation frequency) can be observed: even for the rather high gyroscopic terms, Ω^s, free of any interference, seems to be very well approximated, though keeping in mind the adjusted formula with the numerically calculated eigenfrequencies. Also the amplitude of variation seems to fulfill the assumption of being a small parameter.

In this way, the approximate symbolic expressions for the characteristic frequencies represent a powerful tool. Being aware of the underlying assumptions and potential errors, it is possible to alleviate some of the errors to a great extent (eigenfrequencies) and, at least, understand and interpret others which cannot be taken care of directly (higher order resonances). But most importantly, the obtained insight allows a full understanding of the highly complex stability behavior of this $\mathbf{MDGKN} + \mathbf{C}(t)$ system.

Characteristic LCEs

In the next step the characteristic LCEs, $\Lambda^{0,s,d}$, are to be evaluated using the approximate symbolic expressions, Eqs. (4.24a)-(4.24b), and the numerical computations. Unlike in the case of characteristic frequencies, the expressions for the LCEs do not contain circular eigenfrequencies $\omega_{1,2}$. Therefore, no adjustment is needed here.

Fig. 8.11 shows the LCEs obtained in the two different ways versus the excitation frequency. Similar to the characteristic frequencies, there is an excellent agreement for the magnitude of the strongest stabilization Λ^s. For $\Omega < 3.2\,\mathrm{s}^{-1}$ the strongest stabilization is determined by Eq. (4.24a), while at $\Omega = 3.2\,\mathrm{s}^{-1}$, the amplitude of variation exceeds the threshold given by Eq. (4.26), so that for $\Omega > 3.2\,\mathrm{s}^{-1}$ the strongest stabilization is equal to the maximum stabilization $\Lambda^{*,s}$, which is determined by the diagonal damping coefficients alone, Eq. (4.33). As the comparison to the numerical Floquet analysis shows, both regions are well captured by the approximate symbolic expressions. The approximation of Λ^0 and Λ^d is also very good for $\Omega < 30\,\mathrm{s}^{-1}$. For higher excitation frequencies, however, as shown in Fig. 8.10, both the transition point as well as the strongest destabilization point interfere with the higher order stabilizing difference combination resonances leading to an increasing deviation between the numerical and the semi-analytical results.

8.2.3 Conclusions

The insights obtained from the previous studies of general $\mathbf{MDGKN} + \mathbf{C}(t)$ systems, section 4.2, have shown to be essential for the understanding of the diverse stability phenomena. Owing to this new knowledge, the stability impact of asymmetry in this minimal model of a disk brake could be fully understood for the first time. Furthermore, the approximate symbolic expressions derived by means of the method of normal forms, proved to be capable of providing reasonable qualitative and quantitative representation even for this system with realistic parameter values. The observations of this particular example emphasized that in systems featuring gyroscopic and circulatory terms subject to asynchronous parametric excitation, the stability impact, either stabilizing or destabilizing, is highly sensitive to several parameters: The stabilizing and destabilizing regions are not necessarily separated and may coexist at a combination resonance frequency, while a small change in the operating conditions or parameter values may lead to dramatic changes in the stability behavior.

Concerning the issue of brake squealing, the example shows that even small asymmetries, barely affecting the system's eigenfrequencies, may have a significant impact on stability

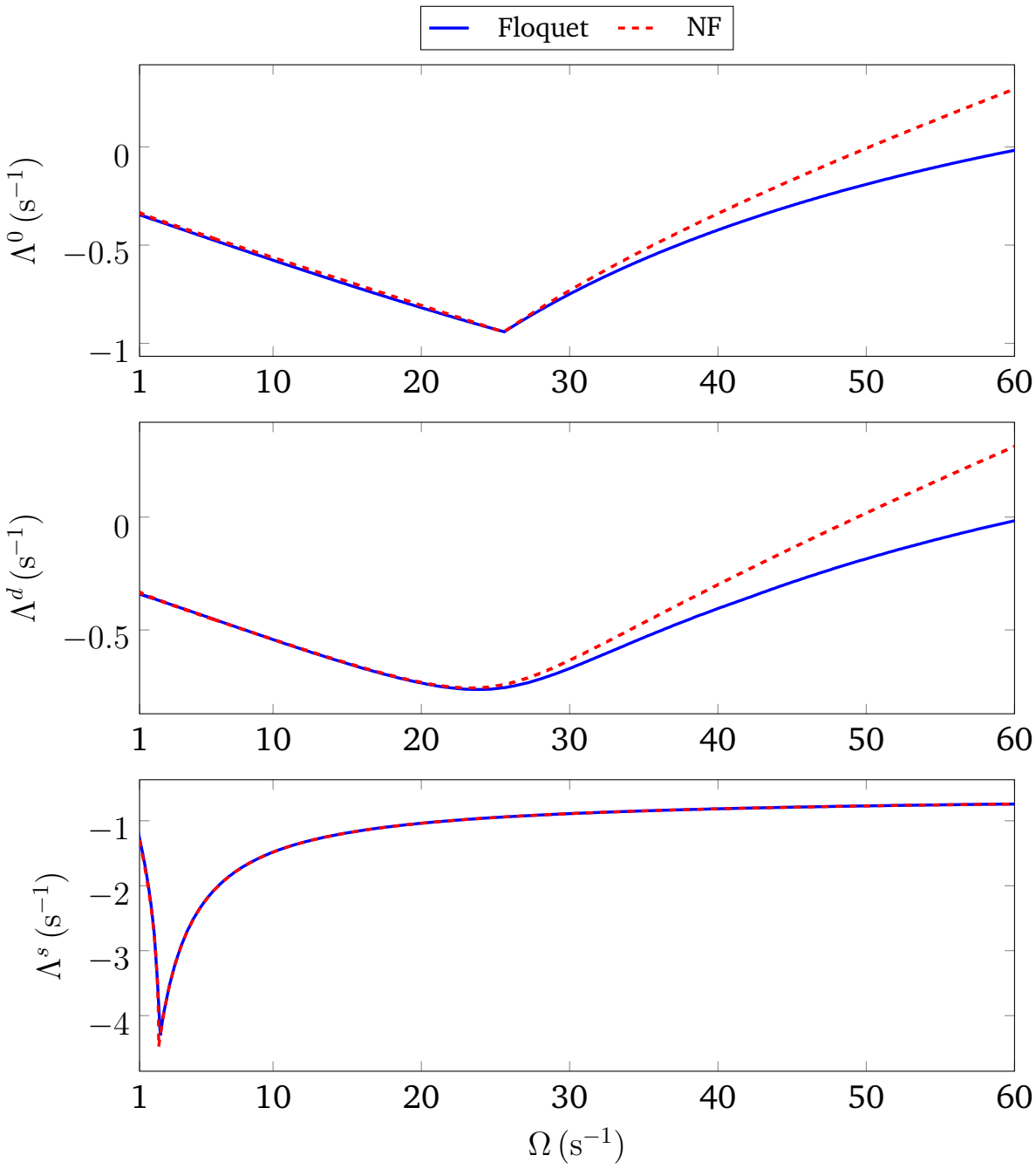

Figure 8.11: Characteristic LCEs for system (8.12): symbolic expressions (NF), Eqs. (4.24a)-(4.24b), versus numerical computations (Floquet) with $\delta = 0$, $\kappa = 1.003$

due to the induced parametric excitation. The obviously high sensitivity to asymmetry indicates that possible asymmetries have to be inspected more carefully and appropriate analysis techniques, accounting for time-periodicity, have to be applied. Further it was shown that previous studies drew an incorrect conclusion on the nature of stabilization through increased asymmetry – the assumed splitting of the eigenfrequencies is not responsible for the stabilization in this particular example, but rather the effect of parametric anti-resonance.

9 Conclusion

The aim of the present work was to extend the studies on parametric excitation with respect to the following aspects. The first aspect deals with the generalization concerning the phase relations in the excitation terms. With most of the studies on time-periodic systems focusing on synchronous excitation, the case of asynchronous excitation was still missing the full picture: The existing studies covered only individual aspects approaching the problem either form the stabilizing or from the destabilizing perspective. Furthermore, the unique phenomenon of total instability caused by a certain kind of asynchronous excitation remained disconnected from the other well studied stability phenomena since its discovery in 1940. The second aspect deals with the generalization with respect to the complexity of the studied systems: Here, the majority of the studies was limited to systems which can be decoupled by modal transformation, i.e., systems featuring neither circulatory nor gyroscopic terms. For these simpler systems a substantial amount of knowledge had been accumulated concerning the appearance of fundamental and combination resonances. However, as soon as circulatory terms appear in the linearized equations of motion, none of the previous knowledge can be directly applied. Even though, numerical stability analysis based on Floquet theory can still be easily performed also for such complex systems, the proper understanding of the effects taking place is still missing.

In order to approach this problem, general MDGKN systems with two degrees of freedom were formulated with displacement- and/or velocity-proportional parametric excitation featuring variable phase relations. Since the fully analytical solution to the stability problem of time-periodic systems is not accessible and the numerical solution does not provide sufficient insight, the semi-analytical method of normal forms was chosen as the main tool for the stability analysis. The method of normal forms, consisting in a series of nonlinear coordinate transformations, provides an approximate autonomous representation of the original time-periodic problem. The stability of this autonomous system can then be more easily obtained by meains of the complex eigenvalue analysis. Even though it is an approximation which is valid in a certain parameter range, it provides excellent insight into the

appearance of different resonance effects and also into the impact of individual parameters. In particular, qualitative statements, e.g., conditions for the appearance of certain kind of resonance, are of great value.

First, the issue of total instability was approached. Total instability, in contrast to the other stability effects, was the only known "global" effect of parametric excitation, i.e., not limited to a narrow frequency range. Deriving the normal form for the non-resonant parametric excitation, which is valid for the whole frequency range except the narrow areas of fundamental and combination resonances, the global stability behavior due to asynchronous parametric excitation could be easily studied. The analysis revealed that total instability is only a special case appearing in systems with uniform damping. Instead, in the more general case with non-uniform damping, there are wide alternating areas with destabilized and stabilized trivial solution. The transition from the stabilizing to the destabilizing effect occurs near the combination resonance frequencies, while the effects reach their maximum right before the transition. The symbolic expressions qualitatively describing the contribution of different parameters to the stability, allowed the formulation of conditions for the appearance of such global effects in general circulatory systems. It was found out that while simpler systems without circulatory terms require a phase shift in the off-diagonal, there are several further possibilities for systems featuring circulatory terms, even with in-phase off-diagonal excitation terms.

The study established connection to other stability effects revealing that the global effects are actually not new separate effects independent from the other common "local" effects. Instead, these are indeed part of the combination resonances and anti-resonances which, in case of asynchronous excitation, are not limited to a narrow frequency range anymore: With the strongest impact still directly in the vicinity of the combination resonance frequencies, the influence of resonances and anti-resonances is extended to the entire excitation frequency range, though quickly getting weaker, if not negligible, with increasing distance from the combination resonance frequencies. For this reason, the global effects, though a unique phenomenon of parametric excitation, are practically insignificant. Of great significance is, however, another implication indicated by this study: Resonance and anti-resonance may coexist at each combination resonance frequency, instead of appearing only separately as believed before.

The coexistence was then studied in detail by deriving corresponding normal forms. The complex stability behavior was described by symbolic expressions obtained for the following characteristic points representing the most significant features: the points of strongest

stabilization and destabilization as well as the transition point. Using the concise symbolical expressions for the characteristic points, the assessment of what kind of resonance to expect (resonance, anti-resonance, or coexistence of both) can now be easily made based on the equations of motion alone, even for a circulatory system.

The coexistence of resonance and anti-resonance represents the core finding of the present work. While the two effects have been individually validated in the past, their simultaneous appearance at a combination resonance frequency was at first a purely theoretical concept identified for abstract mathematical models. In order to provide more significance to the phenomenon of coexistence, a simulation-based validation was performed reproducing the experimental setup of an electronic system used in the past by other researcher. The close-to-experiment simulation using the electronic circuit simulation software confirmed the theoretical findings.

Further, the theoretical studies on circulatory systems under asynchronous parametric excitation were completed by analyzing the fundamental resonances as well. Even though no special effects occur in this case, the results provide missing information on the contribution of the circulatory terms to the magnitude and appearance of fundamental resonances. Again, using the normal form transformation, symbolic expressions were derived and analyzed, revealing some interesting aspects. For example, in circulatory systems fundamental resonances appear even without excitation in the main diagonal.

Finally, the newly obtained knowledge on circulatory systems with asynchronous parametric excitation was applied to two mechanical examples. The first simple example featuring synchronous excitation is used to demonstrate that in the presence of circulatory terms, difference combination resonances may easily appear. In systems without circulatory terms, these are very rare as a skew-symmetric parametric excitation, i.e., phase shift of π in the antidiagonal, is required.

In the second example featuring a complex minimal model of a disk brake with gyroscopic and circulatory terms as well as with asynchronous excitation. The previously derived expressions for the characteristic points, in particular for the characteristic frequencies, are used to explain the unusual stability pattern with frequently alternating stabilized and destabilized regions. The knowledge about the coexistence with the very sensitive transition form the stabilizing to the destabilizing effects provided the explanation for the observed behavior emphasizing the practical significance of coexistence. Moreover, the analysis provided also new insights with respect to the disk brake model. Originally, the asymmetries were introduced to demonstrate the effectiveness of the eigenfrequency splitting regarding

the issue of stability, i.e., brake squealing. However, the present study showed that the splitting itself does not significantly affect the stability behavior – the changes are primarily due to the parametric resonance effects. These findings are supposed draw attention to more careful study of possible asymmetries and therefore parametric excitation in disk brakes.

Summarizing the main results of the thesis, the following main findings are to be highlighted:

- for asynchronous parametric excitation in general
  - there are global stabilizing and destabilizing effects with total instability being only a special case for uniform damping
  - resonance and anti-resonance coexist at each combination resonance frequency, instead of appearing only separately
- for circulatory systems in particular
  - several phase relations in the excitation terms lead to coexistence and global effects, even with in-phase off-diagonal terms
  - fundamental resonances can appear with only antidiagonal excitation
  - combination resonances can appear with only main-diagonal excitation
- concerning the disk brakes
  - the stability impact of asymmetry might be rather due to the parametric resonance effects than due to the eigenfrequency splitting itself
  - even small asymmetries might significantly affect the stability, while the resulting impact (stabilization or destabilization) is not certain and is very sensitive to parameter changes

The future research should be directed towards the exploration of potential applications of the newly discovered stability effects. The symbolic expressions for the characteristic points represent a useful tool for designing systems with desired stability behavior. Possible applications in the area of amplification and filtering might benefit from the coexistence of resonance and anti-resonance with a sharp transition between them. In particular the possibility to flexibly introduce parametric excitation, including asynchronous excitation, in electromechanical systems, e.g., MEMS, might improve the existing applications or initiate new ones.

Bibliography

[1] Analog Devices Inc. *LTspice XVII*. Version XVII. Sept. 1, 2019. URL: https://www.analog.com.

[2] Becker, L. *Experimentelle und numerische Untersuchung von Kombinationsresonanzen (Experimental and numerical investigation of combination resonances)*. PhD thesis. Karlsruhe, Germany: University of Karlsruhe, 1972.

[3] Bobryk, R. V. and Yurchenko, D. "On enhancement of vibration-based energy harvesting by a random parametric excitation". In: *J. Sound Vib.* 366 (2016), pp. 407–417.

[4] Bolotin, V. V. *The Dynamic Stability of Elastic Systems*. Holden-Day, 1964.

[5] Breunung, T., Dohnal, F., and Pfau, B. "An approach to account for interfering parametric resonances and anti-resonances applied to examples from rotor dynamics". In: *Nonlinear Dyn.* 97 (2019), pp. 1837–1851.

[6] Busch-Vishniac, I. J. *Electromechanical Sensors and Actuators*. Springer-Verlag New York, 1999.

[7] Bylov, B. F. et al. *The theory of Lyapunov exponents and its applications to problems of stability (in Russian)*. Moscow, USSR: Nauka, 1966.

[8] Cartmell, M. C. *Introduction to Linear, Parametric and Non-Linear Vibrations*. Springer Netherlands, 1990.

[9] Cesari, L. *Asymptotic Behavior and Stability Problems in Ordinary Differential Equations*. Ergebnisse der Mathematik und ihrer Grenzgebiete. 2. Folge. Springer-Verlag Berlin Heidelberg, 1963.

[10] Cesari, L. *Sulla stabilità delle soluzioni dei sistemi di equazioni differenziali lineari a coefficienti periodici (On the stability of systems of linear differential equations with periodic coefficients)*. Rome, Italy: Reale Accademia d'Italia, 1940.

[11] Chasalevris, A. and Dohnal, F. “A journal bearing with variable geometry for the suppression of vibrations in rotating shafts: Simulation, design, construction and experiment”. In: *Mech. Syst. Signal Process* 52-53 (2015), pp. 506–528.

[12] Chasalevris, A. and Dohnal, F. “Improving stability and operation of turbine rotors using adjustable journal bearings”. In: *Tribol. Int.* 104 (2016), pp. 369–382.

[13] De Broeck, L. *Stability analysis of extended parametrically excited systems by application of normal forms method*. Bachelors thesis. Darmstadt, Germany: Technical University of Darmstadt, 2017.

[14] Dohnal, F. “Damping by Parametric Stiffness Excitation: Resonance and Anti-Resonance”. In: *J. Vib. Control* 14.5 (2008), pp. 669–688.

[15] Dohnal, F. *Damping of Mechanical Vibrations by Parametric Excitation: Parametric Resonance and Anti-Resonance*. Germany: Südwestdeutscher Verlag für Hochschulschriften, 2009.

[16] Dohnal, F. “Experimental studies on damping by parametric excitation using electromagnets”. In: *Proc. Inst. Mech. Eng., Part C: J. Mech. Eng. Sci.* 226.8 (2012), pp. 2015–2027.

[17] Dohnal, F. “General parametric stiffness excitation – anti-resonance frequency and symmetry”. In: *Acta Mech.* 196.1 (2008), pp. 15–31.

[18] Dohnal, F. “Suppressing self-excited vibrations by synchronous and time-periodic stiffness and damping variation”. In: *Journal of Sound and Vibration* 306.1 (2007), pp. 136–152. ISSN: 0022-460X.

[19] Dohnal, F. and Tondl, A. “Suppressing Flutter Vibrations by Parametric Inertia Excitation”. In: *J. Appl. Mech.* 76.3 (Mar. 2009).

[20] Dohnal, F. and Tondl, A. “Using Time-Periodicity for Inducing Energy Transfer Between Vibration Modes”. In: vol. Volume 7B: 9th International Conference on Multibody Systems, Nonlinear Dynamics, and Control. International Design Engineering Technical Conferences and Computers and Information in Engineering Conference. Aug. 2013.

[21] Dohnal, F. and Verhulst, F. “Averaging in vibration suppression by parametric stiffness excitation.” In: *Nonlinear Dyn.* 54 (Mar. 2008), pp. 231–248.

[22] Dolev, A. and Bucher, I. “Tuneable, non-degenerated, nonlinear, parametrically-excited amplifier”. In: *J. Sound Vib.* 361 (2016), pp. 176–189.

[23] Drozd, A. L. “Selected methods for validating computational electromagnetic modeling techniques”. In: *2005 International Symposium on Electromagnetic Compatibility, 2005. EMC 2005.* Vol. 1. IEEE, 2005, 301–306 Vol. 1.

[24] Eicher, N. *Ein Iterationsverfahren zur Berechnung des Stabilitätsverhaltens zeitvarianter Schwingungssysteme (An iterative method for analysis of stability behavior of time-varying vibration systems)*. Fortschritt-Berichte VDI.: Schwingungstechnik, Lärmbekämpfung. Düsseldorf, Germany: VDI-Verlag, 1984.

[25] Eicher, N. *Einführung in die Berechnung parametererregter Schwingungen (An introduction to parametrically excited vibrations)*. TUB-Dokumentation Weiterbildung. Berlin: Technical University of Berlin, 1981.

[26] Eicher, N. *Parametererregte Schwingungen in Theorie und Praxis (Parametrically excited vibrations in theory and application)*. TUB-Dokumentation Weiterbildung. Berlin, Germany: Technical University of Berlin, 1982.

[27] Eicher, N. “Parameterresonanzen 1. und 2. Art bei Schwingungssystemen mit allgemeinen harmonischen Erregermatrizen (Parametric resonances of first and second kind in vibration systems with general harmonic excitation matrices)”. In: *Ingenieur-Archiv* 54.3 (1984), pp. 188–204.

[28] Faraday, M. “On a Peculiar Class of Acoustical Figures; and on Certain Forms Assumed by Groups of Particles upon Vibrating Elastic Surfaces”. In: *Philos. Trans. Royal Soc.* 121 (1831), pp. 299–340.

[29] Hagedorn, P. “Kombinationsresonanz und Instabilitätsbereiche zweiter Art bei parameterregten Schwingungen mit nichtlinearer Dämpfung (Combination resonance and instability areas of second kind in parametrically excited vibrations with nonlinear damping)”. In: *Ingenieur-Archiv* 38.2 (1969), pp. 80–96.

[30] Hagedorn, P. and Hochlenert, D. *Technische Schwingungslehre: Schwingungen linearer diskreter mechanischer Systeme.* Verlag Europa-Lehrmittel, 2015.

[31] Hale, J. K. *Ordinary differential equations*. Pure and applied mathematics. Huntington, N.Y: R.E. Krieger Pub. Co, 1980.

[32] Hill, G. W. “On the part of the motion of the lunar perigee which is a function of the mean motions of the sun and moon”. In: *Acta Math.* 8 (1886), pp. 1–36.

[33] Hochlenert, D. “Dimension reduction and domains of attraction of nonlinear dynamical systems”. In: *Machine Dynamics Research* 35.4 (2011), pp. 32–48.

[34] Hochlenert, D. *Normalformen und Einzugsbereiche nichtlinearer dynamischer Systeme: Beispiele und technische Anwendungen (Normal forms and domains of attraction of nonlinear dynamical systems: examples and technical applications)*. Habilitation thesis. Berlin, Germany: Technische Universität Berlin, 2012.

[35] IEEE. "IEEE Standard for Validation of Computational Electromagnetics Computer Modeling and Simulations". In: *IEEE Std. 1597.1-2008* (2008), pp. c1–41.

[36] IEEE. "List of IEEE Milestones". In: *Engineering and Technology History Wiki* (Sept. 1, 2019). URL: https://ethw.org/Milestones:List_of_IEEE_Milestones.

[37] Jekel, D. "Optimization of Damping in Self-Excited Mechanical Systems". PhD thesis. Technical University of Darmstadt, 2018.

[38] Karev, A., De Broeck, L., and Hagedorn, P. "Some remarks on parametric excitation in circulatory systems". In: *PAMM* 18.1 (2018).

[39] Karev, A. and Hagedorn, P. "Asynchronous parametric excitation: validation of theoretical results by electronic circuit simulation". In: *Nonlinear Dyn.* (June 2020).

[40] Karev, A. and Hagedorn, P. "Global stability effects of parametric excitation". In: *J. Sound Vib.* 448C (2019), pp. 34–52.

[41] Karev, A. and Hagedorn, P. "Non-conservative dynamical systems under asynchronous parametric excitation". In: *Proceedings of the International Conference on Structural Engineering Dynamics*. Viana do Castelo, Portugal, June 24, 2019.

[42] Karev, A. and Hagedorn, P. "Simultaneous Resonance and Anti-Resonance in Dynamical Systems Under Asynchronous Parametric Excitation". In: *J. Comput. Nonlinear Dyn.* (Feb. 2020).

[43] Karev, A., Hochlenert, D., and Hagedorn, P. "Asynchronous parametric excitation, total instability and its occurrence in engineering structures". In: *J. Sound Vib.* 428 (2018), pp. 1–12.

[44] Klotter, K. *Technische Schwingungslehre. Zweiter Band: Schwinger von mehreren Freiheitsgraden (Mehrläufige Schwinger) (Technical vibration theory. Second volume: Oscillators of several degrees of freedom)*. Berlin Heidelberg: Springer, 1981.

[45] Kovacic, I., Rand, R., and Mohamed Sah, S. "Mathieu's Equation and Its Generalizations: Overview of Stability Charts and Their Features". In: *Applied Mechanics Reviews* 70.2 (Feb. 2018).

[46] Lord Rayleigh, F.R.S. “XXXIII. On maintained vibrations”. In: *Philos. Mag.* 15.94 (1883), pp. 229–235.

[47] Lyapunov, A. M. *General problem of the stability of motion (in Russian)*. Classics of natural science. Moscow-Leningrad, USSR: State Publishing House of Technical-Theoretical Literature (GITTL), 1950.

[48] Malkin, J. G. *Theorie der Stabilität einer Bewegung (Theory of stability of motion)*. Munich: R. Oldenbourg, 1959.

[49] *Mathematica, Version 11.2*. Wolfram Research, Inc. Champaign, Illinois, 2020.

[50] Mathieu, É. “Mémoire sur le mouvement vibratoire d’une membrane de forme elliptique.” fre. In: *J. Math. Pures Appl.* 13 (1868), pp. 137–203.

[51] *MATLAB, Version 9.4.0.813654 (R2018a)*. The Mathworks, Inc. Natick, Massachusetts, 2020.

[52] Melde, F. “Über die Erregung stehender Wellen eines fadenförmigen Körpers”. In: *Ann. Phys. (Leipzig)* 187.12 (1860), pp. 513–537.

[53] Mettler, E. “Allgemeine Theorie der Stabilität erzwungener Schwingungen elastischer Körper”. In: *Ingenieur-Archiv* 17 (1949), pp. 418–449.

[54] Moran, K. et al. “A review of parametric resonance in microelectromechanical systems”. In: *Nonlinear Theory and Its Applications, IEICE* 4.3 (2013), pp. 198–224.

[55] Murdock, J. *Normal Forms and Unfoldings for Local Dynamical Systems*. Springer Monographs in Mathematics. Springer New York, 2003.

[56] Nayfeh, A. H. *The Method of Normal Forms*. New York: Wiley-VCH Verlag GmbH & Co. KGaA, 2011.

[57] Nayfeh, A.H. and Mook, D.T. *Nonlinear Oscillations*. Pure and Applied Mathematics: A Wiley Series of Texts, Monographs and Tracts. Wiley, 1979.

[58] Okamoto, H. et al. “Rapid switching in high-Q mechanical resonators”. In: *Applied Physics Letters* 105.8 (2014), p. 083114.

[59] Olkhovets, A. et al. “Non-degenerate nanomechanical parametric amplifier”. In: *Technical Digest. MEMS 2001. 14th IEEE International Conference on Micro Electro Mechanical Systems (Cat. No.01CH37090)*. IEEE. 2001, pp. 298–300.

[60] Peng, K. et al. “Full-circuit SPICE simulation based validation of dynamic delay estimation”. In: *2010 15th IEEE European Test Symposium*. IEEE, 2010, pp. 101–106.

[61] Pfau, B. *Ein verstellbares Zweiflächengleitlager zur Schwingungsminderung flexibler Rotoren*. Berichte aus dem Maschinenbau. Shaker Verlag, 2018.

[62] Pontryagin, L. S. *Ordinary Differential Equations*. Adiwes international series in mathematics. Addison-Wesley, 1962.

[63] Prakash, G. et al. "Theoretical basis of parametric-resonance-based atomic force microscopy". In: *Phys. Rev. B* 79.9 (2009).

[64] Ramírez-Barrios, M., Dohnal, F., and Collado, J. "Enhanced vibration decay in high-Q resonators by confined of parametric excitation". In: *Archive of Applied Mechanics* 90.8 (Aug. 2020), pp. 1673–1684.

[65] Rhoads, J. F., Guo, C., and Fedder, G. K. "Parametrically Excited Micro-and Nanosystems". In: *Resonant MEMS: Fundamentals, Implementation, and Application* (2015).

[66] Rohatgi, A. *WebPlotDigitizer*. San Francisco, California, USA, 2019.

[67] Schmidt, G. *Parametererregte Schwingungen*. VEB Deutscher Verlag der Wissenschaften, 1975.

[68] Schmieg, H. *Kombinationsresonanz bei Systemen mit allgemeiner harmonischer Erregermatrix (Combination resonance in systems with general harmonic excitation matrix)*. PhD thesis. Karlsruhe, Germany: University of Karlsruhe, 1976.

[69] Spelsberg-Korspeter, G. "Breaking of symmetries for stabilization of rotating continua in frictional contact". In: *J. Sound Vib.* 322.4-5 (2009), pp. 798–807.

[70] Spelsberg-Korspeter, G. and Hagedorn, P. "Complex Eigenvalue Analysis and Brake Squeal: Traps, Shortcomings and their Removal". In: *SAE Int. J. Passeng. Cars - Mech. Syst.* 5.4 (2012), pp. 1211–1216.

[71] Spelsberg-Korspeter, G., Hochlenert, D., and Hagedorn, P. "Non-linear investigation of an asymmetric disk brake model". In: *Proc. IMechE, Part C: J. Mechanical Engineering Science* 225.10 (2011), pp. 2325–2332.

[72] Tondl, A. *On the interaction between self-excited and parametric vibrations*. In Monographs and Memoranda 25. Prague, Czechoslovakia: National Research Institute for Machine Design Bechovice, 1978.

[73] Turner, K. L. and Zhang, W. "Design and analysis of a dynamic MEM chemical sensor". In: *Proceedings of the 2001 American Control Conference. (Cat. No.01CH37148)*. Vol. 2. 2001, 1214–1218 vol.2.

[74] Verhulst, F. “Parametric and Autoparametric Resonance”. In: *Acta Applicandae Mathematica* 70.1 (Jan. 2002), pp. 231–264.

[75] Wagner, U. von, Hochlenert, D., and Hagedorn, P. “Minimal models for disk brake squeal”. In: *J. Sound Vib.* 302.3 (2007), pp. 527–539.

[76] Yakubovich, V. A. and Starzhinskii, V. M. *Linear Differential Equations with Periodic Coefficients*. Israel Program for Scientific Translations. Jerusalem: John-Wiley & Sons New York-Toronto, 1975.

[77] Yang, W. and Towfighian, S. “A parametric resonator with low threshold excitation for vibration energy harvesting”. In: *J. Sound Vib.* 446 (2019), pp. 129–143.